LUND UNIVERSITY

The strength of glulam beams with holes - A probabilistic fracture mechanics method and experimental tests

Danielsson, Henrik

2009

[Link to publication](#)

Total number of authors:
1

THE STRENGTH OF GLULAM BEAMS WITH HOLES
A Probabilistic Fracture Mechanics Method and Experimental Tests

HENRIK DANIELSSON

Licentiate Dissertation

THE STRENGTH OF GLULAM BEAMS WITH HOLES
A Probabilistic Fracture Mechanics Method and Experimental Tests

HENRIK DANIELSSON

Acknowledgements

Lund, February 2009

Henrik Danielsson

Abstract

This thesis deals with experimental tests and methods for strength analysis of glulam beams with holes. Test results and methods for strength analysis available in literature are compiled and discussed. The methods considered comprise both code strength design methods and more general methods for strength analysis.

New strength tests of beams with quadratic holes with rounded corners are presented. The test programme included investigations of four important design parameters: material strength class, bending moment to shear force ratio, beam size and hole placement with respect to beam height. One important finding from these tests is the strong beam size influence on the strength. This finding is in line with previous test results found in literature but the beam size effect is however not accounted for in all European timber engineering codes.

A probabilistic fracture mechanics method for strength analysis is presented. The method is based on a combination of Weibull weakest link theory and the mean stress method which is a generalization of linear elastic fracture mechanics. Combining these two methods means that the fracture energy and the stochastic nature of the material properties are taken into account. The probabilistic fracture mechanics method is consistent with Weibull weakest link theory in the sense that the same strength predictions are given by these two methods for an ideally brittle material. The probabilistic fracture mechanics method is also consistent with the mean stress method in the sense that the same strength predictions are given by these two methods for a material with deterministic material properties.

A parameter study of the influence of bending moment to shear force ratio, beam size, hole placement with respect to beam height and relative hole size with respect to beam height is presented for the probabilistic fracture mechanics method.

Strength predictions according to the probabilistic fracture mechanics method is also compared to the present and previous test results found in literature and also to other methods for strength analysis including code design methods. The probabilistic fracture mechanics method shows a good ability to predict strength, with the exception of very small beams.

Keywords: glulam, hole, stress, strength, test, design, Weibull, fracture mechanics, probabilistic fracture mechanics.

Contents

APPENDED PAPERS

Paper A

    Strength Tests of Glulam Beams with Quadratic Holes – Test Report
    Henrik Danielsson
    Report TVSM-7153, Division of Structural Mechanics, Lund University, 2008.

Paper B

    Strength of Glulam Beams with Holes –
    Tests of Quadratic Holes and Literature Test Results Compilation
    Henrik Danielsson and Per Johan Gustafsson
    CIB-W18/41-12-4, St Andrews, Canada, 2008.

Paper C

    A Probabilistic Fracture Mechanics Method for Strength Analysis
    of Glulam Beams with Holes
    Henrik Danielsson and Per Johan Gustafsson
    submitted to European Journal of Wood and Wood Products
    (previous journal title: Holz als Roh- und Werkstoff)

SEPARATE REPORT BEING PART OF THESIS

    The Strength of Glulam Beams with Holes –
    A Survey of Tests and Calculation Methods
    Henrik Danielsson
    Report TVSM-3068, Division of Structural Mechanics, Lund University, 2007.

Chapter 1

Introduction

1.1   Background

The mechanical properties of wood are very different for different orientations of loading with respect to material direction. Wood is very weak when exposed to tensile stress perpendicular to grain, the tensile strength perpendicular to grain is only a few percent of the tensile strength parallel to grain. Due to the low strength, special attention should hence be given when designing timber structures in order to avoid or at least limit this type of stress. Fracture caused by tension perpendicular to grain commonly has a brittle course which emphasizes the need for careful design considerations even more. Avoiding tension perpendicular to grain all in all when designing is not a trivial task. There are a number of common and in many respects appealing technical solutions that however introduce risk of fracture due to perpendicular to grain stresses. Three such examples are shown in Figure 1.1; a beam with a hole, an end-notched beam and a curved beam. There are also other possible causes for perpendicular to grain stresses, for example various types of joints and development of an uneven moisture content due to variations in temperature and relative humidity.

Introducing a hole through a beam drastically changes the stress state and reduces the strength significantly due to the high perpendicular to grain tensile stresses and shear stresses appearing in the vicinity of the hole. It is however sometimes necessary to make holes through glulam beams, for example for installations as can be seen in Figure 1.2.
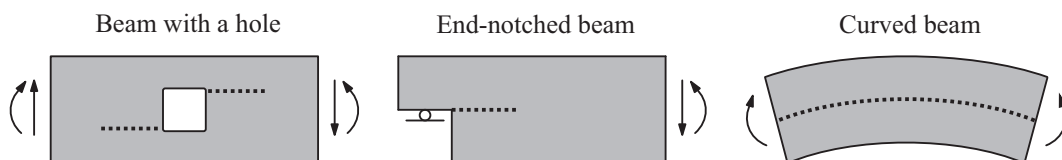
Figure 1.1: *Structural timber elements with perpendicular to grain tensile stresses.*

Figure 1.2: *Examples of structures with glulam beams with holes. Indoor swimming pool, Västerås, Sweden (with permission for Martinssons Trä AB) and Restaurant Ideon, Lund, Sweden.*

There are several available methods for rational strength analysis when it comes to timber engineering. Timber is in many aspects a complex construction material which is partly due to the anisotropic properties and the large differences in strength between loading modes. The choice of method for strength analysis depends on the application. Assumptions and simplifications for a certain method and material model may be acceptable for some applications but may for other cases lead to unreliable results if the analysis is possible to perform at all. A distinction can be made between *deterministic* and *stochastic* material models. In the deterministic models, wood is viewed as a homogeneous material with the same material properties in all points. In the stochastic models, the natural heterogeneity due to knots and other defects is considered by some type of statistical measure. For both deterministic and stochastic models, another distinction can be made concerning whether the material strength is assumed to have a *finite* or an *infinite* value. Distinctions between different models can also be made based on properties of fracture energy, where the material can be assumed to be either *ideally brittle* (zero fracture energy) or be assumed to show *fracture ductility* (nonzero fracture energy). Based on the distinctions mentioned above, various kinds of methods for rational strength analysis of timber elements can be categorized as in Table 1.1.

There are also other types of methods which do not fit in the categorization presented here, for example empirically based methods. Such methods are here defined as a method where empirical relations between material-, geometry-, load parameters and load carrying capacity are established based only on experimental tests. This type of method is to be considered as a last resort when more rational methods, such as the ones presented above, are not useful for some reason. Empirical and semi-empirical methods are found in various codes and handbooks as will be shown below. Among the methods presented here, the applicability for strength analysis of glulam beams with holes varies.

Table 1.1: *Methods for rational strength analysis in timber engineering.*

	Deterministic (homogeneous strength)		Stochastic (heterogenous strength)	
	finite material strength	infinite material strength	finite material strength	infinite material strength
Ideally brittle	Conventional stress analysis	-	Weibull weakest link theory	-
With fracture ductility	Generalized linear elastic fracture mechanics Nonlinear fracture mechanics	Linear elastic fracture mechanics	Probabilistic generalized linear elastic fracture mechanics Probabilistic nonlinear fracture mechanics	Probabilistic linear elastic fracture mechanics

Looking at the literature concerning the strength of glulam beams with holes, it can be seen that several experimental and theoretical investigations have been carried out within this field over the last decades. A brief summary is given below while a more comprehensive literature review, focusing on experimental tests but also relating to methods for strength analysis, is presented in [7]. This report is published separately but is however also a part of this thesis.

Among the early work within the field, contributions concerning experimental tests were presented by Bengtsson & Dahl [4] 1971, Kolb & Frech [18] 1977 and Penttala [20] 1980. Rather comprehensive experimental investigations and also different methods for strength analysis were presented by Johannesson [17] 1983. Based on the test results, an empirical method for strength analysis was proposed and this method is now one of the two methods found in the Swedish design handbook Limträhandbok. This method is presented in Section 3.3. Theoretical investigations presented by Kolb & Epple [19] 1985, partly dealt with stress analysis of beams with holes and a design method was presented. The design procedure in the German code DIN 1052, which is presented in Section 3.4, is based on this method.

From the 1990's and forward, much of the theoretical work have focused on approaches based on fracture mechanics. Various fracture mechanics methods have been investigated and contributions within this field are for example presented by: Pizio [22] 1991, Hallström [15] 1995, Riipola [24] 1995, Aicher, Schmidt & Brunhold [1] 1995, Petersson [21] 1995, Gustafsson, Petersson & Stefansson [13] 1996, Scheer & Haase [25] and [26] 2000 and Stefansson [28] 2001.

The studies presented by Höfflin [16] 2005 and Aicher & Höfflin [2] 2006 deal with the strength of glulam beams with circular holes and are two of the most recent and also two of the most comprehensive studies. Substantial test programmes were carried out including investigations of influence of beam height, relative hole size and bending moment to shear force ratio. A design method based on Weibull weakest link theory was also proposed. This method is presented in Section 3.5.

The study presented by Rautenstrauch, Franke and Franke [23] 2007 deals with the strength of glulam beams with rectangular or circular holes. Contact-free measurements by so called *close range photogrammetry* was used to measure the strain field in the vicinity of the holes.

One of the most important overall aims of timber engineering research is to incorporate findings in design codes and handbooks since they are the everyday tools used by practising structural engineers. Looking at design recommendations for glulam beams with holes in European timber engineering codes and handbooks over the last decades, it can be seen that the issue has been treated in many different ways. The theoretical backgrounds on which the recommendations are based show fundamental differences and both empirically based methods and more rationally based methods are found. In spite of the research effort in this field, there are still major discrepancies between the predicted strengths according to the different codes and also between codes and experimental test results. This reflects the lack of knowledge in the area which is further emphasized by the fact that the contemporary version of Eurocode 5 [8] does not state any equation concerning design of glulam beams with holes and the design recommendations for glulam beams with rectangular holes were withdrawn from the German code DIN 1052 [5] during 2007.

1.2 Problem statement

The lack of reliable design recommendations in European timber engineering codes reflects the insufficient knowledge of the strength of glulam beams with holes in particular and of fracture caused by high perpendicular to grain stresses in general. The assumption of a homogeneous and ideally brittle material behavior commonly adopted in timber engineering seems to be inadequate for strength predictions of glulam beams with holes.

1.3 Aim and objectives

The aim of the work presented in this thesis is to develop a *probabilistic fracture mechanics method* for strength analysis of glulam beams with holes, taking into consideration the nonzero fracture energy of the material and also accounting for the heterogeneity in material properties. The method derived and implemented here is based on the so called *mean stress method* (generalized linear elastic fracture mechanics) and *Weibull weakest link theory*. The specific objectives are to determine influence of four important design parameters on the strength according to the probabilistic fracture mechanics method and to evaluate the correlation with experimental test results. The considered design parameters are:

- Bending moment to shear force ratio
- Beam size
- Hole placement with respect to beam height
- Relative hole size with respect to beam height

1.4 Research approach and limitations

The research approach adopted in the work presented in this thesis can in general terms be described as development of a rational method for strength analysis which is based on (and consistent with) established theories relating to strength analysis. The method is then evaluated by comparison to previous and new experimental test results.

The probabilistic fracture mechanics method presented in this thesis is founded on a combination of Weibull weakest link theory and the so called mean stress method. Weibull weakest link theory is often put forward as an explanatory theory for the well known size-strength dependency found for various applications within timber engineering. The mean stress method is based on a generalization of linear elastic fracture mechanics. Different approaches based on fracture mechanics have over the last decades received increasing interest within the timber engineering research community and are generally believed to have great potential for applications where failure is caused by high perpendicular to grain tensile stresses.

In order make a thorough evaluation of the purposed method, comparison to a wide and reliable base of experimental tests results is needed. There are however a number of problems related to this. Costly and time consuming full-scale experimental tests are needed since model-scale testing generally are of little value due to the strong size-strength dependency. Another issue is the relatively high variability which is characteristic to timber as a material. The strength is further dependent on many different parameters relating to beam geometry, material properties and loading conditions. Based on time and economical considerations, the number of nominally equal tests within a test series needed for reliable results stands against the number of parameters that can be investigated. For the tests presented in Paper A, four nominally equal tests were used in each test series and four design parameters were (to various extent) investigated in the study. The comparisons between different test results and also between the proposed method and test results are partly based on results presented in [2] and [16]. There are some inevitable epistemic risks involved with using test results from other sources. The tests are in these two studies are however very well documented.

The four design parameters mentioned in Section 1.3 are consequently considered regarding experimental tests, design codes and also the computational parameter study. This is not to say that these parameters are the most important ones, or that other parameters are unimportant, but the work presented within this thesis has been limited to these four design parameters. The computational parameter study does furthermore comprises material parameters of the present probabilistic fracture mechanics method. The aim with the work presented is not to propose a design method suitable for design codes but rather to increase the knowledge of the strength of glulam beams with holes and to investigate the possibilities with the proposed method.

1.5 Structure of thesis

This thesis consists of this main report and a separately published report [7]. The thesis is structured in the following way:

Chapter 1 - Introduction

Chapter 2 - Strength tests of glulam beams with holes
    Strength tests of glulam beams with quadratic holes are presented and compared to test results of previously performed tests.

Chapter 3 - Code design methods for glulam beams with holes
    Design methods according to some European timber engineering design codes are review and compared.

Chapter 4 - Weibull weakest link theory
    The basics of Weibull weakest link theory are presented and some comments on influence of volume and heterogeneity in stress distribution are given.

Chapter 5 - Fracture mechanics
    The basics of linear elastic fracture mechanics and generalized linear elastic fracture mechanics, in particular the mean stress method, are presented.

Chapter 6 - A probabilistic fracture mechanics method – PFM
    A probabilistic fracture mechanics (PFM) method based on Weibull weakest link theory and the mean stress method is derived and illustrated.

Chapter 7 - Implementation of the PFM method
    An implementation of the PFM method based on finite element stress analysis and numerical integration of stresses is presented.

Chapter 8 - Parameter study and verification
    A parameter study and verification concerning design parameters is presented for the PFM method. The study also comprises experimental tests.

Chapter 9 - Concluding Remarks
    Some concluding remarks concerning the strength of glulam beams with holes and the PFM method are given.

Paper A
    A detailed description of the strength tests of beams with quadratic holes.

Paper B
    CIB-paper concerning the strength tests of beams with quadratic holes, literature test result compilation and also comparison between tests results and design codes.

Paper C
    Journal-paper concerning the probabilistic fracture mechanics method.

Separately published report
    This report holds a literature review focusing mostly on experimental tests but also relating to methods for strength analysis.

Chapter 2

Strength tests of glulam beams with holes

2.1   General

There are numerous experimental investigations found in literature concerning the strength of glulam beams with holes. The experimental test results published by the authors mentioned in Chapter 1 prior to 2007 are reviewed in [7] and a compilation of the results is also found in Paper B. Although these tests all in all represent much work the review reveals that important parameters such as mode of loading, beam size and hole placement with respect to beam height have often been varied only within a very limit range. It seems for example that all beams tested have had a hole centrically placed with respect to beam height.

2.2   Tests of glulam beams with quadratic holes

With the aim of widening the experimental data base, tests of beams with quadratic holes were carried out at Lund University during the spring of 2008. The test programme consisted of nine test series with four nominally equal tests in each series. Four design parameters were investigated; *material strength class*, *bending moment to shear force ratio*, *beam size* and the previously overlooked design parameter *hole placement with respect to beam height*.

Test setups and hole placements with respect to beam height used in the test series are illustrated in Figure 2.1. Two different test setups were designed in order to investigate the influence of bending moment to shear force ratio. Three different hole placements were tested in test setup 1 in order to investigate the influence of hole placement with respect to beam height. The influence of beam size was investigated by scaling all in-plane dimensions while the out-of-plane dimension was constant. Two different beam cross sections ($T \times H = 115 \times 180$ and 115×630 mm^2) were used for test setup 1 and all three hole placements with respect to beam height. The material strength class GL 32h was used for all test setups and all hole

7

placements. For test setup 1 with a centrically placed hole, beams of the Swedish material strength class L40 were also tested. All holes were quadratically shaped with rounded corners. The side lengths of the holes were $a = b = H/3$ and the corner radius was $r = 7$ mm for $H = 180$ mm and $r = 25$ mm for $H = 630$ mm.

A more thorough presentation of the tests is given in Paper A and Paper B where density, moisture content, test procedure, recorded load levels and other characteristics of the tests are given. The findings concerning the four investigated design parameters are here summarized only in general terms:

Material strength class
There was no significant difference in strength between the different material strength classes. The results of these two test series are however comparatively scattered.

Bending moment to shear force ratio
The beams with holes placed in a position of zero bending moment show on average slightly higher capacity compared to the beams with holes placed in a position of combined bending moment and shear force.

Beam size
The test results indicate a strong beam size effect on the strength. Increasing the beam size by a factor 3.5 gave about 30-35 % reduction of nominal capacity.

Hole placement with respect to beam height
Slightly lower capacities were found for the beams with eccentrically placed holes compared to the beams with centrically placed holes.
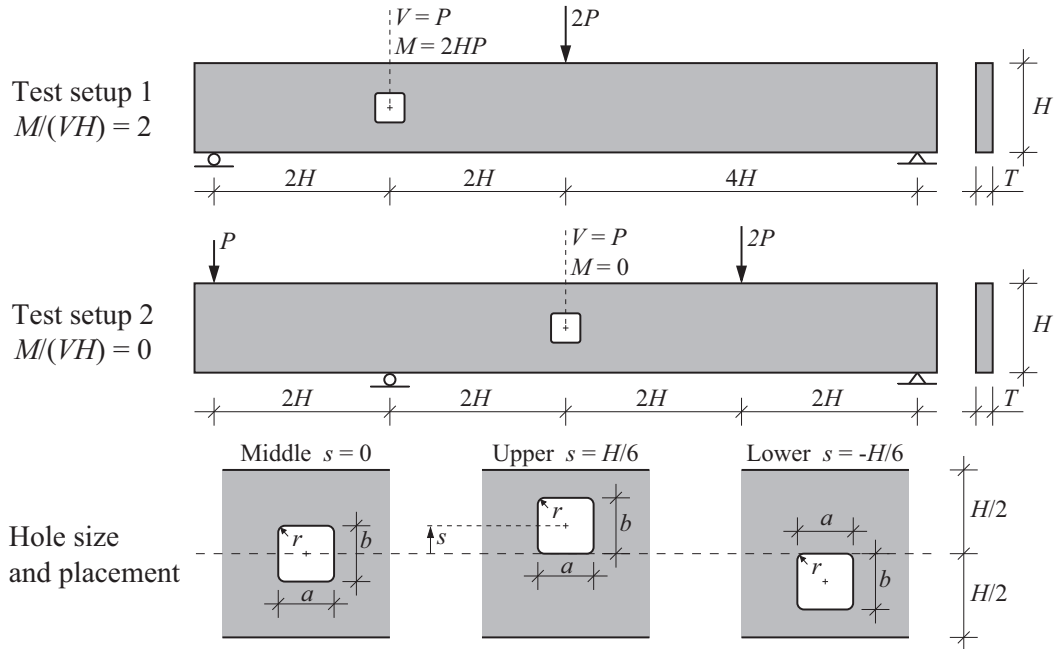
Figure 2.1: *Test setups, hole size and placements with respect to beam height.*

2.3   Comparison of test results

In order to relate the tests of beams with quadratic holes to previously performed tests on glulam beam with holes, test results concerning the four design parameters stated in Section 1.3 are presented: *bending moment to shear force ratio*, *beam size*, *hole placement with respect to beam height* and *relative hole size*. These design parameters are also the ones considered in Chapter 3 and Chapter 8.

The comparisons are based on the results of the tests of beams with quadratic holes (quadratic marks and solid lines) and on the results of beams with circular holes presented by Höfflin [16] and by Aicher & Höfflin [2] (circular marks and dashed lines). The nominal shear strength V_c/A_{net} given in the figures relate to the mean strength values of the test series where each test series consists of 4-6 individual tests. The value of shear force V_c is that at the instant of crack development across the entire beam width. A_{net} refer to the beam net cross section area at hole center and ϕ is the hole diameter for circular holes. All test results relate to beams of material strength class GL 32h. Lines connecting two or more marks indicate that these test series are identical concerning the four parameters considered here, except the particular parameter illustrated in the respective figures.

Since there seems to be no previous tests of beams with eccentrically placed holes with respect to beam height, the comparison of test results for this design parameter is only based on the tests of quadratic holes presented in the previous section. These tests do however not include any study of the influence of relative hole size, and this comparison is hence only based on the previously performed tests.

As illustrated in Figure 2.2, the influence of the bending moment to shear force ratio seems to be rather small. The test results suggest only a small decrease in strength with increasing bending moment to shear force ratio. Concerning beam size, illustrated in Figure 2.3, the test results indicate a strong influence. For uniformly scaled in-plane dimensions and constant out-of-plane dimensions, the beam size effect can be expressed according $V_c/A_{net} \sim (H^2)^{-1/m}$. The parameter m describes the beam size effect and can be determined from two test series of different scales. The values of m are for the nine pair of test series given in Figure 2.3. As an example, $m = 4$ corresponds to $V_c/A_{net} \sim 1/\sqrt{H}$. Note that this definition of m differs from the definition in Paper B. As illustrated in Figure 2.4 and mentioned in the previous section, the tests of beam with quadratic holes indicate somewhat lower strength for beams with eccentrically placed holes. Concerning the relative hole size, illustrated in Figure 2.5, the test results seem to indicate a small decrease in strength considering the nominal shear strength V_c/A_{net}. Considering the absolute values of the shear force V_c and constant beam cross section, the strength decreases significantly with increasing hole size.

Among the presented results, there is one test series with a surprisingly low strength and there seems to be no obvious explanation for it. The mean strength of this test series is lower than the strength of the test series with the same beam cross section and bending moment to shear force ratio but with a larger hole. This deviating test series is in the figures indicated by a filled mark.
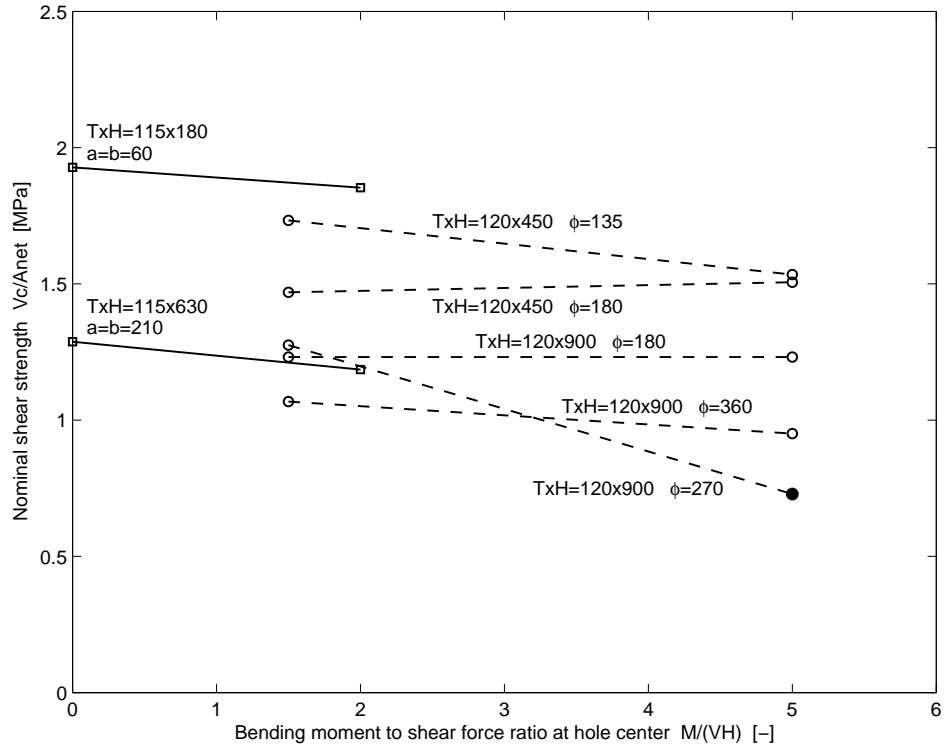
Figure 2.2: *Influence of bending moment to shear force ratio.*
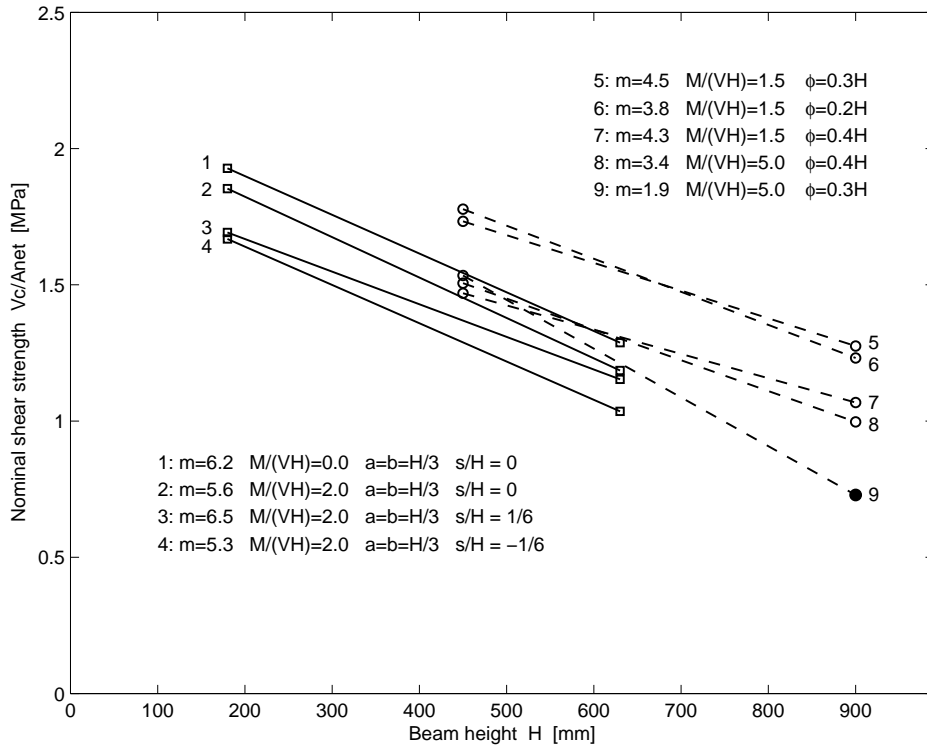
Figure 2.3: *Influence of beam size.*
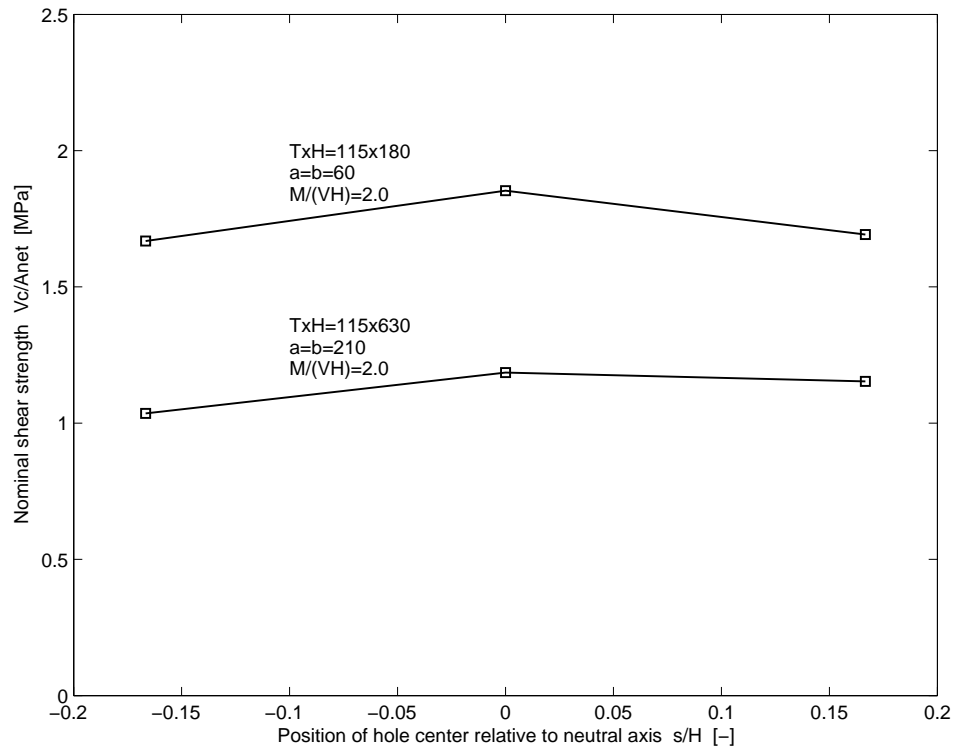
Figure 2.4: *Influence of hole placement with respect to beam height.*
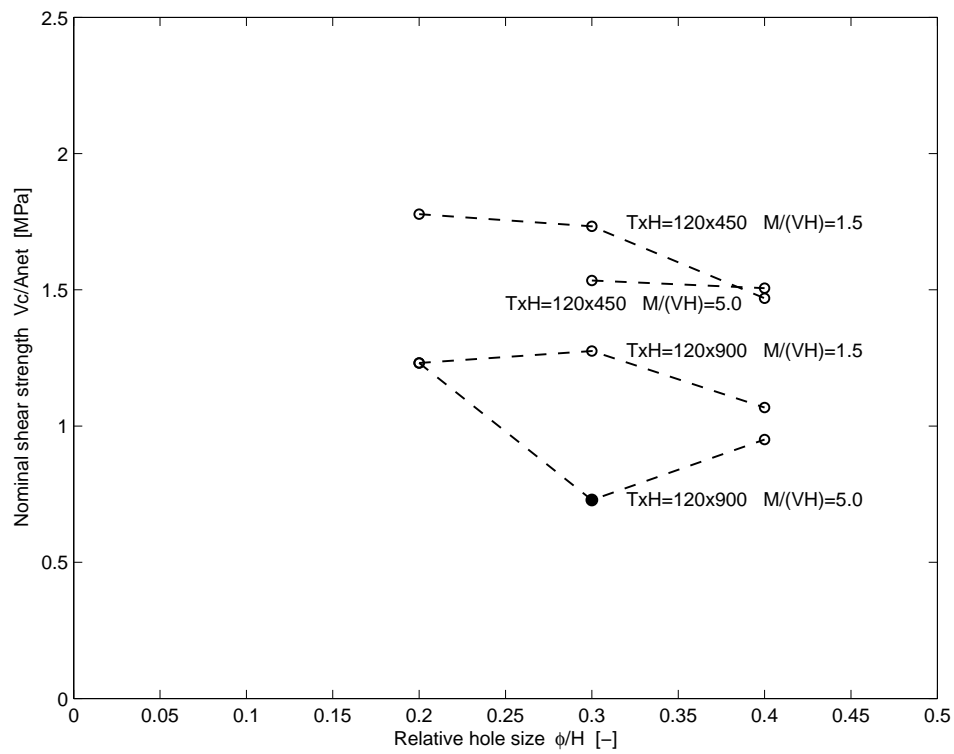
Figure 2.5: *Influence of relative hole size.*

Chapter 3

Code design methods for glulam beams with holes

3.1 General

Looking at design recommendations for glulam beams with holes in European timber engineering codes and handbooks over the last decades, it can be seen that the issue has been treated in many different ways. The theoretical backgrounds on which the recommendations are based show fundamental differences and there are also major discrepancies between the strength estimations according to the different codes as well as between tests and estimations according to codes. Finding a simple, general and reliable method for design of glulam beams with holes seems to be a difficult task which is reflected in several ways:

- The contemporary version of Eurocode 5 [8] does not state any equation concerning design of glulam beams with holes although it was included in a previous draft version of the code [9].

- The recommendations in the German code DIN 1052 [5] concerning rectangular holes were withdrawn during the fall of 2007 since they were believed to lead to unsafe design.

- The Swiss timber design code is currently under revision and the design approach for glulam beams with holes is likely to be altered [29].

- The fact that empirical and semi-empirical methods play an important role in contemporary design codes shows the need for further development of methods for strength analysis.

Some of the design recommendations which are found or have been found in European timber design codes are reviewed in the following sections. There are in general some basic rules concerning for example hole placement, maximum allowed hole sizes and corner radius for rectangular holes and so on that need to be fulfilled.

13

Examples of these are presented in Table 3.1 and Figure 3.1. It is generally recommended to place the hole in the neutral axis of the beam. This is probably partly because it is believed to give the highest capacity and partly due to the fact that, with exception of recent tests performed at Lund University, all previous tests seem to have been performed on beams with holes placed in the neutral axis [7].

Table 3.1: *Regulations concerning hole geometry and placement.*

	Limträhandbok [6]	DIN 1052:2004 [5]
l_a	-	$\geq 0.5H$
l_v	-	$\geq H$
l_z	$\geq H$	$\geq H$ and ≥ 300mm
h_u	$\geq 0.15H$	$\geq 0.25H$
h_l	$\geq 0.15H$	$\geq 0.25H$
a	$\leq 3b$	$\leq H$
b or ϕ	$\leq 0.5H$	$\leq 0.4H$
r	≥ 25 mm	≥ 15 mm
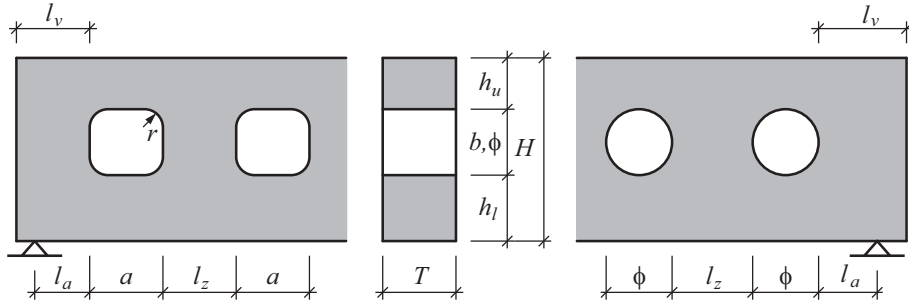
Figure 3.1: *Notations for regulations concerning hole geometry and placement.*

3.2 Draft version of Eurocode 5

As mentioned earlier, there are no design recommendations stated in the contemporary version of Eurocode 5 [8]. In a previous draft version of the code from 2002 [9] there is however a section on design of glulam beams with holes. The method stated is the same as the "end-notched beam" analogy method in Limträhandbok.

3.3 Swedish handbook - Limträhandbok

Limträhandbok (Glulam Handbook) [6] is not an official Swedish code but rather a tool for recommendations concerning design of glulam structures. Two different methods for design of glulam beams with holes are stated in the handbook; an empirically based method and a method based on estimations by means of comparison with fracture mechanics analysis of end-notched beams.

Method 1 - Empirically based design

This method was originally proposed by Johannesson [17] as a simple but rather crude estimation of strength for glulam beams with holes. The method is based on short term loading tests of some 50 beams with more or less the same beam cross section ($90{\times}500$ mm^2). Beams with holes of various geometries were tested, with all holes placed centrically with respect to beam height. The design criterion consists of a comparison of shear stress τ and a reduced shear strength $f_{v,red}$ according to Equation (3.1). The shear stress τ is due to the shear forces V_i where index i indicates that either the upper (u) or lower (l) part of the beam is considered. The total shear force at hole center V can be divided between the upper and lower part based on the relative stiffness but $V_{tot} = V_u + V_l$ must of course always hold. The shear strength f_v is reduced by the factors k_{vol} and k_{hole} accounting for a beam width effect (but no beam height effect) and an influence of hole size respectively. There is also a comment found relating to design with respect to bending moment of the net cross section but the description of how this should be done is rather unclear. Definitions of loads and geometry parameters are shown in Figure 3.2.

$$\tau = \frac{3}{2}\frac{V_i}{Th_i} \le f_{v,red} \qquad \text{where index } i = u \text{ or } l \qquad (3.1)$$

$$f_{v,red} = k_{vol}k_{hole}f_v$$

$$k_{vol} = \left(\frac{90}{T}\right)^{0.2} \qquad \text{for } 90 \le T \le 215 \text{ mm}$$

$$k_{hole} = \begin{cases} 1 - 555(D/H)^3 & \text{for } D/H \le 0.1 \\[2mm] \dfrac{1.62}{(1.8 + D/H)^2} & \text{for } D/H > 0.1 \end{cases}$$

$$D = \begin{cases} \sqrt{a^2 + b^2} & \text{for rectangular hole} \\ \phi & \text{for circular hole} \end{cases}$$
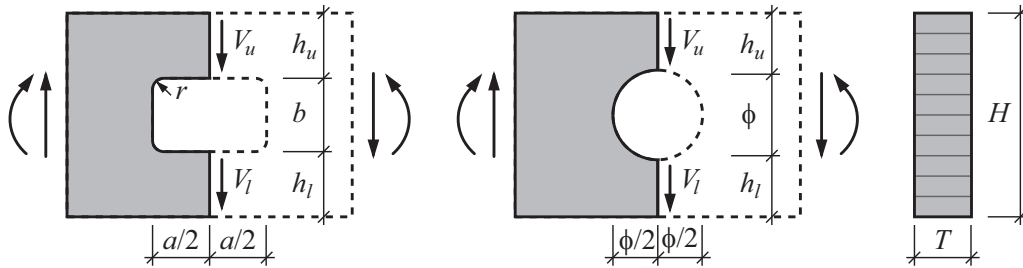
Figure 3.2: *Notations for design according to method 1, Limträhandbok.*

Method 2 - "End-notched beam" analogy

There is also another method suggested for design of glulam beams with holes placed in a shear force dominated region presented in Limträhandbok. This method is based on the assumption that the stress distribution in the vicinity of a hole is rather alike the stress distribution in an end-notched beam. Hence, the design method for end-notched beams can be used in a slightly modified way. The original method for end-notched beams is derived in [10] and based on a fracture mechanics approach. As for the empirically based method, the design criterion formally reads as a comparison of shear stress τ and a reduced shear strength $f_{v,red}$ according to Equation (3.2). Both corners with perpendicular to grain stresses must be checked. The shear strength f_v is reduced by the factor k_v in analogy with the strength reduction for a corresponding end-notched beam. A rectangular hole is assumed to correspond to a right angled end-notch while a circular hole is assumed to correspond to a 1:1 tapered end-notch. Influence of possible bending moment is not considered in method 2 and neither in method 1. Definitions of loads and geometry parameters are shown in Figure 3.3.

$$\tau \;=\; \frac{3}{2}\frac{V_i}{Th_i} \le f_{v,red} \qquad \text{where index } i = u \text{ or } l \qquad (3.2)$$

$$f_{v,red} \;=\; k_v f_v$$

$$k_v \;=\; \min \begin{cases} 1.0 \\[2mm] \dfrac{6.5\left(1+\dfrac{1.1j^{1.5}}{\sqrt{h}}\right)}{\sqrt{h}\left(\sqrt{\alpha-\alpha^2}+0.8\dfrac{e}{h}\sqrt{\dfrac{1}{\alpha}-\alpha^2}\right)} \end{cases}$$

$$h = h_i + b/2 \qquad [\text{mm}]$$

$$\alpha = h_i/h$$

$$j = \begin{cases} 0 & \text{for rectangular hole} \\ 1.0 & \text{for circular hole} \end{cases}$$

$$e = \begin{cases} a/2 & \text{for rectangular hole} \\ 0 & \text{for circular hole} \end{cases}$$
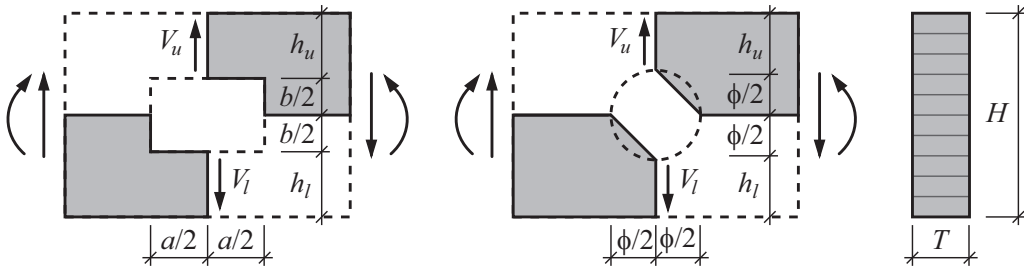
Figure 3.3: *Notations for design according to method 2, Limträhandbok.*

3.4 German code - DIN 1052

Design of glulam beams with holes is treated rather differently in the German code DIN 1052 [5] compared to the two methods in Limträhandbok. The German method can be referred to as a semi-empirical method since it is partly based on analysis of the stress field in the vicinity of the hole and partly based on results from experimental tests. The method is based on the work presented in [19]. The design criterion is a comparison between tension stress perpendicular to grain and perpendicular to grain tensile strength according to Equation (3.3). The perpendicular to grain tension force $F_{t,90}$ consists of contributions due to shear force V ($F_{t,V}$) and bending moment M ($F_{t,M}$) and both sections 1 and 2 should be checked. The perpendicular to grain stress is assumed to have a triangular shaped distribution over a length $l_{t,90}$. Definitions of loads and geometry parameters are shown in Figure 3.4. As mentioned earlier, the design recommendations for rectangular holes were withdrawn during the fall of 2007 since they were believed to lead to unsafe design.

$$\sigma_{90} = \frac{F_{t,90}}{0.5 l_{t,90} T} \leq f_{t,90} \tag{3.3}$$

$$F_{t,90} = F_{t,V} + F_{t,M}$$

$$F_{t,V} = \frac{V_i x}{4H} \left(3 - \frac{x^2}{H^2} \right) \qquad \text{where index } i = 1 \text{ or } 2$$

$$F_{t,M} = 0.008 \frac{M_i}{h_r} \qquad \text{where index } i = 1 \text{ or } 2$$

for rectangular holes:

$$l_{t,90} = 0.5(b + H)$$
$$x = b$$
$$h_r = \min \left\{ \begin{array}{c} h_u \\ h_l \end{array} \right.$$

for circular holes:

$$l_{t,90} = 0.353\phi + 0.5H$$
$$x = 0.7\phi$$
$$h_r = \min \left\{ \begin{array}{c} h_u + 0.15\phi \\ h_l + 0.15\phi \end{array} \right.$$
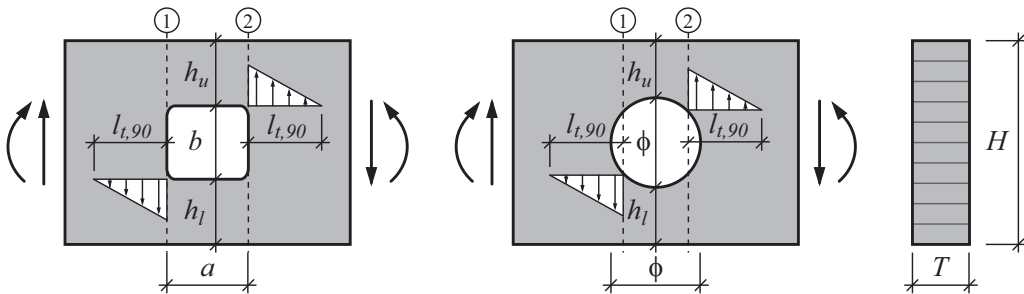
Figure 3.4: *Notations for design according to DIN 1052.*

3.5 Design proposal by Höfflin and Aicher

A design proposal for glulam beams with circular holes based on Weibull weakest link theory is presented in [16] and [2]. The design criterion is stated in Equation (3.4) as a comparison of maximum perpendicular to grain tensile stress $\sigma_{t,90}$ and the perpendicular to grain tensile strength $f_{t,90}$. In accordance with Weibull weakest link theory, the strength is modified depending on the size of the stressed volume and on the level of heterogeneity in the stress distribution. The stress distribution, the magnitude and location for the maximum tensile stress $\sigma_{t,90}$ were for different types of loading (for different relations between shear force V and bending moment M) investigated by 2D plane stress finite element analysis. Based on this analysis, the below stated expression for the maximum perpendicular to grain tensile stress $\sigma_{t,90}$ was assumed to be a good approximation for a general case. The choice of volume for integration of stresses is not obvious but based on the finite element analysis, the volume Ω according to Figure 3.5 was chosen. Considering only this volume, the level of heterogeneity of the stress distribution (described by the distribution factor $k_{dis} = \sigma_{t,90}/\sigma_{wei}$) was determined for various relations of shear force V and bending moment M. The strength is further modified depending on the relation between the reference volume Ω_{ref} and the considered volume Ω.

$$\sigma_{t,90} \leq f_{t,90}k_{dis}c\left(\frac{\Omega_{ref}}{\Omega}\right)^{1/5} \tag{3.4}$$

$$\sigma_{t,90} = \frac{3}{2}\frac{V}{TH}\left(1.23 + 0.82\frac{\phi}{H}\right) + \frac{0.6M}{TH^2}\frac{\phi}{H}$$

$$k_{dis} = \begin{cases} 1.79 & \text{for} & 0 \leq M/(VH) & \leq 2 \\ 1.83 & \text{for} & M/(VH) & = 5 \\ 1.88 & \text{for} & M/(VH) & = 10 \\ 2.04 & \text{for} & M/(VH) & = \infty \end{cases}$$

$$c = 1.16 \qquad \text{empirical calibration factor}$$
$$\Omega_{ref} = 10^7 \qquad \text{reference volume [mm}^3\text{]}$$
$$\Omega = \phi/2\left(\phi/2\cos 20° - \phi/2\cos 80°\right)T = 0.1915\phi^2 T \qquad \text{[mm}^3\text{]}$$
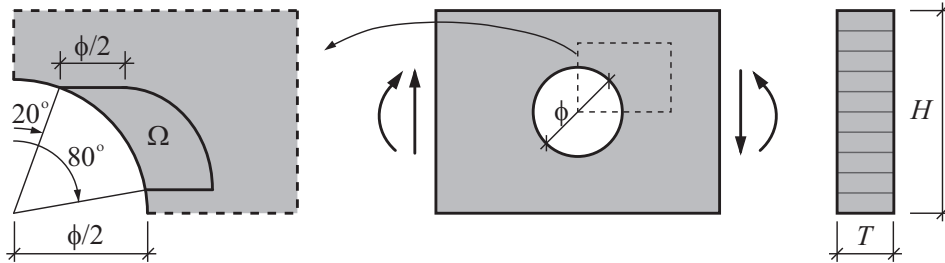
Figure 3.5: *Notations for design according to Höfflin's proposal.*

3.6 Comparison of code design methods

To make a simple comparison of the predicted strengths according to the different methods, influence of four design parameters stated in Section 1.3 are illustrated in Figure 3.6. The comparison is based on a reference beam with cross section $T \times H = 120 \times 450$ mm^2, a circular hole of diameter $\phi = 0.3H$ placed with its center in the neutral axis ($s = 0$) and in a position of bending moment to shear force ratio of $M/(VH) = 1.5$. Characteristic shear strength $f_{v,k} = 3.8$ MPa and characteristic perpendicular to grain tensile strength $f_{t,90,k} = 0.5$ MPa (based on values for GL 32h stated in [27]) are used for the comparison. In the graphs a)-d); one design parameter is varied while the others are kept constant and V/A_{net} refers to the characteristic nominal shear stress at failure. It is worth pointing out that the strong beam size effect suggested by test results, shown in Figure 2.3, is not taken into account in design of glulam beams with holes according to DIN 1052 and method 1 in Limträhandbok.
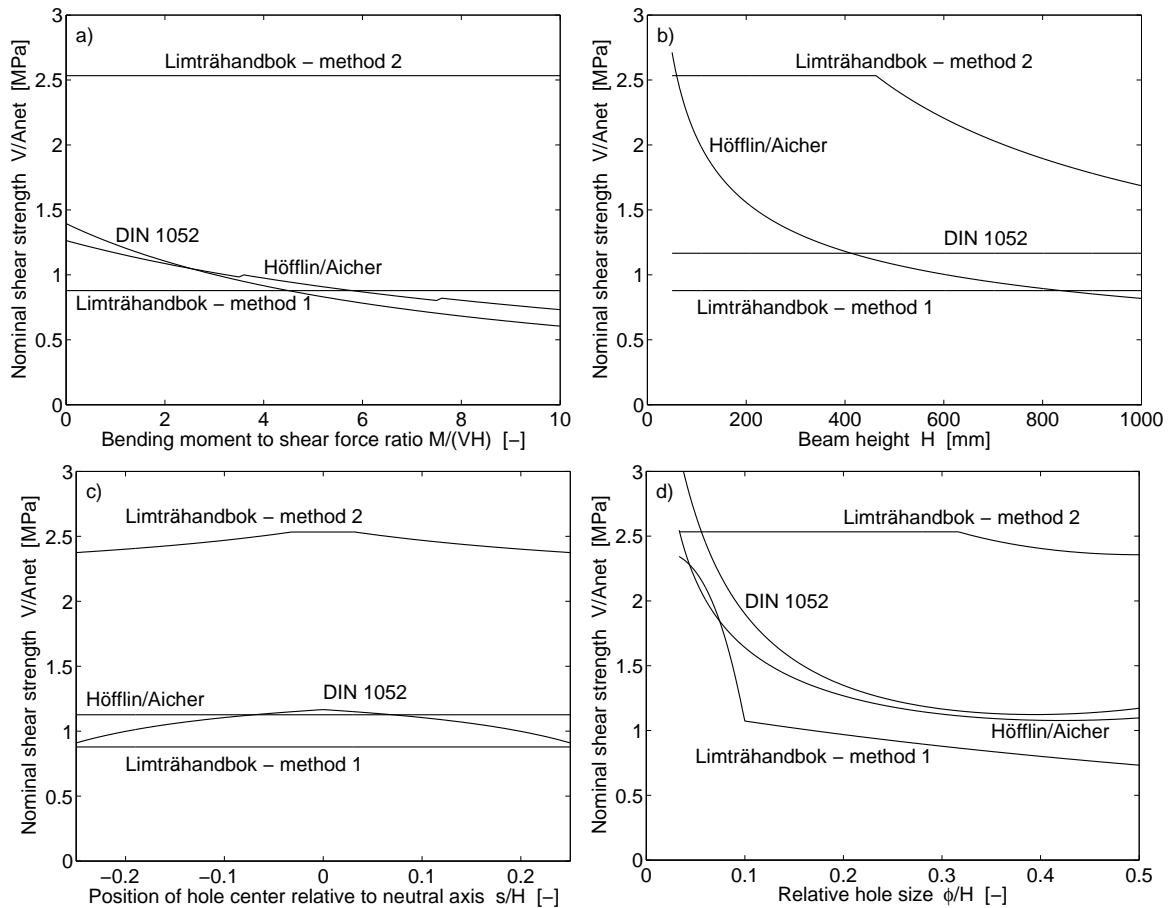
Figure 3.6: *Influence of design parameters a) bending moment to shear force ratio, b) beam size, c) hole placement with respect to neutral axis and d) relative hole size on the characteristic strength of glulam beams with holes according to codes.*

Chapter 4

Weibull weakest link theory

4.1 General

The Weibull weakest link theory [30] enables a probabilistically based approach to strength analysis. This means that the probability of failure at a certain state of stresses for a certain volume of a material can be determined with knowledge of the magnitude and the scatter of the strength of the material. The global strength perpendicular to grain is for wood strongly dependent on the size of the stressed volume, the larger the volume the more likely it is that severe defects are present in the volume and thereby reducing the strength. This makes the theory very useful for timber applications considering the heterogeneity of the material due to annual rings, knots and other defects. The material is assumed to be ideally brittle and since structural failure due to tensile stresses perpendicular to grain or shear stresses parallel to grain commonly has a brittle course (although the material is not ideally brittle) the theory may appear appropriate for analyzing perpendicular to grain tensile failure. A general drawback of the Weibull weakest link theory is that it can not be applied to strength analysis of structural elements with a stress singularity caused for instance by a crack or a sharp corner [11].

The basic assumption in Weibull weakest link theory is, as the name suggests, that global failure occurs when the strength of the weakest link is reached. The theory can be derived considering a system of links loaded in tension and a general body loaded in tension according to Figure 4.1.
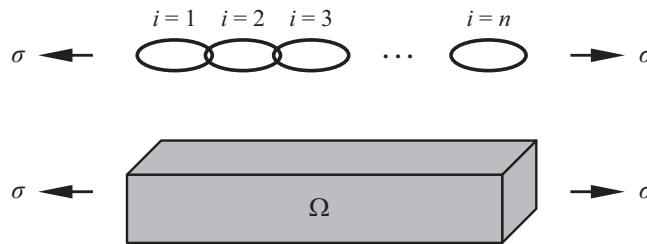
Figure 4.1: *System of n serial coupled links and volume Ω loaded in tension.*

Considering the system of n links coupled in series and loaded by a tensile stress σ, the probability of global survival S is

$$S = S_1 S_2 S_3 ... S_n = e^{\ln S_1 + \ln S_2 + \ln S_3 + ... + \ln S_n} = e^{\sum_{i=1}^{n} \ln S_i} \qquad (4.1)$$

where S_i is the survival probability for link i, which is a function of the stress σ_i. Note that the stress σ_i may be different for different links although the simple illustration in Figure 4.1 suggests equal stress in all links. Assuming statistically equal properties for all links, the survival probability S_i can for all links be expressed as a function $g = g(\sigma_i)$ according to

$$S_i = e^{-g(\sigma_i)} \qquad \text{or} \qquad \ln S_i = -g(\sigma_i) \qquad (4.2)$$

where $g(\sigma_i)$ is a monotonically increasing function, referred to as the *material function*, that defines the strength properties of the link. The global failure probability F of a chain with n links is then found to be

$$F = 1 - S = 1 - e^{\sum_{i=1}^{n} -g(\sigma_i)} \qquad (4.3)$$

Moving from a chain with n links to a body or material volume Ω made up of $n = \Omega/\Delta\Omega$ smaller volumes $\Delta\Omega$ and then letting $\Delta\Omega \to d\Omega$, the probability of global failure is found to be

$$F = 1 - e^{-\int_{\Omega} g(\sigma) \, d\Omega} \qquad (4.4)$$

where there are two suggestions for the material function $g(\sigma)$

$$\text{2-parameter model:} \quad g(\sigma) = \left(\frac{\sigma}{\sigma_0} \right)^m \qquad (4.5)$$

$$\text{3-parameter model:} \quad g(\sigma) = \begin{cases} \left(\dfrac{\sigma - \sigma_u}{\sigma_0} \right)^m & \text{for } \sigma \geq \sigma_u \\ 0 & \text{for } \sigma < \sigma_u \end{cases} \qquad (4.6)$$

where σ is the stress in the body and where σ_0, σ_u and m relate to the magnitude and scatter in the strength of the material. These three parameters are often referred to as the *scale parameter* σ_0, *location parameter* σ_u and *shape parameter* m. The failure probability distribution and density functions for a stress σ in a unit volume $d\Omega$ are illustrated in Figure 4.2 for the 2- and 3-parameter models for some different values of the shape parameter m.
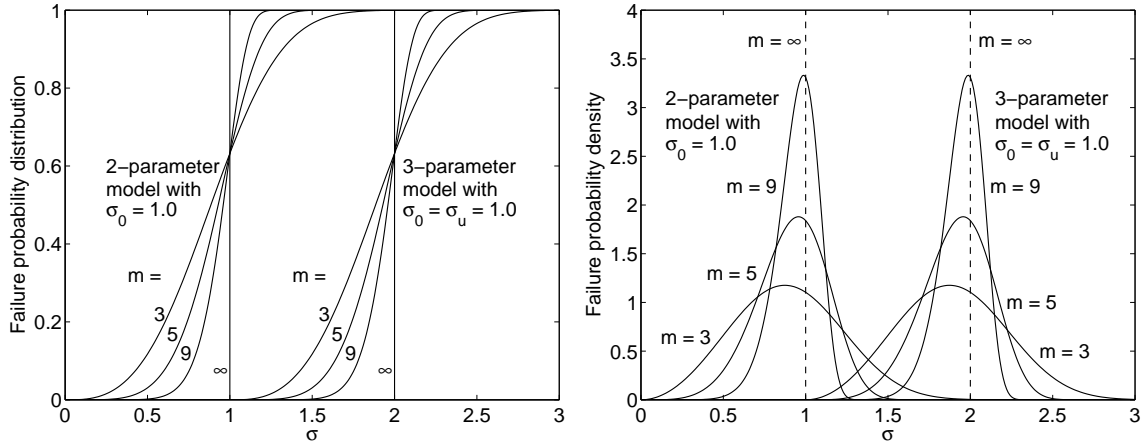
Figure 4.2: *Failure probability distribution* $(F = 1 - e^{-g(\sigma)})$ *and density functions.*

4.2 Volume and stress distribution effects

According to Weibull weakest link theory, there is a volume influence as well as an influence of the heterogeneity of the stress distribution on the probability of global failure. The global strength of a body is not only dependent on the value of the stress in the most stressed point but also on the distribution of stresses and the stressed volume. The influence of volume and stress distribution can be investigated by assuming equal probability of failure for bodies of different volume and/or with different stress distributions. According to Equation (4.4), the condition for equal probability of failure for body 1 with stress σ_1 and body 2 with stress σ_2 is

$$\int_{\Omega_1} g(\sigma_1)\, d\Omega = \int_{\Omega_2} g(\sigma_2)\, d\Omega \qquad (4.7)$$

which for the 2-parameter model according to Equation (4.5) gives

$$\int_{\Omega_1} \left(\frac{\sigma_1(x,y,z)}{\sigma_0} \right)^m d\Omega = \int_{\Omega_2} \left(\frac{\sigma_2(x,y,z)}{\sigma_0} \right)^m d\Omega \qquad (4.8)$$

The volume and stress distribution effects can be established by considering the different cases concerning volume and stress distribution according to Figure 4.3.
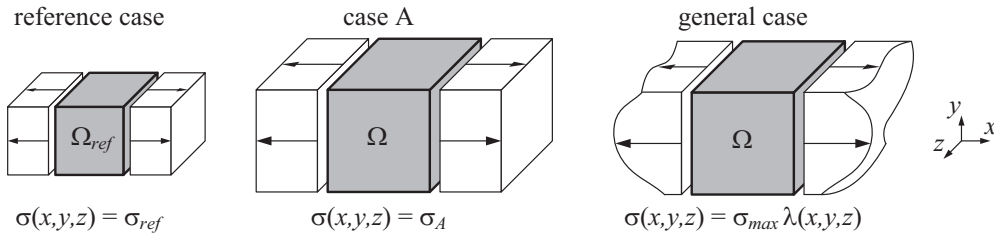
Figure 4.3: *Considered cases for illustration of volume and stress distribution effects.*

In the reference case, a body of volume Ω_{ref} is exposed to a homogeneous stress distribution $\sigma(x, y, z) = \sigma_{ref}$. In case A, a body of volume Ω is exposed to a homogeneous stress distribution $\sigma(x, y, z) = \sigma_A$. In the general case, a body of volume Ω is exposed to a heterogeneous stress distribution $\sigma(x, y, z) = \sigma_{max} \, \lambda(x, y, z)$ where $\lambda(x, y, z) = \sigma(x, y, z)/\sigma_{max}$ and hence $0 \leq \lambda(x, y, z) \leq 1$. Consider now a large number of nominally equal bodies and describing the mean strengths related to the three cases by the mean values of the stress in the most stressed point (σ_{ref}, σ_A and σ_{max}) at failure. These mean strengths are denoted f_{ref}, f_A and f for the reference case, case A and the general case respectively. The influence of volume and heterogeneity in stress distribution on the mean strength can then be derived by assuming equal probability of failure according to Equation (4.8) for two of the cases in Figure 4.3.

Pure volume effect

The influence of stressed volume on the strength is found by comparing the reference case and case A which both have a homogeneous stress distribution but different volumes. The influence of the volume on the strength is found to be

$$f_A \;=\; f_{ref} \left(\frac{\Omega}{\Omega_{ref}} \right)^{-1/m} \tag{4.9}$$

which shows that the theory predicts decreasing strength with increasing volume.

Pure stress distribution effect

The influence of a heterogeneous stress distribution is found by comparing case A and the general case which both have a stressed volume Ω but with different stress distributions. The influence of the heterogeneity in the stress distribution is found to be

$$f \;=\; f_A \left(\frac{1}{\Omega} \int_\Omega \lambda^m(x, y, z) \, d\Omega \right)^{-1/m} \tag{4.10}$$

which shows that the theory predicts increasing strength for increasing heterogeneity in stress distribution since $\lambda(x, y, z) \leq 1$.

Combined volume and stress distribution effect

The combined influence of volume and heterogeneity in stress distribution on the strength is found by comparing the reference case and the general case or inserting Equation (4.9) in Equation (4.10). The combined influence is hence found to be

$$f \;=\; f_{ref} \left(\frac{\Omega}{\Omega_{ref}} \right)^{-1/m} \left(\frac{1}{\Omega} \int_\Omega \lambda^m(x, y, z) \, d\Omega \right)^{-1/m} \tag{4.11}$$

A convenient way of comparing the probability of failure between structural elements with different stress distribution is the so called the Weibull stress (or equivalent Weibull stress or effective Weibull stress). The Weibull stress is a fictive homogeneous stress in the volume Ω that yields the same probability of failure as the the actual heterogeneous state of stress for the volume Ω considered.

$$\sigma_{wei} = \left(\frac{1}{\Omega} \int_{\Omega} \sigma^m(x,y,z) \, d\Omega \right)^{1/m} \tag{4.12}$$

The level of heterogeneity in the stress distribution is often expressed by the distribution factor k_{dis} which is defined as the ratio between the maximum stress in the body σ_{max} and the Weibull stress σ_{wei} according to

$$k_{dis} = \frac{\sigma_{max}}{\sigma_{wei}} = \left(\frac{1}{\Omega} \int_{\Omega} \lambda^m(x,y,z) \, d\Omega \right)^{-1/m} \tag{4.13}$$

where $k_{dis} = 1$ for a homogeneous stress distribution and $k_{dis} > 1$ for all other stress distributions. The distribution factor k_{dis} can be identified as the last parts of Equation (4.10) and of Equation (4.11).

4.3 Interpretations of the material function

Using the expression for the Weibull stress σ_{wei} according to Equation (4.12) and the distribution factor k_{dis} according to Equation (4.13) in Equation (4.11) for the mean strength, the following expression can be obtained

$$\frac{\sigma_{max}}{f} = \left(\frac{1}{\Omega_{ref}} \int_{\Omega} \left(\frac{\sigma(x,y,z)}{f_{ref}} \right)^m d\Omega \right)^{1/m} \tag{4.14}$$

where σ_{max} is the maximum stress in the body of volume Ω, f is the mean of σ_{max} at the instant of failure and f_{ref} is the mean strength valid for a homogeneous stress distribution in the volume Ω_{ref}.

The ratio σ_{max}/f can be interpreted as a *global effective dimensionless stress parameter* α_{global} and $\sigma(x,y,z)/f_{ref}$ as an *effective dimensionless stress field* $\alpha(x,y,z)$ defined in the volume Ω. The expression can then be rewritten as

$$\alpha_{global} = \left(\frac{1}{\Omega_{ref}} \int_{\Omega} \alpha^m(x,y,z) \, d\Omega \right)^{1/m} \tag{4.15}$$

where the value of α_{global} for the effective dimensionless stress field $\alpha(x,y,z)$ in the volume Ω corresponds to equal probability of failure as for the constant value of $\alpha(x,y,z) = \alpha_{global}$ for a homogeneous stress in the volume Ω_{ref}. Since f_{ref} is here defined as the mean strength of the reference volume Ω_{ref}, $\alpha_{global} = 1.0$ will for the volume Ω give the mean failure value of σ_{max}. It is in calculation of the external load that give $\alpha_{global} = 1.0$ convenient that $\sigma(x,y,z)$ and then also $\alpha(x,y,z)$ and α_{global} are proportional to the load.

The effective dimensionless stress field $\alpha(x, y, z)$ may for a multi-axial stress state also be chosen to consider both tensile stresses and shear stresses according to

$$\alpha(x, y, z) = \left(\left(\frac{\sigma(x, y, z)}{f_\sigma} \right)^2 + \left(\frac{\tau(x, y, z)}{f_\tau} \right)^2 \right)^{1/2} \tag{4.16}$$

where $\sigma(x, y, z)$ is the tensile stress, $\tau(x, y, z)$ is the shear stress and f_σ and f_τ are the corresponding mean strengths valid for a volume Ω_{ref}. In the same way as described above, $\alpha_{global} = 1.0$ corresponds to the mean failure stress state since f_σ and f_τ are the mean strengths valid for the reference volume Ω_{ref}.

4.4 Example: Beam in bending

The volume and stress distribution effects predicted by the Weibull weakest link theory can be illustrated by considering a beam according to Figure 4.4. The ratio between the bending moments at the two ends of the beam is $\eta = M_L/M_R$ and $0 \leq \eta \leq 1$. Weibull weakest link theory is applied considering only the tensile stresses perpendicular to grain and assuming a mean perpendicular to grain tensile strength f_σ valid for the volume Ω_{ref}. The global effective dimensionless stress parameter α_{global} according to Equation (4.15) and the mean value of the bending moment at failure $M_{R,failure}$ (obtained for $\alpha_{global} = 1.0$) are then found to be

$$\alpha_{global} = \frac{6M_R}{TH^2 f_\sigma} \left(\frac{LHT}{2\Omega_{ref}} \frac{1}{(m+1)^2} \frac{1 - \eta^{m+1}}{1 - \eta} \right)^{1/m}$$

$$M_{R,failure} = \frac{TH^2 f_\sigma}{6} \left(\frac{LHT}{2\Omega_{ref}} \frac{1}{(m+1)^2} \frac{1 - \eta^{m+1}}{1 - \eta} \right)^{-1/m}$$

Details of the derivation of the above given equations are found in Appendix A. For the case of a constant bending moment M_R along the beam length ($\eta = 1.0$), the expressions are reduced to

$$\alpha_{global} = \frac{6M_R}{TH^2 f_\sigma} \left(\frac{LHT}{2\Omega_{ref}} \frac{1}{m+1} \right)^{1/m}$$

$$M_{R,failure} = \frac{TH^2 f_\sigma}{6} \left(\frac{LHT}{2\Omega_{ref}} \frac{1}{m+1} \right)^{-1/m}$$

For the special case $m \to \infty$, corresponding to conventional deterministic stress analysis, the global effective dimensionless stress parameter α_{global} and the bending moment at failure $M_{R,failure}$ are found to be

$$\alpha_{global} = \frac{6M_R}{TH^2 f_\sigma}$$

$$M_{R,failure} = \frac{TH^2 f_\sigma}{6}$$

irrespective of the value of η. The load bearing capacity is hence determined by the value of the stress in the most stressed point only and independent of the stressed volume and stress distribution.
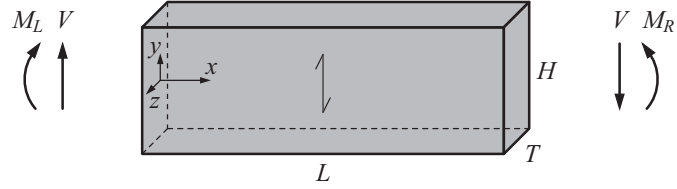
Figure 4.4: *Beam in bending analyzed by Weibull weakest link theory.*

Chapter 5

Fracture mechanics

5.1 Linear elastic fracture mechanics

Linear elastic fracture mechanics (LEFM) deals with analysis of cracks and propagation of cracks. The theory presented in this chapter is based on [3], where fracture mechanics theories for timber applications are presented. LEFM is based on the existence of a crack (or a sharp notch) and the assumption of an ideally linear elastic behavior of the material. A consequence of the assumed material behavior is that stresses at the tip of a crack theoretically are infinite, see Figure 5.1, but this is however accepted in LEFM as long as the fracture process region is small compared to the length of the crack and also compared to the distance to loads and supports. For wood, the fracture process region is approximately one to a few centimeters. Although stresses and strains may be very large in the vicinity of the tip of the crack, the theory of small strains is used.
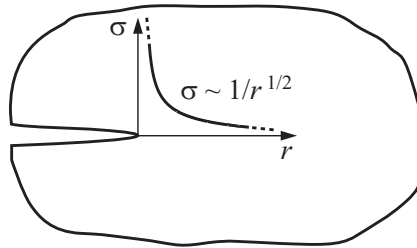
Figure 5.1: *Linear elastic stress distribution at the tip of a crack.*

For a given plane of a crack, there are three possible types of relative displacements which can be referred to as modes of loading. These modes are illustrated in Figure 5.2 where mode I represent fracture due to pure tensile stress perpendicular to the plane of fracture while mode II and mode III represent fracture due to in-plane shear stresses and transverse shear stress respectively. The general case consists of a mixture of the three modes but for most applications, the most common cases are modes I and II. Hence, the term *mixed mode* is often used to refer to a mixture of mode I and mode II only.
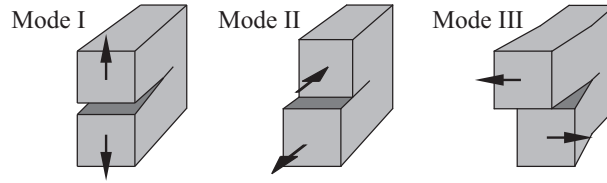
Figure 5.2: *Loading modes I, II and III.*

LEFM can not be used to determine where and when one can expect a crack in a stressed body to arise but it can be used for analysis of whether an existing crack will propagate or not. Crack propagation analysis can be done by considering the energy balance of the system, by considering the so called stress intensity factors or by some similar method.

Energy balance approach

One approach when analyzing crack propagation is to consider the energy balance and how a virtual extension of the crack will effect the energy of the system. The *energy release rate G* (sometimes also called the crack driving force) is defined as the decrease in potential energy U of the system at an infinitely small increase of the crack area A according to

$$ G \;\; = \;\; -\frac{\partial U}{\partial A} \tag{5.1} $$

where the potential energy U of the system consists of elastic strain energy and the potential energy of the loads acting on the structure. The value of the energy release rate G is dependent on the geometry of the structure, the geometry of the crack, the boundary conditions, the applied loads and the stiffness properties of the material. In order to determine whether a crack will propagate or not, the energy release rate G is compared to the *critical energy release rate G_c* (sometimes also called the crack resistance) which is a material property. The general crack propagation criterion can thus be expressed as $G = G_c$, which says that a crack is just about to propagate when the crack driving force equals the crack resistance or in other terms when the energy release rate equals its critical value.

There are three possible crack propagation scenarios; stable, semi-stable and unstable crack growth. Unstable crack growth corresponds to the common case of increasing G with increasing crack area. It is however also possible that G decreases with increasing crack area and if the value of G falls below the critical energy release rate G_c, the crack propagation will stop and the crack growth is termed stable. Semi-stable crack growth corresponds constant G with increasing crack area.

As mentioned earlier, there are three possible modes of loading and the critical energy release rate may have different values for the different modes. It is also possible to separate the energy release rate G into the three modes and obtaining G_I, G_{II} and G_{III}. For an ideal elastic material, the critical energy release rate G_c is equal to the *fracture energy G_f*.

Stress intensity factor approach

Another approach for analysis of crack propagation is to consider the distribution of stresses in the vicinity of the tip of the crack by consideration of the *stress intensity factors* K_I, K_{II} and K_{III}. With coordinate system and stresses according to Figure 5.3, the stress intensity factors are defined as

$$K_I = \lim_{r \to 0} \sigma_{yy}(r)\sqrt{2\pi r} \qquad \text{for } \theta = 0 \tag{5.2}$$

$$K_{II} = \lim_{r \to 0} \tau_{xy}(r)\sqrt{2\pi r} \qquad \text{for } \theta = 0 \tag{5.3}$$

$$K_{III} = \lim_{r \to 0} \tau_{yz}(r)\sqrt{2\pi r} \qquad \text{for } \theta = 0 \tag{5.4}$$
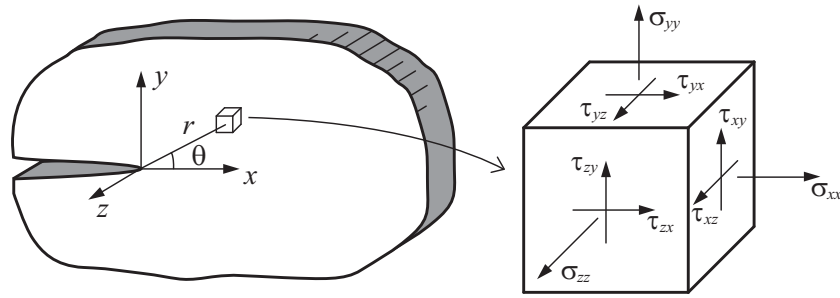
Figure 5.3: *Stresses used in definition of stress intensity factors.*

The values of the stress intensity factors are governed by the geometry of the structure, the geometry of the crack, the boundary conditions and the applied load. The factors are also effected by by possible anisotropic properties of the material. Due to the linear elastic assumption, stresses and thereby also the stress intensity factors are proportional to the applied load. The crack propagation criterion is a comparison of the stress intensity factor K and the *fracture toughness* K_c (also known as critical stress intensity) and can in general terms be expressed as $K = K_c$.

Relation between energy release rate and fracture toughness

The relationship between G and K for mode I and II for an orthotropic material considering a plane state of stress and a fracture plane which is oriented parallel to the direction of grain (x-direction) are given by

$$K_I = \sqrt{E_I G_I} \qquad \text{where} \qquad E_I = \sqrt{\frac{2E_x E_y}{\sqrt{\dfrac{E_x}{E_y}} + \dfrac{E_x}{2G_{xy}} - \nu_{yx}\dfrac{E_x}{E_y}}} \tag{5.5}$$

and

$$K_{II} = \sqrt{E_{II} G_{II}} \qquad \text{where} \qquad E_{II} = \sqrt{\frac{2E_x^2}{\sqrt{\dfrac{E_x}{E_y}} + \dfrac{E_x}{2G_{xy}} - \nu_{yx}\dfrac{E_x}{E_y}}} \tag{5.6}$$

where E_x is the modulus of elasticity parallel to grain, E_y is the modulus of elasticity perpendicular to grain, G_{xy} is the shear modulus and ν_{yx} is Poisson's ratio defined as $\nu_{yx} = -\epsilon_x/\epsilon_y$ for uniaxial loading in the y-direction. Equations (5.5) and (5.5) are found in [3].

5.2   Generalized linear elastic fracture mechanics

The theory concerning LEFM suffers from one obvious limitation: it is based on the assumption of an existing crack or sharp notch giving rise to a square root stress singularity. Conventional stress analysis with a stress based failure criterion is on the other hand not applicable when such a singularity is present. The LEFM-theory can however be modified (generalized) in order to overcome this limitation and make it valid for a general case, with or without a stress singularity. Two different methods, namely the the *initial crack method* and the *mean stress method*, are presented in [3] but here only the latter of the two methods will be dealt with.

The basic idea of the mean stress method is to consider not the stress state in a point of the material but instead the mean stresses acting across a *potential fracture area*. These stresses, which has a finite value also for the case of presence of a stress singularity, are then used in a conventional stress based failure criterion. The size of the potential fracture area is related to the size of the fracture process region at the instant of start of unstable crack growth and is derived in such a way that the method will give the same strength prediction for a body in a homogeneous state of stress as the conventional stress based failure criterion used and also give the same strength prediction as LEFM for a body with a square root stress singularity.

The following section is based on assumptions of a body in plane stress, a fracture plane which coincides with the direction of grain (x-direction) and mixed mode I and mode II loading. Two basic criteria need to be chosen, a conventional stress analysis failure criterion and a LEFM crack propagation criterion. The stress failure criterion can for example be chosen as the criterion of Norris

$$\left(\frac{\sigma}{f_\sigma}\right)^2 + \left(\frac{\tau}{f_\tau}\right)^2 = 1.0 \tag{5.7}$$

where σ is the perpendicular to grain tensile stress, τ is the shear stress and f_σ and f_τ are the corresponding strength values. The LEFM crack propagation criterion can for example be chosen as the criterion of Wu

$$\frac{K_I}{K_{IC}} + \left(\frac{K_{II}}{K_{IIC}}\right)^2 = 1.0 \tag{5.8}$$

where K_I and K_{II} are the mode I and mode II stress intensity factors and K_{IC} and K_{IIC} are the corresponding fracture toughness. Considering now the mean stresses acting across a potential fracture area instead of the stress state in a point, the stress failure criterion is then

$$\left(\frac{\bar{\sigma}}{f_\sigma}\right)^2 + \left(\frac{\bar{\tau}}{f_\tau}\right)^2 = 1.0 \tag{5.9}$$

where $\bar{\sigma}$ and $\bar{\tau}$ are the mean values of the perpendicular to grain tensile stress σ and the shear stress τ in the potential fracture area. Using the definitions of the stress intensity factors according to Equation (5.2) and (5.3), the stresses in front of a crack tip can be expressed as

$$\sigma(x) \;=\; \frac{K_I}{\sqrt{2\pi x}} + ... \tag{5.10}$$

$$\tau(x) \;=\; \frac{K_{II}}{\sqrt{2\pi x}} + ... \tag{5.11}$$

where the first term in these series are dominating for small values of x. The size of the potential fracture area is given by the width T of the plane stress body and a length a_{ms} in the grain direction. Assuming a small length a_{ms} compared to other dimensions in the body, the mean stresses in a potential fracture area starting from the surface of the body can be expressed as

$$\bar{\sigma} \;=\; \frac{1}{a_{ms}} \int_0^{a_{ms}} \sigma(x)\; dx \;=\; \sqrt{\frac{2K_I^2}{\pi a_{ms}}} \tag{5.12}$$

$$\bar{\tau} \;=\; \frac{1}{a_{ms}} \int_0^{a_{ms}} \tau(x)\; dx \;=\; \sqrt{\frac{2K_{II}^2}{\pi a_{ms}}} \tag{5.13}$$

The length a_{ms} is then derived by inserting the expressions for the mean stresses $\bar{\sigma}$ and $\bar{\tau}$ according to Equations (5.12) and (5.13) into Equation (5.9), using Equation (5.8) and introducing the mixed mode ratio $k = K_{II}/K_I = \bar{\tau}/\bar{\sigma}$. The length a_{ms} is then found to be

$$a_{ms} = \frac{2E_I G_{IC}}{\pi f_\sigma^2} \frac{E_x}{E_y} \left(\frac{G_{IIc}}{G_{Ic}}\right)^2 \frac{1}{4k^4} \left(\sqrt{1 + 4k^2 \sqrt{\frac{E_y}{E_x}\frac{G_{Ic}}{G_{IIc}}}} - 1\right)^2 \left(1 + k^2 \frac{f_\sigma^2}{f_\tau^2}\right) \tag{5.14}$$

and depends hence on material properties (stiffness, fracture toughness, shear- and perpendicular to grain tensile strengths) and also the mixed mode ratio k. Determining the length a_{ms} is hence an iterative process where an initial guess of the mixed mode ratio k is needed. The expression can be simplified for pure mode I or pure mode II according to

$$a_{ms} \;=\; \frac{2E_I G_{IC}}{\pi f_\sigma^2} \qquad \text{for pure mode I, } k = 0 \tag{5.15}$$

$$a_{ms} \;=\; \frac{2E_{II} G_{IIC}}{\pi f_\tau^2} \qquad \text{for pure mode II, } k \to \infty \tag{5.16}$$

As mentioned above, the strength prediction of the mean stress method derived here will be the same as when using the conventional stress analysis failure criterion for a body in homogeneous stress and also the same when using the LEFM crack propagation criterion for a deep crack in a large body. Moving from the extreme

of a body in homogeneous stress towards a increasing stress gradient, the influence on the strength prediction of the size, stiffness and fracture toughness of the body increases whereas the influence of the material strength parameters decreases. One can in general expect the mean stress method to give accurate strength predictions only if the length a_{ms} is reasonably small as compared to relevant dimensions of the body analyzed.

5.3   Example: Beam in bending

The mean stress method can be illustrated considering the same beam as in Section 4.4. As shown in Figure 5.4, the beam is exposed to a constant bending moment M along the beam length and the grain direction coincide with the y-direction. For this loading condition, the failure criterion according to Equation (5.9) is reduced to $\bar{\sigma} = f_\sigma$. The mean perpendicular to grain tensile stress $\bar{\sigma}$ acting across a potential fracture area from the bottom and of length a_{ms} in the y-direction and the bending moment at failure $M_{failure}$ (obtained for $\bar{\sigma} = f_\sigma$) are hence

$$\bar{\sigma} = \frac{1}{a_{ms}} \int_{-\frac{H}{2}}^{-\frac{H}{2}+a_{ms}} -\frac{12M}{TH^3}y \ dy = \frac{6M}{TH^2}\left(1 - \frac{a_{ms}}{H}\right)$$

$$M_{failure} = \frac{TH^2 ft}{6} \frac{1}{1 - a_{ms}/H}$$

$$\text{where } a_{ms} = \frac{2E_I G_{Ic}}{\pi f_\sigma^2} \qquad \text{since } k = 0$$

To expect reasonably accurate results of $M_{failure}$, a_{ms} must be significantly less than $H/2$ since there are tensile stress only in the lower half of the beam. For the case of an ideally brittle material ($G_{Ic} = 0$), corresponding to conventional stress analysis, the length of the potential fracture area is zero and the bending moment at failure $M_{failure}$ is hence

$$M_{failure} = \frac{TH^2 ft}{6}$$

which was also found in Section 4.4 for Weibull weakest link theory when $m \to \infty$.
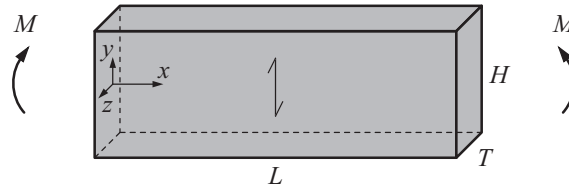
Figure 5.4: *Beam in bending analyzed by mean stress method.*

Chapter 6

A probabilistic fracture mechanics method – PFM

6.1 General

Using Weibull weakest link theory (presented in Chapter 4) means that the heterogeneity of the material is taken into account in a statistical sense by acknowledging stochastic scatter in the strength of the material. The failure is however considered to be ideally brittle due to the assumption that a body will fail as soon as the strength of the weakest point of the body is reached. In linear elastic fracture mechanics and generalized linear elastic fracture mechanics (presented in Chapter 5) on the other hand, fracture ductility is considered but the material is assumed to have deterministic properties meaning that homogeneous material properties are assumed throughout the body. Combining some fracture mechanics theory, taking into account the fracture ductility of the material, and Weibull weakest link theory or some other statistical method, taking into account the stochastic strength of the material, results in something that can be called *probabilistic fracture mechanics*. A proposal for such a method, based on the mean stress method and Weibull weakest link theory, is briefly outlined in [12] and will be further developed here.

The starting point for the description of this probabilistic fracture mechanics method is the reformulation of *Weibull weakest link theory* in Section 4.3. Based on analysis of different volumes and stress distributions with equal probability of failure, the global effective dimensionless stress parameter α_{global} was introduced as

$$\alpha_{global} \quad = \quad \left(\frac{1}{\Omega_{ref}} \int_{\Omega} \alpha^m(x, y, z) \, d\Omega \right)^{1/m} \tag{6.1}$$

where $\alpha(x, y, z)$ is an effective dimensionless stress field, Ω is the considered volume, Ω_{ref} is the reference volume and m is the Weibull shape parameter. The value of α_{global} in the volume Ω corresponds to equal probability of failure as the constant value of $\alpha(x, y, z) = \alpha_{global}$ for a homogeneous stress in the volume Ω_{ref}.

For a body in plane stress and considering both perpendicular to grain tensile stresses and shear stresses, the effective dimensionless stress field can be chosen according to

$$\alpha(x,y) \;=\; \left(\left(\frac{\sigma(x,y)}{f_\sigma} \right)^2 + \left(\frac{\tau(x,y)}{f_\tau} \right)^2 \right)^{1/2} \tag{6.2}$$

where $\sigma(x,y)$ is the perpendicular to grain tensile stress, $\tau(x,y)$ is the shear stress and f_σ and f_τ are the corresponding mean strengths valid for the reference volume Ω_{ref}. Acknowledging the heterogeneity in the material strength in this way, the strength prediction will depend both on the volume and the distribution of the stress fields but the material is still assumed to behave ideally brittle.

In order to account also for the fracture toughness of the material, other choices of the effective dimensionless stress field $\alpha(x,y)$ than stated above can be made. In accordance with the *mean stress method* presented in Section 5.2, it can be useful to consider not the stresses in a point but instead the mean stresses acting across a potential fracture area. Assuming a fracture plane which coincides with the grain direction, the effective dimensionless stress field can be chosen according to

$$\alpha(x,y) \;=\; \left(\left(\frac{\bar{\sigma}(x,y)}{f_\sigma} \right)^2 + \left(\frac{\bar{\tau}(x,y)}{f_\tau} \right)^2 \right)^{1/2} \tag{6.3}$$

where $\bar{\sigma}(x,y)$ and $\bar{\tau}(x,y)$ are the mean values of the perpendicular to grain tensile stress σ and the shear stress τ in the potential fracture area. If the mean stress perpendicular to grain is compressive, the contribution $\bar{\sigma}(x,y)$ is ignored and the effective dimensionless stress field $\alpha(x,y)$ is determined by the mean shear stress $\bar{\tau}(x,y)$ only. The effective dimensionless stress field $\alpha(x,y)$ is hence defined in the entire body and the value in a material point (x,y) is determined by the values of $\sigma(x,y)$ and $\tau(x,y)$ along a potential fracture plane in the grain direction in the vicinity of the material point.

Since f_σ and f_τ are here defined as the mean strengths valid for the reference volume Ω_{ref}, $\alpha_{global} = 1.0$ will for the volume Ω correspond to the mean failure stress state. For example, $\alpha_{global} = 0.5$ in the volume Ω corresponds to the equal probability of failure as the homogeneous dimensionless stress $\alpha(x,y,z) = 0.5$ in the volume Ω_{ref}. Accordingly, to obtain the probability of failure in volume Ω corresponding to $\alpha_{global} = 1.0$ and hence to equal probability of failure for the homogeneous stress $\alpha(x,y,z) = 1$ in Ω_{ref}, the stress in Ω should be doubled.

The physical interpretation of the method is that all points in the body are considered as potentially weak points where fracture initiation may occur. The material is, due to fracture toughness and ductility, assumed to have the ability to distribute stresses over the fracture area and it is hence the mean stresses acting within this area which are considered. In accordance with Weibull weakest link theory, the resistance to fracture is not homogeneous but viewed as a stochastic property. Since fracture may start from any point in the body, all possible points need to be considered.

The strength prediction of the probabilistic fracture mechanics method depends, among other parameters, on the value of the Weibull shape parameter m and the fracture energy parameters G_{Ic} and G_{IIc}. For an ideally brittle material ($G_{Ic} = G_{IIc} = 0$), the method will break down to Weibull weakest link theory. This is also true for a body with a homogeneous stress distribution, since the mean stresses then are equal to the actual stresses. The probabilistic fracture mechanics method will also approach Weibull weakest link theory for increasing size of the considered body since the relative size of the potential fracture area decreases. For a material which is assumed to show fracture ductility ($G_{Ic} \neq 0$ and $G_{IIc} \neq 0$) but where the material properties are assumed to be deterministic ($m \to \infty$), the probabilistic fracture mechanics method will break down to the mean stress method meaning that the potential fracture area with the most severe combined action of $\bar{\sigma}$ and $\bar{\tau}$ will be decisive. For the special case of a a deep crack in a large body, the mean stress method will in turn break down to conventional linear elastic fracture mechanics. For an ideally brittle material with deterministic properties, the strength prediction of the probabilistic fracture mechanics method will be the same as according to conventional stress analysis and the material point with the most severe combined action of σ and τ will be decisive.
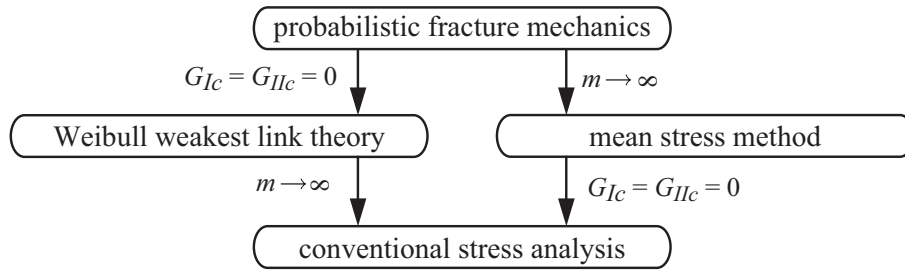
Figure 6.1: *Relation between methods for strength analysis.*

6.2 Size of the potential fracture area

As shown in the previous section, the effective dimensionless stress field $\alpha(x, y)$ depends on the stress fields $\sigma(x, y)$ and $\tau(x, y)$, the corresponding strength values f_σ and f_τ and also on the size of the potential fracture area used for integration of stresses. How to determine the appropriate size of the potential fracture area is however not obvious and there are two separate considerations that need to be taken into account.

According to mean stress method described in Section 5.2, the size of the potential fracture area depends on material properties (stiffness, fracture toughness, shear- and perpendicular to grain tensile strengths) and also the mixed mode ratio $k = \bar{\tau}/\bar{\sigma}$. For the general case with arbitrary stress distributions, the size of the potential fracture area hence depends on the location of the considered material point since the mixed mode ratio k in general varies throughout the body.

There is however also another reason why the size of the potential fracture area depends on the location of the considered point. The expression stated in Equation (5.14) for the length a_{ms} is valid for a potential fracture area starting from the surface of the considered body, which corresponds to interpreting a defect on the surface as a surface crack. The integration of $\alpha(x,y)$ should however be carried out over the entire considered volume meaning that points on the surfaces as well as points in the interior of the body need to be considered.

For a point far from the surfaces, a defect in the material can be interpreted as an interior crack which hence has two tips. In accordance with the mean stress method, the potential fracture area used for determining mean stresses should hence be twice that valid for a surface crack. For points which are not on a surface, but neither far from them, some approximation needs to be made. Aiming for a smooth transition of the size of the potential fracture area when moving from a point on the surface of the material to a point far from the surface, the length of the potential fracture area a_m is in the present implementation determined as expressed mathematically in Equation (6.4) and illustrated in Figure 6.2.

$$a_m(x) = \begin{cases} a_{ms} & \text{for} & 0 \leq x < a_{ms}/2 \\ 2x & \text{for} & a_{ms}/2 \leq x < a_{ms} \\ 2a_{ms} & \text{for} & a_{ms} \leq x \end{cases} \qquad (6.4)$$

Figure 6.2: *Interpretation of length of the potential fracture area for different positions of a material point with respect to a surface at $x = 0$.*

6.3 Example: Beam in bending

The probabilistic fracture mechanics method can be illustrated by considering the same example as in Section 4.4 and Section 5.3 with a constant bending moment M along the beam length according to Figure 6.3. The probabilistic fracture mechanics method is applied assuming a mean perpendicular to grain tensile strength f_σ valid for the volume Ω_{ref}. The global effective dimensionless stress parameter α_{global} according to Equation (6.1) and the mean bending moment at failure $M_{failure}$

(obtained for $\alpha_{global} = 1.0$) are then found to be

$$\alpha_{global} = \frac{6M}{TH^2 f_\sigma} \left(1 - \frac{a_{ms}}{H}\right) \left(\frac{LHT}{2\Omega_{ref}} \left(\frac{a_{ms}}{H} + \frac{1}{m+1} - \frac{1}{m+1}\frac{a_{ms}}{H}\right)\right)^{1/m}$$

$$M_{failure} = \frac{TH^2 f_\sigma}{6} \frac{1}{1 - a_{ms}/H} \left(\frac{LHT}{2\Omega_{ref}} \left(\frac{a_{ms}}{H} + \frac{1}{m+1} - \frac{1}{m+1}\frac{a_{ms}}{H}\right)\right)^{-1/m}$$

$$\text{where } a_{ms} = \frac{2E_I G_{Ic}}{\pi f_\sigma^2} \quad \text{since } k = 0$$

Details of the derivation of the above given equations are found in Appendix A. For an ideally brittle material ($G_{Ic} = 0$), corresponding to Weibull weakest link theory, the length of the potential fracture area is zero and the global effective dimensionless stress parameter α_{global} and the bending moment at failure $M_{failure}$ are hence

$$\alpha_{global} = \frac{6M}{TH^2 f_\sigma} \left(\frac{LHT}{2\Omega_{ref}} \frac{1}{m+1}\right)^{1/m}$$

$$M_{failure} = \frac{TH^2 f_\sigma}{6} \left(\frac{LHT}{2\Omega_{ref}} \frac{1}{m+1}\right)^{-1/m}$$

which are the same expressions as found in Section 4.4 for Weibull weakest link theory. For the case $G_{Ic} \neq 0$ and $m \to \infty$, corresponding to the mean stress method, the bending moment at failure $M_{failure}$ is found to be

$$M_{failure} = \frac{TH^2 f_\sigma}{6} \frac{1}{1 - a_{ms}/H}$$

which is the same expression as found in Section 5.3 for the mean stress method.

For $G_{Ic} = 0$ and $m \to \infty$, the probabilistic method breaks down to conventional deterministic stress analysis and in the same way as Weibull weakest link theory and the mean stress method.
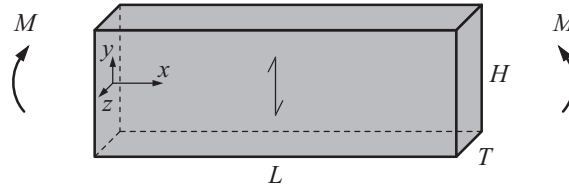

Figure 6.3: *Beam in bending analyzed by probabilistic fracture mechanics method.*

Chapter 7

Implementation of the PFM method

7.1 General

This chapter deals with implementation of the probabilistic fracture mechanics method for glulam beams with holes derived in Chapter 6. Plane stress conditions are assumed to be valid and the combined action of perpendicular to grain tensile stress σ and shear stress τ is assumed to be decisive. The strength is hence determined by the effective dimensionless stress field $\alpha(x,y)$ and the global effective dimensionless stress parameter α_{global} according to

$$\alpha(x,y) = \left(\left(\frac{\bar{\sigma}(x,y)}{f_\sigma} \right)^2 + \left(\frac{\bar{\tau}(x,y)}{f_\tau} \right)^2 \right)^{1/2} \tag{7.1}$$

$$\alpha_{global} = \left(\frac{1}{\Omega_{ref}} \int_\Omega \alpha^m(x,y) \, d\Omega \right)^{1/m} \tag{7.2}$$

where $\bar{\sigma}(x,y)$ and $\bar{\tau}(x,y)$ are the mean stresses and f_σ and f_τ are corresponding mean strengths valid for the reference volume Ω_{ref}. The strength prediction is given by the external loads that corresponds to stress fields $\sigma(x,y)$ and $\tau(x,y)$ which give a global effective dimensionless stress parameter $\alpha_{global} = 1.0$.

The implementation of the method can been seen as being composed of three parts:

1. Determination of stress fields $\sigma(x,y)$ and $\tau(x,y)$ by the finite element method.

2. Determination mean stresses $\bar{\sigma}(x,y)$ and $\bar{\tau}(x,y)$ and the effective dimensionless stress fields $\alpha(x,y)$ according to Equation (7.1).

3. Integration of $\alpha(x,y)$ according to Equation (7.2) to obtain the global effective dimensionless stress parameter α_{global}. Knowing α_{global} for the present magnitude of the loads, the failure load corresponding to $\alpha_{global} = 1$ is easily obtained since α_{global} is proportional to the applied load.

7.2 Finite element stress analysis

The stress fields $\sigma(x, y)$ and $\tau(x, y)$ are determined by 2D plane stress finite element analysis. The entire beam is not modeled but only a part of the beam close to the hole as illustrated in Figure 7.1 where also beam geometry and load parameters are defined. The length $1.5H + 1.5H$ is consistently used for all models. This approach is adopted since it decreases the computational demands and enables an easy way of changing load conditions. Another advantage is that a possible disturbance of the stress fields near beam supports and point loads is avoided. This approach should not influence the results for holes that are placed reasonable far from the supports and point loads since the high perpendicular to grain tensile stresses, which are believed to be the most decisive for the strength, are limited to the close vicinity of the hole. The shear forces V and the bending moments M_L and M_R are applied as parabolic shear stress distributions and linear normal stress distributions respectively.

An orthotropic and linear elastic material model is used for the finite element stress analysis. With this model, material directions are only distinguished as parallel and perpendicular to grain. The influence of a possible uneven stress distribution in the beam width direction due to the difference in stiffness between radial and tangential direction with respect to annual rings is hence ignored. The values of the modulus of elasticity parallel to grain $E_{xx} = 13700$ MPa and the shear modulus $G_{xy} = 850$ MPa are based on mean values stated in [27] for strength class GL 32h. The value for the modulus of elasticity perpendicular to grain $E_{yy} = 460$ MPa is based on the commonly used relation $E_{yy} \approx E_{xx}/30$. Poisson's ratio (defined as $\nu_{xy} = -\epsilon_{yy}/\epsilon_{xx}$ for uniaxial loading in the x-direction) is set to $\nu_{xy} = 0.35$. The stress-strain relationship can be expressed in matrix notation according to Equation (7.3). The stress component σ_{yy} is the perpendicular to grain normal stress component which in this thesis in general is referred to as σ (without index).

$$
\begin{bmatrix} \epsilon_{xx} \\ \epsilon_{yy} \\ \gamma_{xy} \end{bmatrix} = \begin{bmatrix} 1/E_{xx} & -\nu_{xy}/E_{xx} & 0 \\ -\nu_{xy}/E_{xx} & 1/E_{yy} & 0 \\ 0 & 0 & 1/G_{xy} \end{bmatrix} \begin{bmatrix} \sigma_{xx} \\ \sigma_{yy} \\ \tau_{xy} \end{bmatrix} \tag{7.3}
$$

The commercial software ABAQUS is used for the finite element stress analysis. 8-node plane stress quadrilateral elements with biquadratic displacement interpolation and reduced integration (denoted CPS8R in ABAQUS) are used throughout. Dynamic and geometrical non-linear effects are not included in the analysis.

Due to the geometry, there are high stress gradients around the hole. In general that means a fine mesh is needed to be able describe the stress field accurately. This problem is however less pronounced since the mean stresses within a certain area are considered. The maximum element size in the regions with a high stress gradient should however be considerably smaller than the size of the potential fracture area used to determine the mean stresses. A typical finite element mesh used for the stress analysis is shown in Figure 7.2. The side length of the elements is typically about $H/600$ at the hole. The number of elements and degrees of freedom are typically 90 000 and 500 000, respectively.
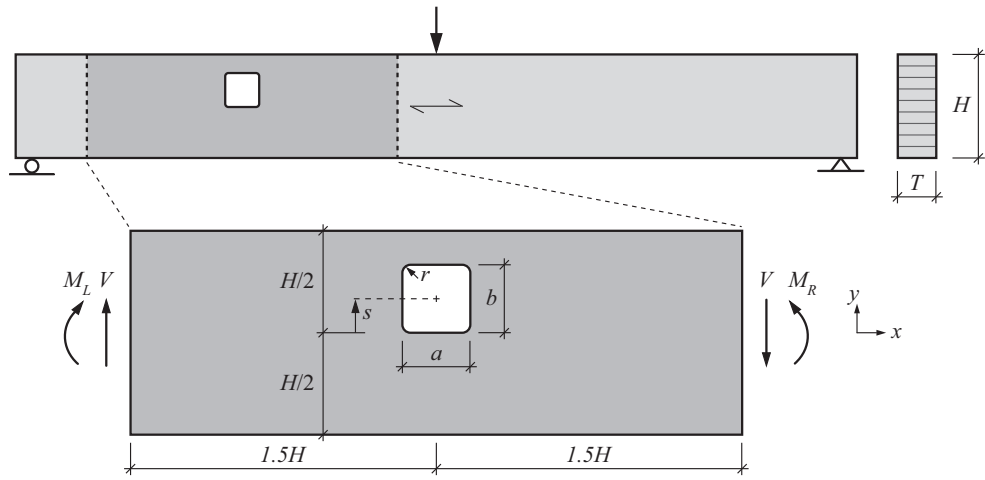
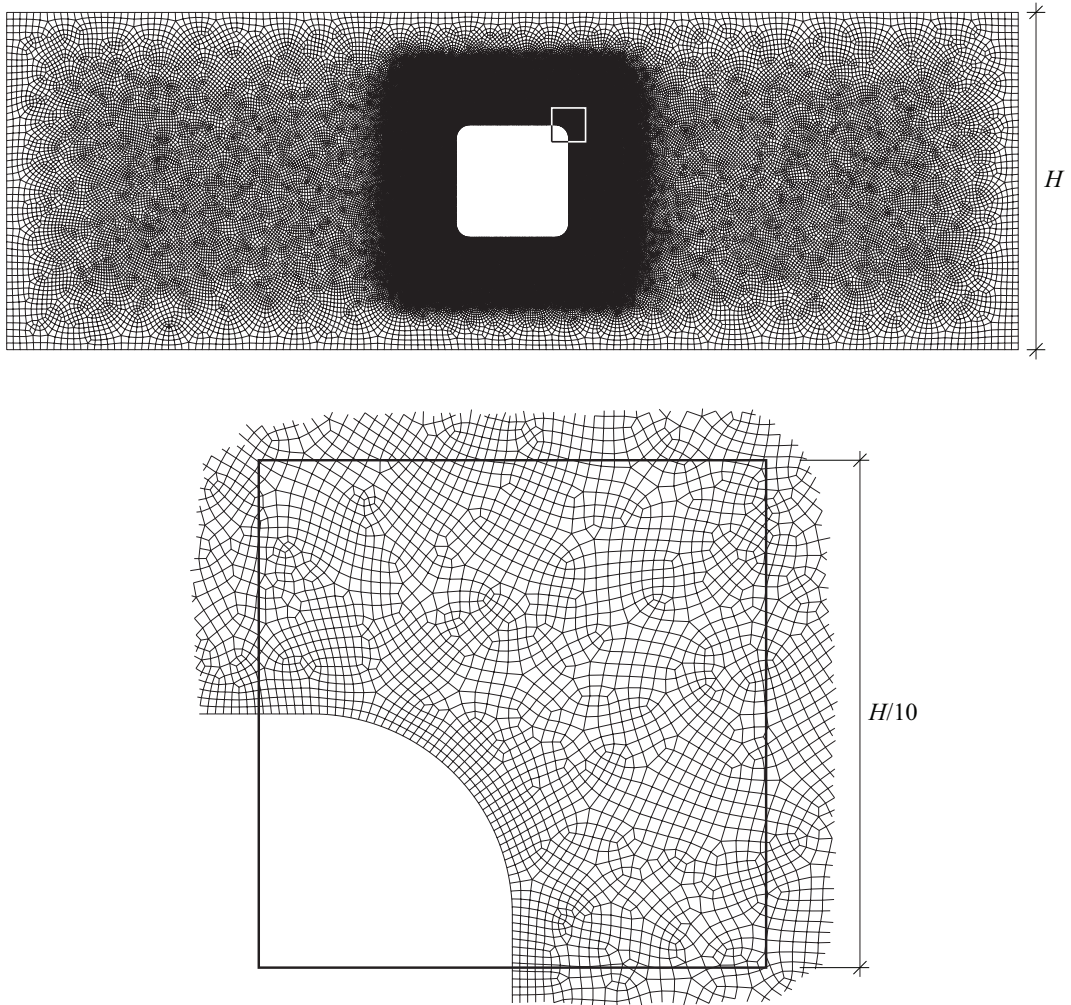Figure 7.1: *Geometry and load parameters for considered part of beam.*

Figure 7.2: *Typical finite element mesh used for the stress analysis.*

7.3   Determination of mean stresses

Once the stress fields $\sigma(x,y)$ and $\tau(x,y)$ are determined by finite element stress analysis in Abaqus, the next steps are to determine the mean stresses $\bar{\sigma}(x,y)$ and $\bar{\tau}(x,y)$, the effective dimensionless stress field $\alpha(x,y)$ and $\alpha^m(x,y)$. These parts, and the also the rest of the implementation, are performed in Matlab.

The output from the finite element stress analysis is taken as the stresses σ and τ in the nodal points of the elements. These stresses are then interpolated at *reference points* in an evenly distributed grid in the body using Matlab build in function `griddata`. The distance between the reference points is equal in x- and y-directions and is denoted a_{rp}. The mean stresses $\bar{\sigma}$ and $\bar{\tau}$ are determined at all reference points by numerical integration of the stresses within the potential fracture area a_m associated with the specific reference point. The effective dimensionless stress field $\alpha(x,y)$ is determined at the reference points according to Equation (7.1).

The considered beam volume $\Omega = LHT$ for the stress parameters $\bar{\sigma}$, $\bar{\tau}$ and α is smaller than the volume used for the finite element stress analysis, see Figure 7.3. The reason for this is that the mean stresses in an interior material point of the body represent stress of both sides of the material point in the x-direction. Hence, the volume where $\bar{\sigma}$, $\bar{\tau}$ and α are determined must be somewhat smaller than the volume where the stresses σ and τ are determined.

An illustration of the grid of reference points is also shown in Figure 7.3. This grid is very coarse compared to the actual grid used in order make the illustration clearer. For the numerical calculations presented in Chapter 8, the length of the volume for determining the mean stresses is $L = 0.75H + 0.75H$ and the distance between the evenly distributed reference points is $a_{rp} = H/1000$.
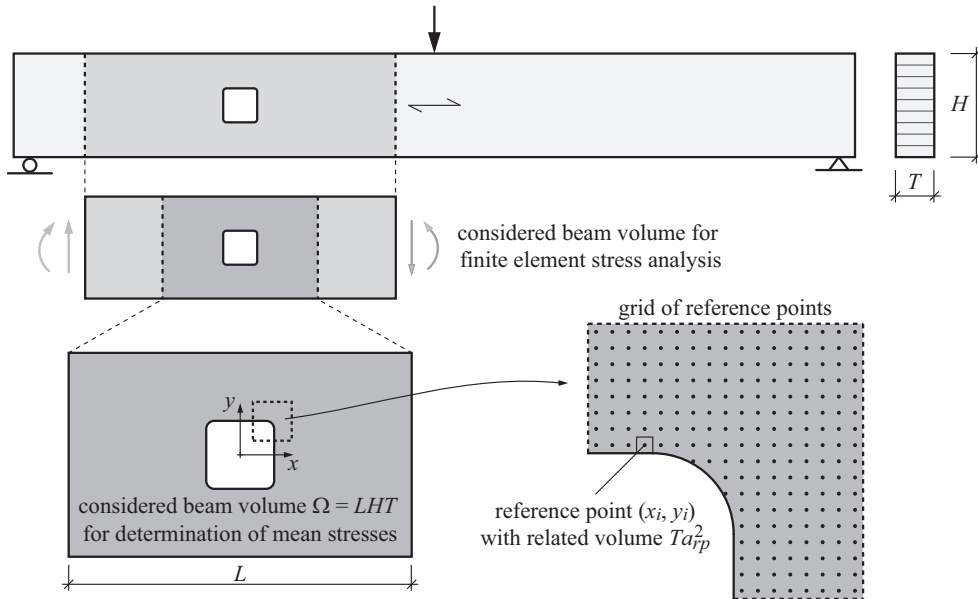
Figure 7.3: *Considered volume Ω for $\bar{\sigma}$, $\bar{\tau}$, α and grid of reference points.*

The size of the potential fracture a_m depends on the mixed mode ratio $k = \bar{\tau}/\bar{\sigma}$ and determining the mean stresses is hence an iterative process where an initial guess of the mixed mode ratio is needed. In this implementation, this iteration is however ignored and the mixed mode ratio is assumed to be determined with sufficient accuracy by the ratio between the stresses in the considered reference point $k = \tau/\sigma$.

Apart from the elastic stiffness properties previously stated, the material properties needed to determine $\bar{\sigma}$, $\bar{\tau}$ and α are based on values stated in [3]. These are the perpendicular to grain tensile strength $f_\sigma = 3.0$ MPa, the shear strength $f_\tau = 9.0$ MPa and the fracture energies $G_{Ic} = 0.300$ Nmm/mm^2 and $G_{IIc} = 1.050$ Nmm/mm^2.

An illustration of typical distributions of σ, τ, α and α^m in the vicinity of a hole is shown in Figure 7.4. The length of the potential fracture area a_m, the perpendicular to grain tensile stress σ, the shear stress τ and the corresponding mean stresses $\bar{\sigma}$ and $\bar{\tau}$ along a line of reference points are shown in Figure 7.5. Both figures are based on the beam geometry and the load given in Figure 7.5.

Figure 7.4: *Distributions of σ, τ, α and α^m in vicinity of a hole.*

Figure 7.5: *Geometry and line of reference points considered in this illustration, length of potential fracture area a_m, perpendicular to grain stress and shear stress.*

7.4 Stress integration and strength prediction

The strength prediction according to the probabilistic fracture mechanics method is implicitly given by the value of the global effective dimensionless stre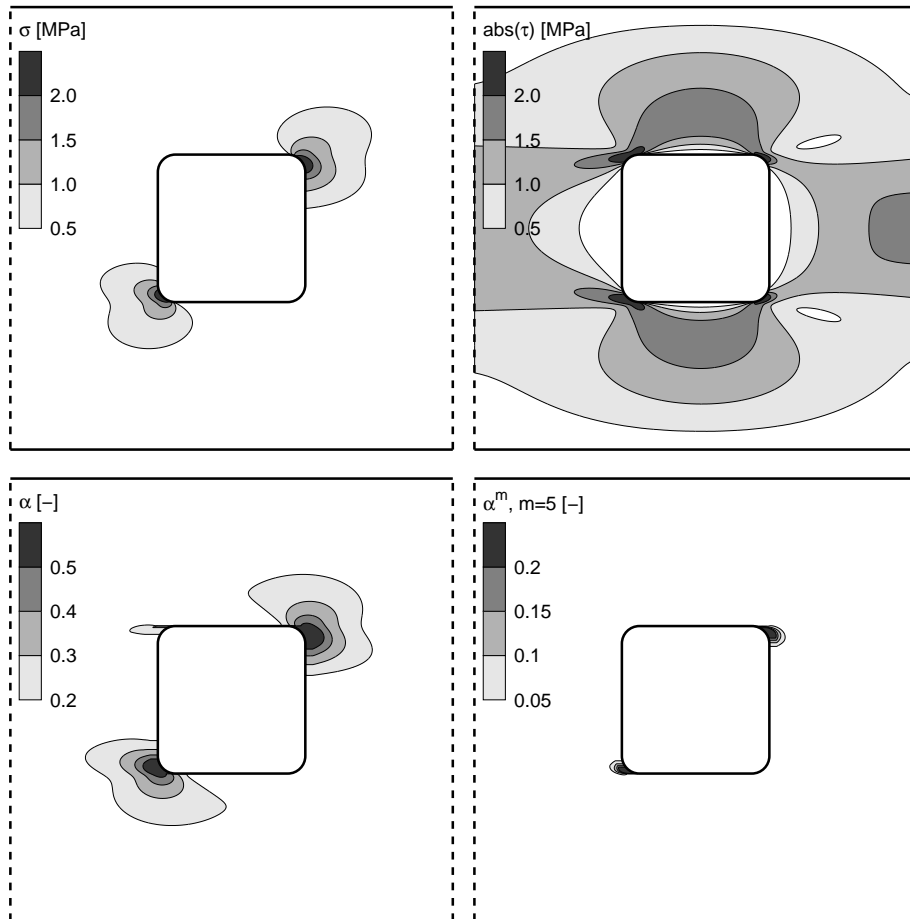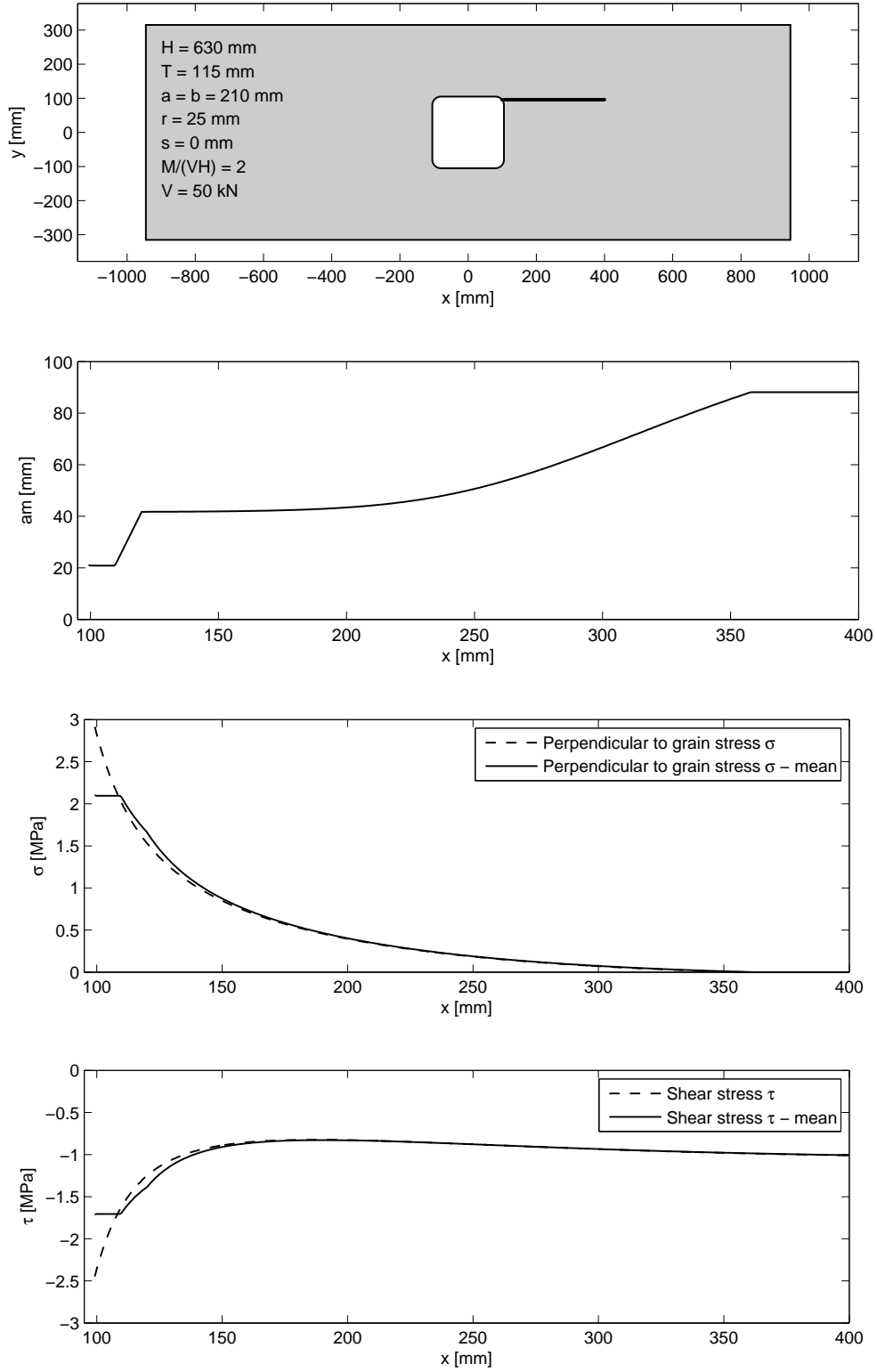ss parameter α_{global}. To obtain this value, the effective dimensionless stress field $\alpha(x, y)$ should be integrated according to Equation (7.2). This integration is carried out numerically according to

$$\alpha_{global} = \left(\frac{Ta_{rp}^2}{\Omega_{ref}} \sum_{i=1}^{n} \alpha^m(x_i, y_i) \right)^{1/m} \tag{7.4}$$

where Ω_{ref} is the reference volume, T is the beam width, a_{rp} is the distance between the reference points, n is the number of reference points in the considered volume Ω, $\alpha(x_i, y_i)$ is the value of the effective dimensionless stress field at reference point i and m is the Weibull shape parameter. The volume Ta_{rp}^2 is the volume related to each reference point.

The strength prediction according to the probabilistic fracture mechanics method is given by $\alpha_{global} = 1.0$. This strength prediction corresponds to the same probability of failure as a body of the reference volume Ω_{ref} in homogeneous stress σ and τ according to

$$\left(\frac{\sigma}{f_\sigma} \right)^2 + \left(\frac{\tau}{f_\tau} \right)^2 = 1.0 \tag{7.5}$$

and since f_σ and f_τ in the present calculations are defined as the mean strengths valid for the reference volume Ω_{ref}, the criterion $\alpha_{global} = 1.0$ hence gives the mean global failure load.

Since the relation between the applied load and α_{global} is linear, the strength prediction according to the probabilistic fracture mechanics method in terms of shear force at failure $V_{failure}$ is given by

$$V_{failure} = \frac{1}{\alpha_{global}} V_{FE} \tag{7.6}$$

where V_{FE} is the shear force applied in the finite element stress analysis and α_{global} is the value obtained from Equation (7.4) for this applied shear force.

In addition to the previously stated material properties, the Weibull shape parameter m and the reference volume Ω_{ref} are needed to determine α_{global}. These parameters are set to $m = 5$ and $\Omega_{ref} = 31250$ mm^3. These values relate to experimental tests of the strength for homogeneous tensile stress perpendicular to grain. The reference volume is determined from the empirical relation $f_\sigma/f_0 = 1.5(\Omega_{ref}/\Omega_0)^{-0.2}$ where $f_0 = 1.0$ MPa and $\Omega_0 = 10^6$ mm^3 which is found in [14]. The value of the Weibull shape parameter corresponds to the volume influence in this empirical relation and also to about 23 % coefficient of variation in strength.

As described in Chapter 6, the probabilistic fracture mechanics method will break down to other methods for strength analysis depending on the choice of material properties. The following methods will be used for comparison of the results of the probabilistic fracture mechanics (PFM) method:

Weibull weakest link theory with $\alpha = ((\sigma/f_\sigma)^2 + (\tau/f_\tau)^2)^{1/2}$
denoted WEI$\sigma\tau$

Weibull weakest link theory with $\alpha = \sigma/f_\sigma$
denoted WEIσ

Mean stress method with failure criterion $(\bar{\sigma}/f_\sigma)^2 + (\bar{\tau}/f_\tau)^2 = 1.0$
denoted MSM

Conventional stress analysis with failure criterion $(\sigma/f_\sigma)^2 + (\tau/f_\tau)^2 = 1.0$
denoted CSA$\sigma\tau$

Conventional stress analysis with failure criterion $\sigma/f_\sigma = 1.0$
denoted CSAσ

Two possible sources of reduced numerical accuracy introduced in the implementation are the length L of the beam volume Ω considered for integration of stresses and the reference point grid density given by a_{rp}. The influence of these implementation parameters is shown in Figure 7.6. The length L has obviously no influence on the conventional stress analysis methods and the mean stress method since the highest stresses are at the very vicinity of the hole. This example indicates that there is some influence, although rather small, on the predicted strength according to the probabilistic fracture mechanics method and the Weibull weakest link theory considering both σ and τ. The grid density of the reference points has a very small influence on the strength prediction according to the probabilistic fracture mechanics method as long as $a_{rp} < 3H/1000$. As expected, strength predictions according to the conventional stress analysis methods are much more influenced by the grid density. The values $L = 1.5H$ and $a_{rp} = H/1000$ are used in Chapter 8.
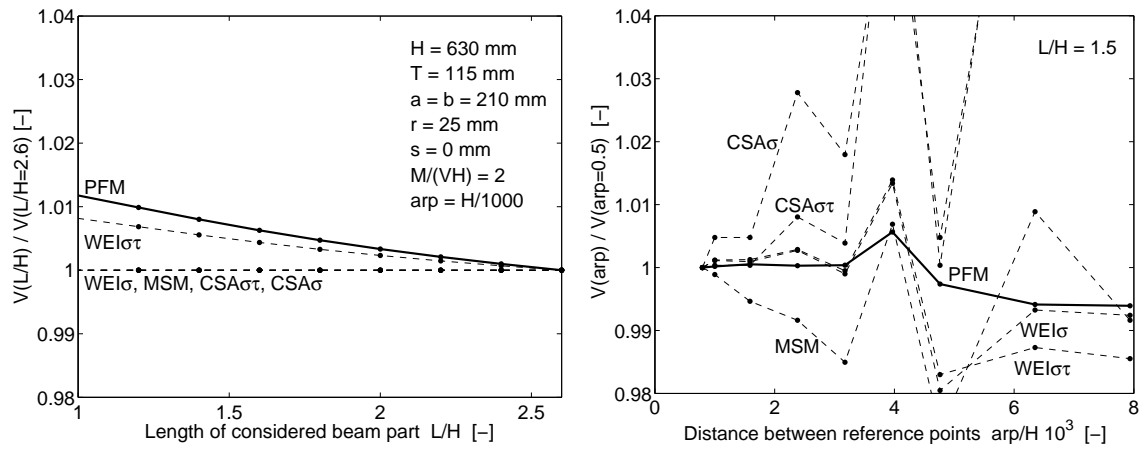
Figure 7.6: *Influence of considered beam length and reference point grid density.*

7.5 Influence of fracture energy and Weibull shape parameter

The influence of the fracture energies G_{Ic} and G_{IIc} and the Weibull shape parameter m on the strength is illustrated in Figure 7.7. The illustration is based on beams with quadratic holes. The beams are of height $H = 180$ mm for the graphs to the left and $H = 630$ mm for the graphs to the right and $T = 115$ mm, $a = b = H/3$, $s = 0$, $M/(VH) = 2$ for both beam heights. Implementation parameters $a_{rp} = H/1000$ and $L = 1.5H$ are used. The graphs are based on the constant ratio $G_{IIc}/G_{Ic} = 3.5$. Material properties other than the ones illustrated in the figures are as previously stated and summarized in Table 8.1.

As discussed above, the probabilistic fracture mechanics breaks down to either the mean stress method, Weibull weakest link theory or conventional stress analysis depending on the choice of the fracture energies and the Weibull shape parameter. It can be noted that the influence of m is not monotonic for a beam with a hole. Peak strength is predicted for intermediate values of m. For a beam without a hole and in pure bending, the influence of m and G_{Ic} is given in Figure 7.9.
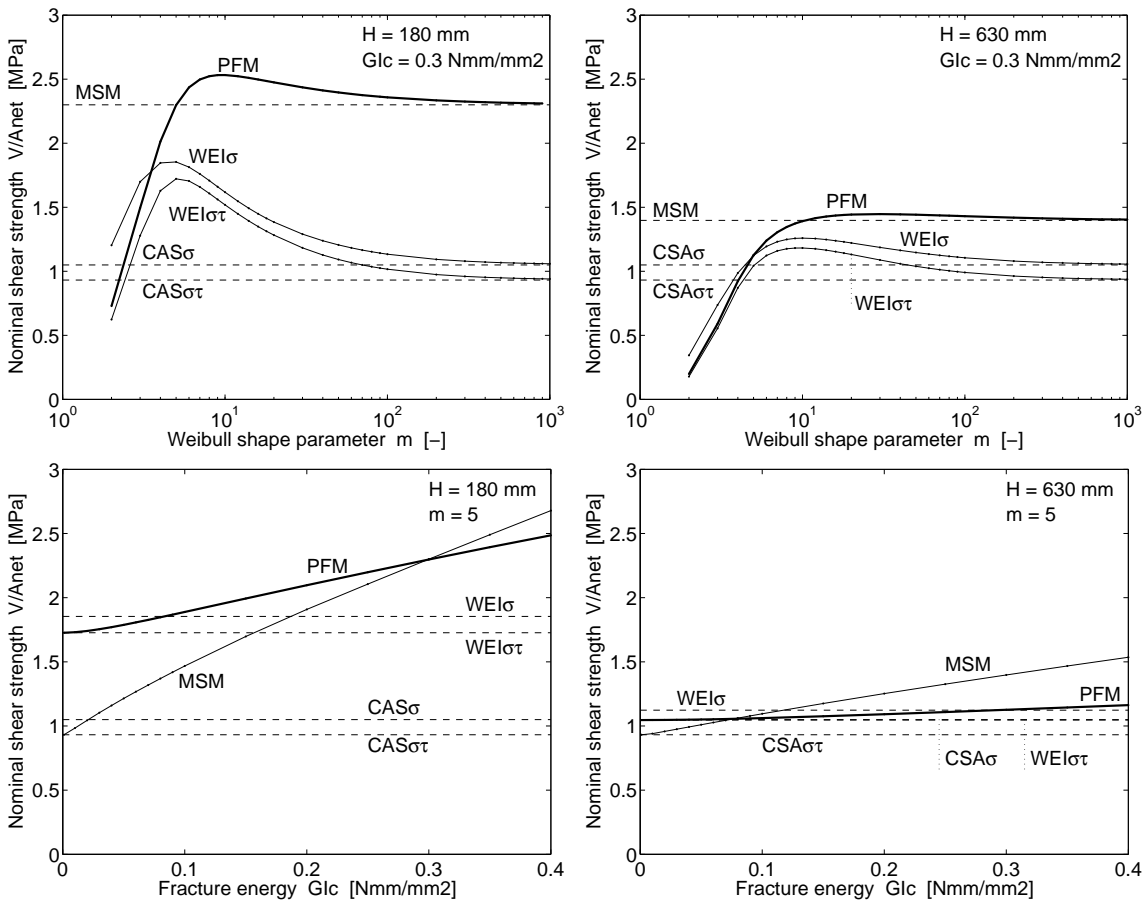
Figure 7.7: *Influence of Weibull shape parameter m and fracture energy G_{Ic}.*

7.6 Verification: Beam in bending

In order to verify the implementation of the probabilistic fracture mechanics method, the method is applied to a beam in bending according to Figure 7.8. The analytical solutions for this example according the different methods for strength analysis are given in Section 4.4, Section 5.3 and Section 6.3. The verification is based on a beam of dimension $L = 2H = 2T = 200$ mm with a constant bending moment M along the beam length. Material properties other than the ones illustrated in the figures are as previously stated and summarized in Table 8.1. Applying a pure bending moment gives a mixed mode ratio $k = 0$ and with the given material properties the length of the potential fracture area is $a_{ms} \approx 21$ mm.

The strength prediction according to the analytical solutions (dashed and solid lines) and the numerical solutions (marks) are for different values of m and G_{Ic} shown in Figure 7.9 for the different methods for strength analysis. The numerical implementation of the probabilistic fracture mechanics method gives almost exactly the same results as the analytical solution.
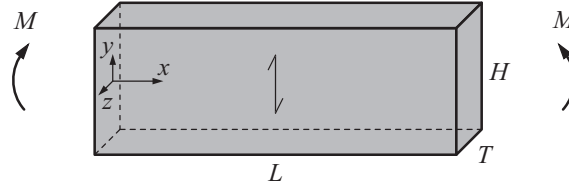
Figure 7.8: *Beam in bending used for verification of the implementation of the probabilistic fracture mechanics method.*
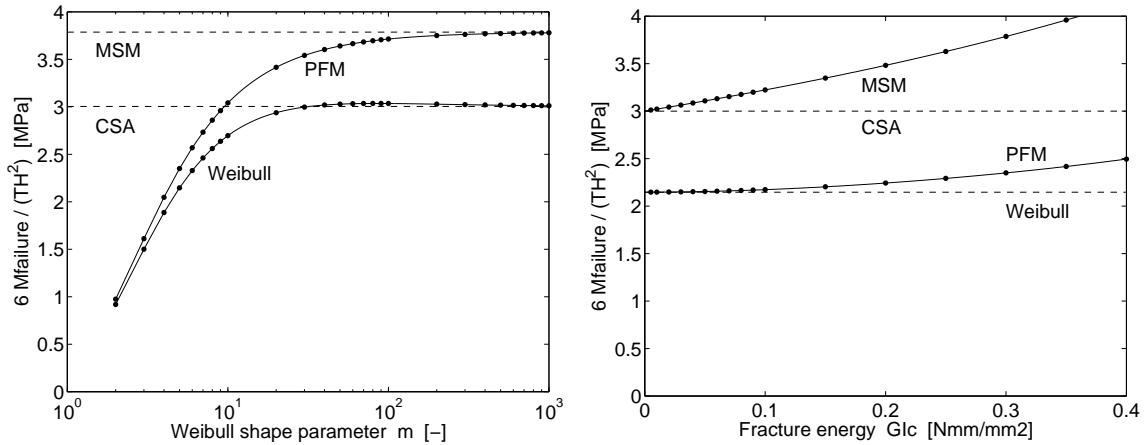
Figure 7.9: *Predicted strength $6M_{failure}/(TH^2)$ for different methods and different choices of Weibull shape parameter m and fracture energy G_{Ic}.*

Chapter 8

Parameter study and verification

8.1 General

The parameter study concerns application of the probabilistic fracture mechanics method on glulam beams with holes. The study comprises the four design parameters *bending moment to shear force ratio*, *beam size*, *hole placement with respect to beam height* and *relative hole size with respect to beam height*. The influence of these design parameters on the strength is illustrated graphically for beams with circular or quadratic holes with rounded corners. A circular hole can formally be regarded as a quadratic hole with corner radius ratio $r/a = r/b = 0.5$. In addition to the circular holes and the quadratic hole with rounded corners, a quadratic hole with sharp corners ($r = 0$) was also analyzed.

The strength according to the probabilistic fracture mechanics method is also compared to experimental test results and other methods for strength analysis.

The length of the considered volume Ω where $\bar{\sigma}$, $\bar{\tau}$ and α are determined is $L = 1.5H$ and the distance between the evenly distributed reference points is $a_{rp} = H/1000$. The material properties used for the parameter study and verification are summarized in Table 8.1.

Table 8.1: *Material properties related to stiffness, strength and fracture energy.*

Modulus of elasticity parallel to grain	E_{xx}	13 700	MPa
Modulus of elasticity perpendicular to grain	E_{yy}	460	MPa
Shear Modulus	G_{xy}	850	MPa
Poisson's ratio	ν_{xy}	0.35	-
Perpendicular to grain tensile strength	f_σ	3.0	MPa
Shear strength	f_τ	9.0	MPa
Fracture energy mode I	G_{Ic}	0.300	Nmm/mm^2
Fracture energy mode II	G_{IIc}	1.050	Nmm/mm^2
Reference volume	Ω_{ref}	31250	mm^3
Weibull shape parameter	m	5	-

8.2 Parameter study

The relative influence of the four design parameters on the strength is illustrated in Figure 8.1 for quadratic holes and in Figure 8.2 for circular holes. The illustrations are based on a reference beam according to the figures. For each of the four graphs in the respective figures, one of the design parameters is varied while the others are constant. The nominal shear strength V/A_{net} is 1.35 MPa for the reference beam with a circular hole ($r/\phi = 0.5$), 1.16 MPa for the reference beam with a quadratic hole and rounded corners ($r/a = r/b \approx 0.14$) and 1.14 MPa for a corresponding quadratic hole with sharp corners ($r = 0$).

The influence of hole placement with respect to beam height is illustrated in Figure 8.3 for different bending moment to shear force ratios and in Figure 8.4 for different beam sizes. The influence of relative hole size is illustrated in Figure 8.5 for different bending moment to shear force ratios and in Figure 8.6 for different beam sizes. Stress distributions for some geometries are illustrated in Figures 8.7-8.10. Some comments concerning the design parameters are given below.

Bending moment to shear force ratio
The influence of bending moment to shear force ratio is comparatively small for holes centrically placed with respect to beam height. This agrees well with the overall behavior found in the experimental tests, see Figure 2.2.

Beam size
The beam size seems to be the most influential parameter out of the four investigated design parameters. The method predicts a strong beam size influence on the strength which was also found in the experimental tests, see Figure 2.3.

Hole placement with respect to beam height
Concerning hole placement with respect to beam height, the influence on the strength is rather complex. For holes placed in position where $M/(VH) = 0$, the strength is greater for eccentrically placed holes than for centrically placed holes. For larger bending moment to shear force ratios, the strength is however considerably lower for the eccentrically placed holes compared to the centrically placed ones. The study comprises only one hole size ($0.30H$) for the eccentrically placed holes. The general behavior shows reasonable agreement with available test results, see Figure 2.4

Relative hole size with respect to beam height
The nominal shear strength decreases with increasing relative hole size. In general, the method suggests greater strength for a beam with a circular hole compared to a beam with a quadratic hole for $a = b = \phi$. The strength reduction for increasing hole size is further greater for the quadratic holes than for the circular holes. Increasing the holes size from $\phi = a = b = 0.20H$ to $0.40H$, the nominal shear strength is reduced by about 25 % for the quadratic holes and about 15 % for the circular holes. The findings seem reasonable compared to experimental test results, see Figure 2.5.
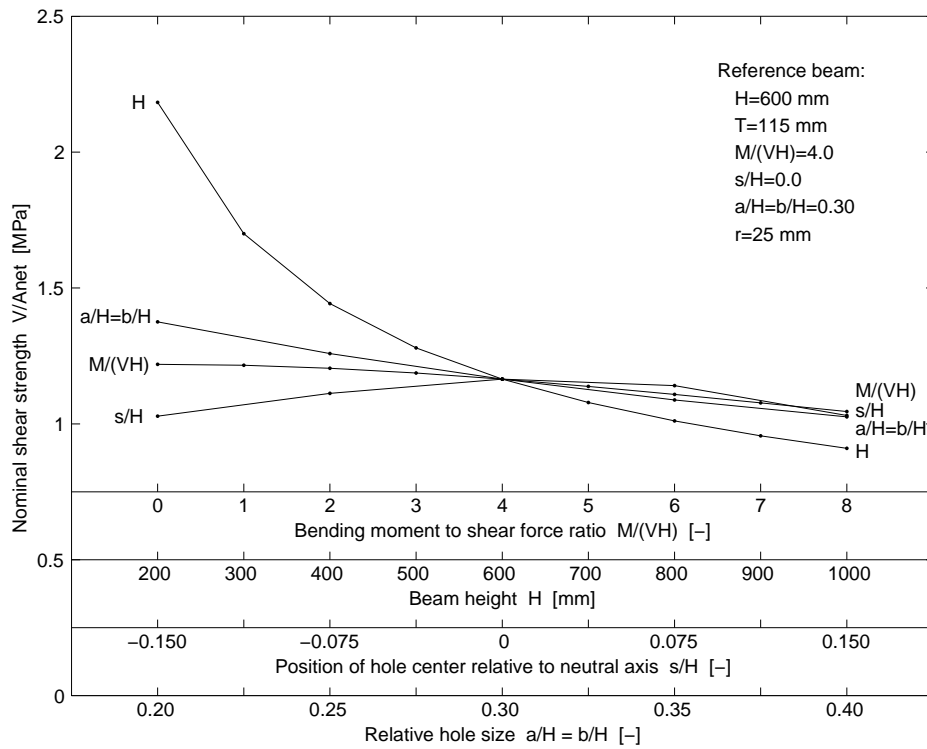
Figure 8.1: *Influence of design parameters for a beam with a quadratic hole.*
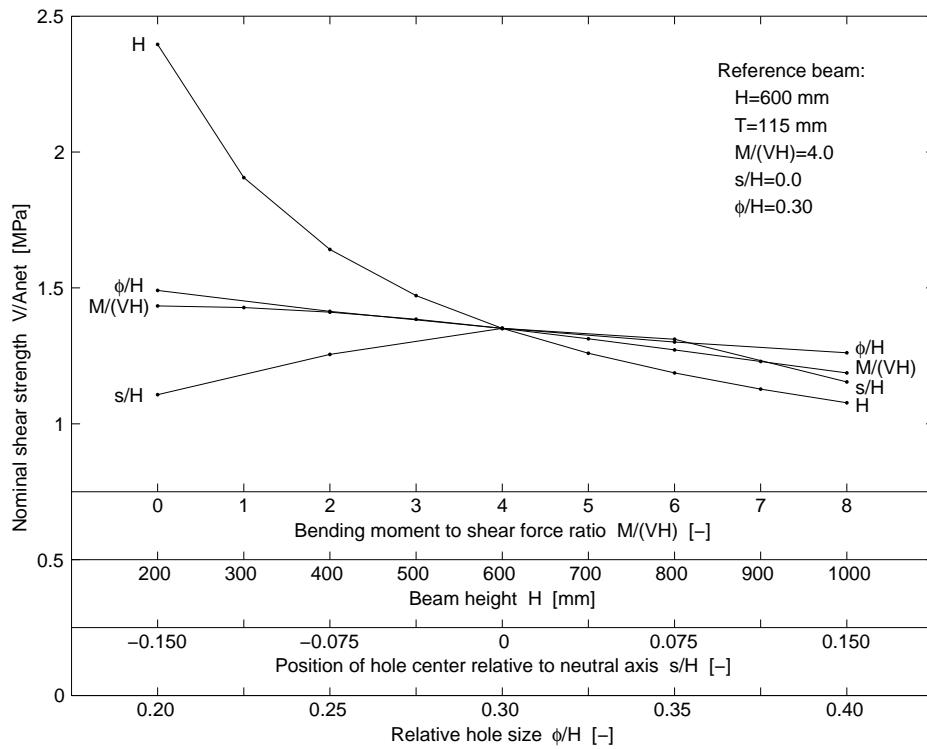
Figure 8.2: *Influence of design parameters for a beam with a circular hole.*
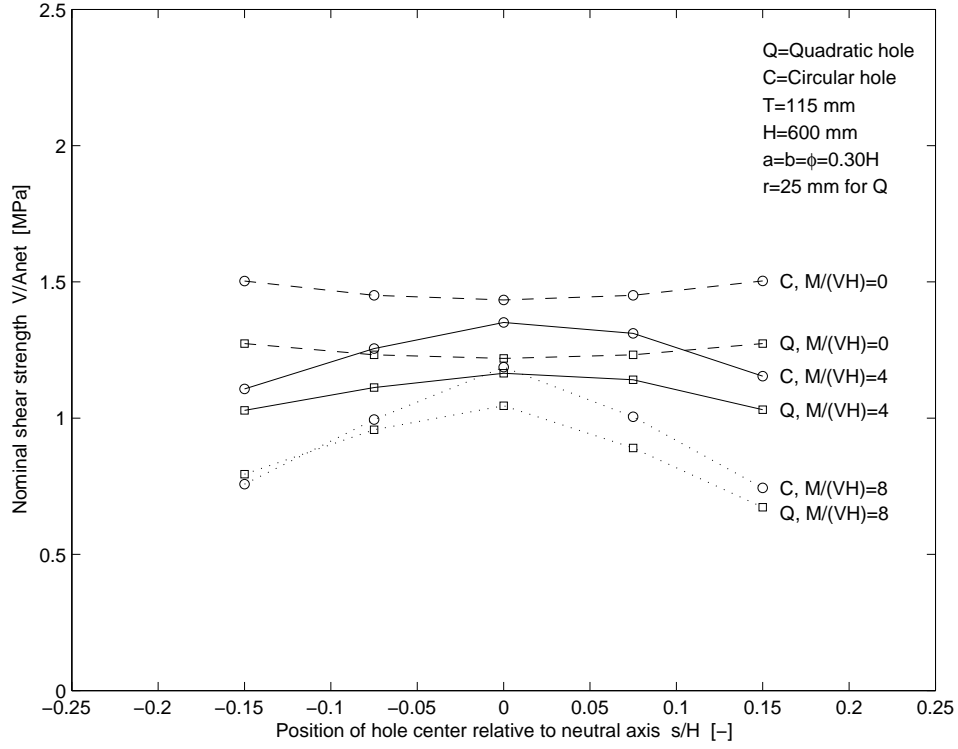
Figure 8.3: *Hole placement with respect to beam height – Bending moment to shear force ratio.*
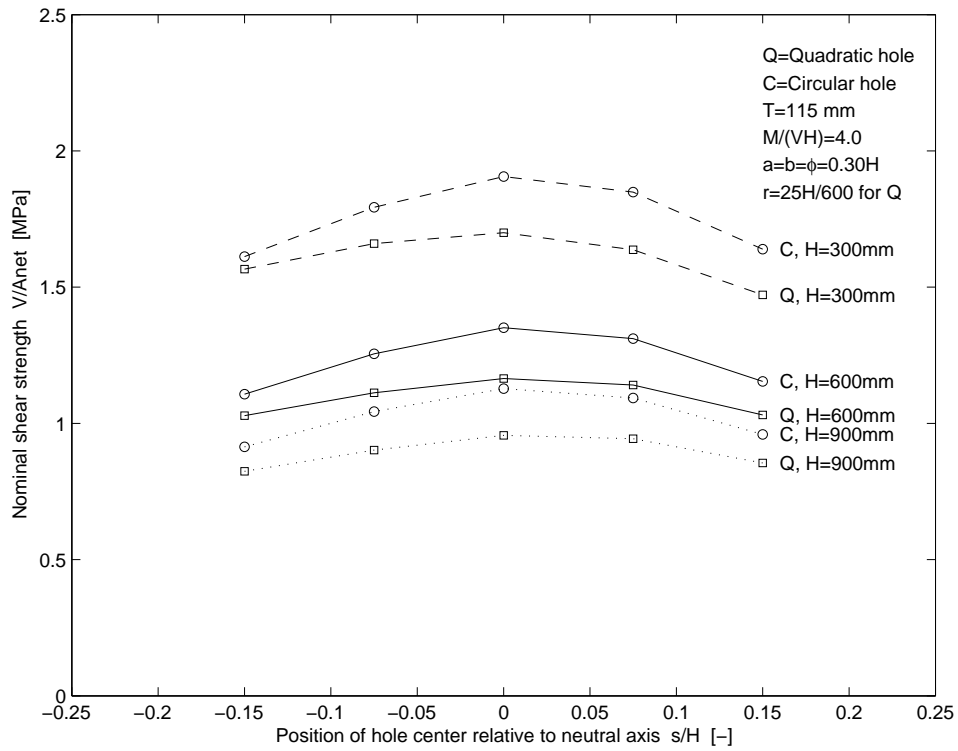
Figure 8.4: *Hole placement with respect to beam height – Beam height.*
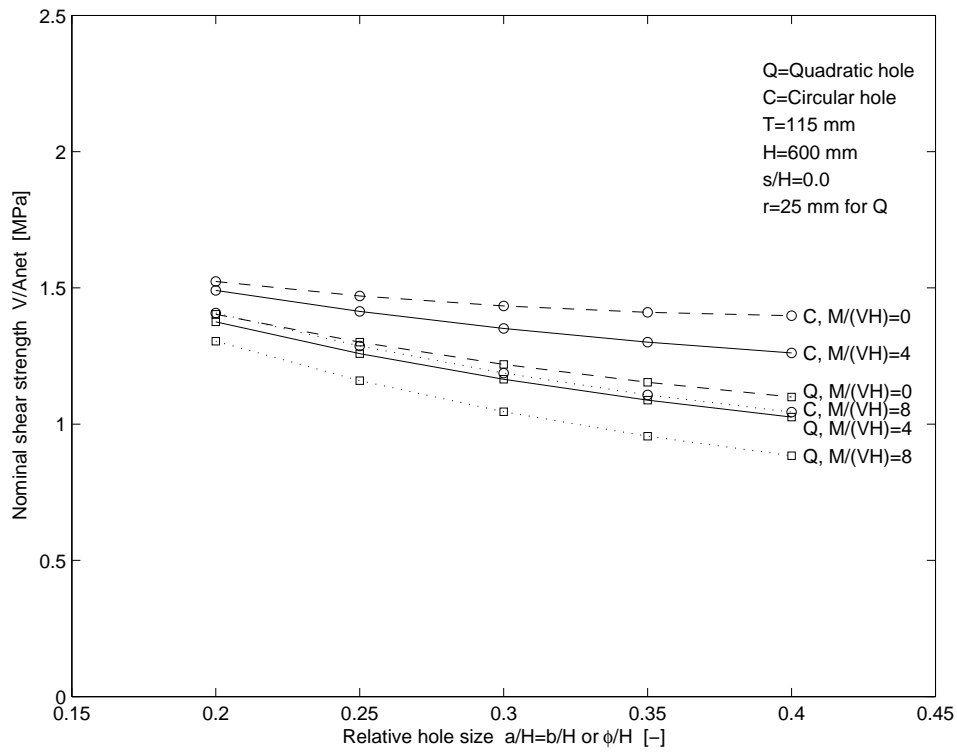
Figure 8.5: *Relative hole size with respect to beam height – Bending moment to shear force ratio.*
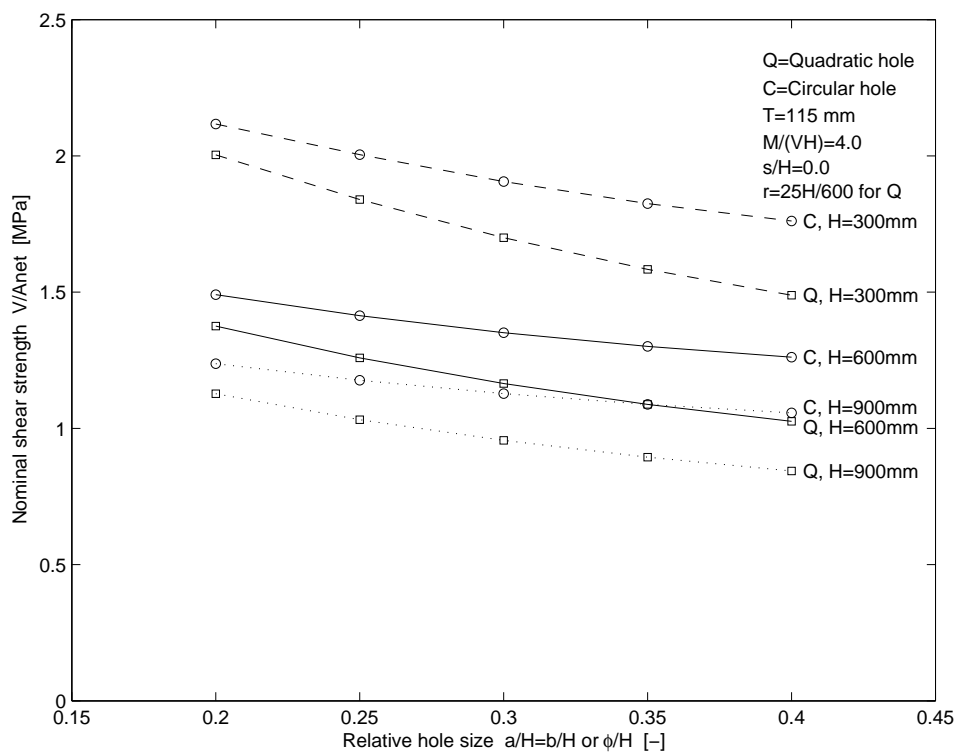
Figure 8.6: *Relative hole size with respect to beam height – Beam height.*
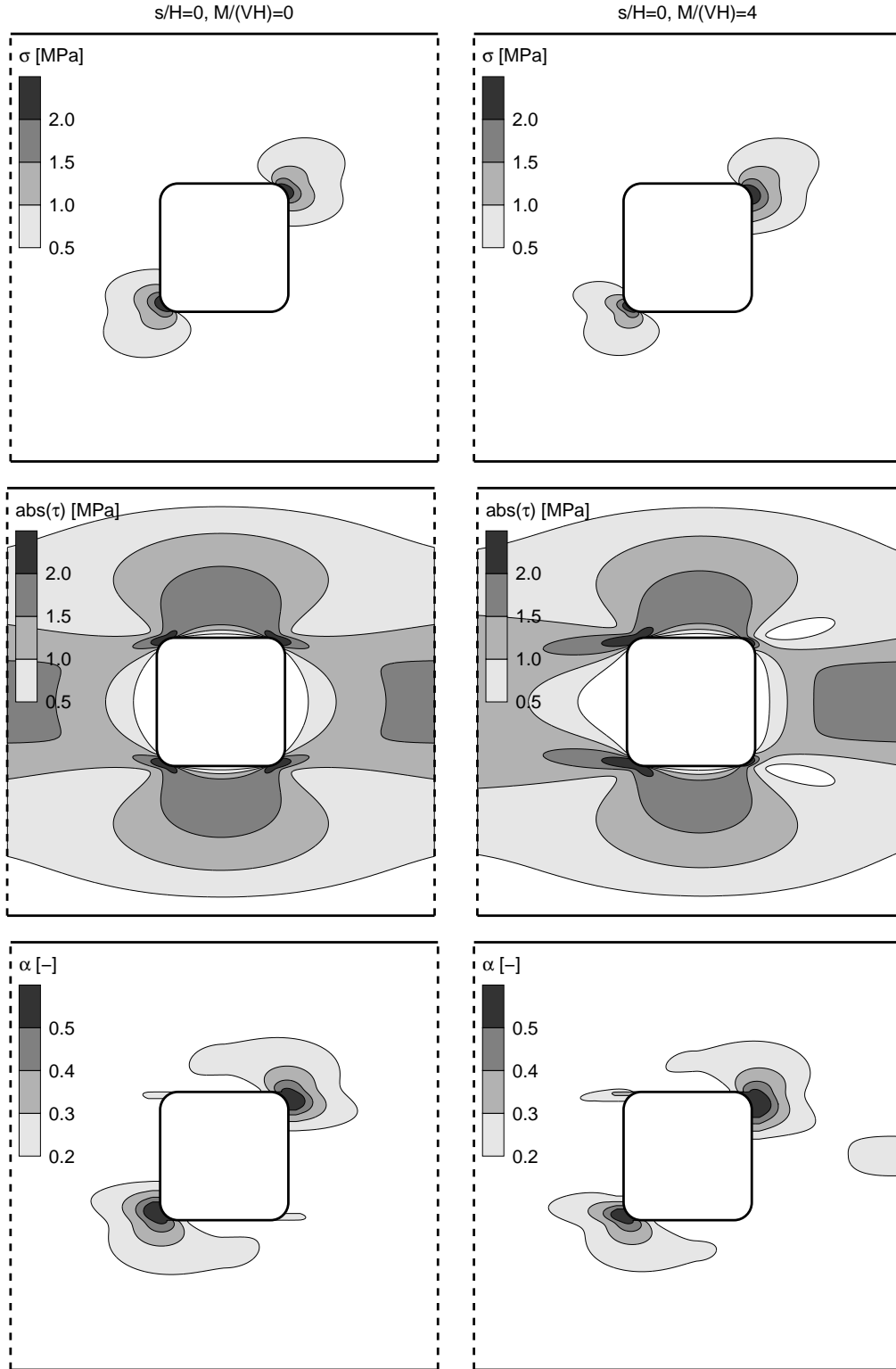
Figure 8.7: *Stress distributions σ, τ and α for beam geometry $H = 600$ mm, $T = 115$ mm, $a = b = 0.3H$, $r = 25$ mm. Applied loads correspond to PFM failure loads: $V/A_{net} = 1.22$ MPa for $M/(VH) = 0$ and $V/A_{net} = 1.16$ MPa for $M/(VH) = 4$.*
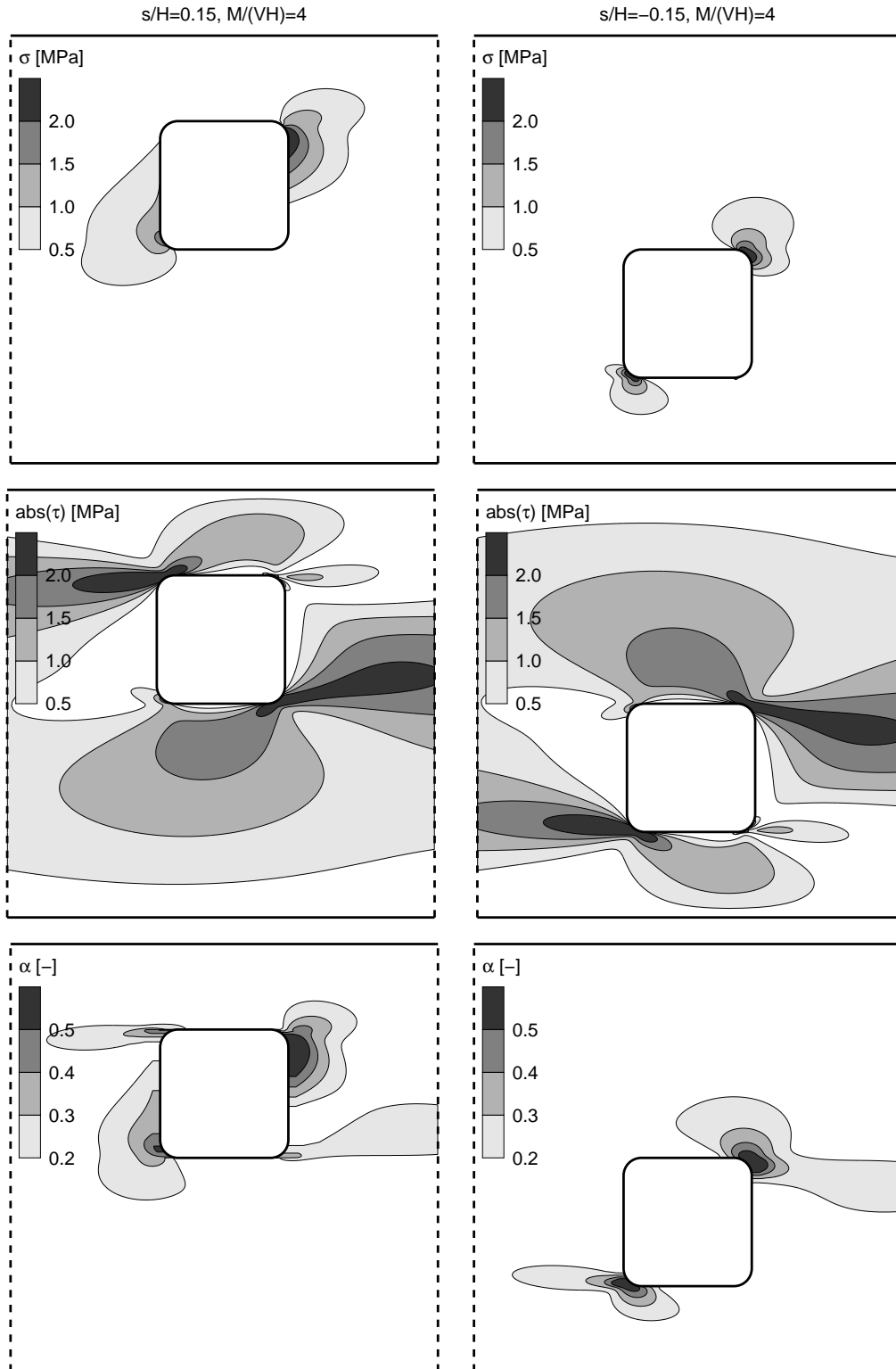
Figure 8.8: *Stress distributions σ, τ and α for beam geometry $H = 600$ mm, $T = 115$ mm, $a = b = 0.3H$, $r = 25$ mm. Applied loads correspond to PFM failure loads: $V/A_{net} = 1.03$ MPa for $s/H = 0.15$ and $V/A_{net} = 1.03$ MPa for $s/H = -0.15$.*

58
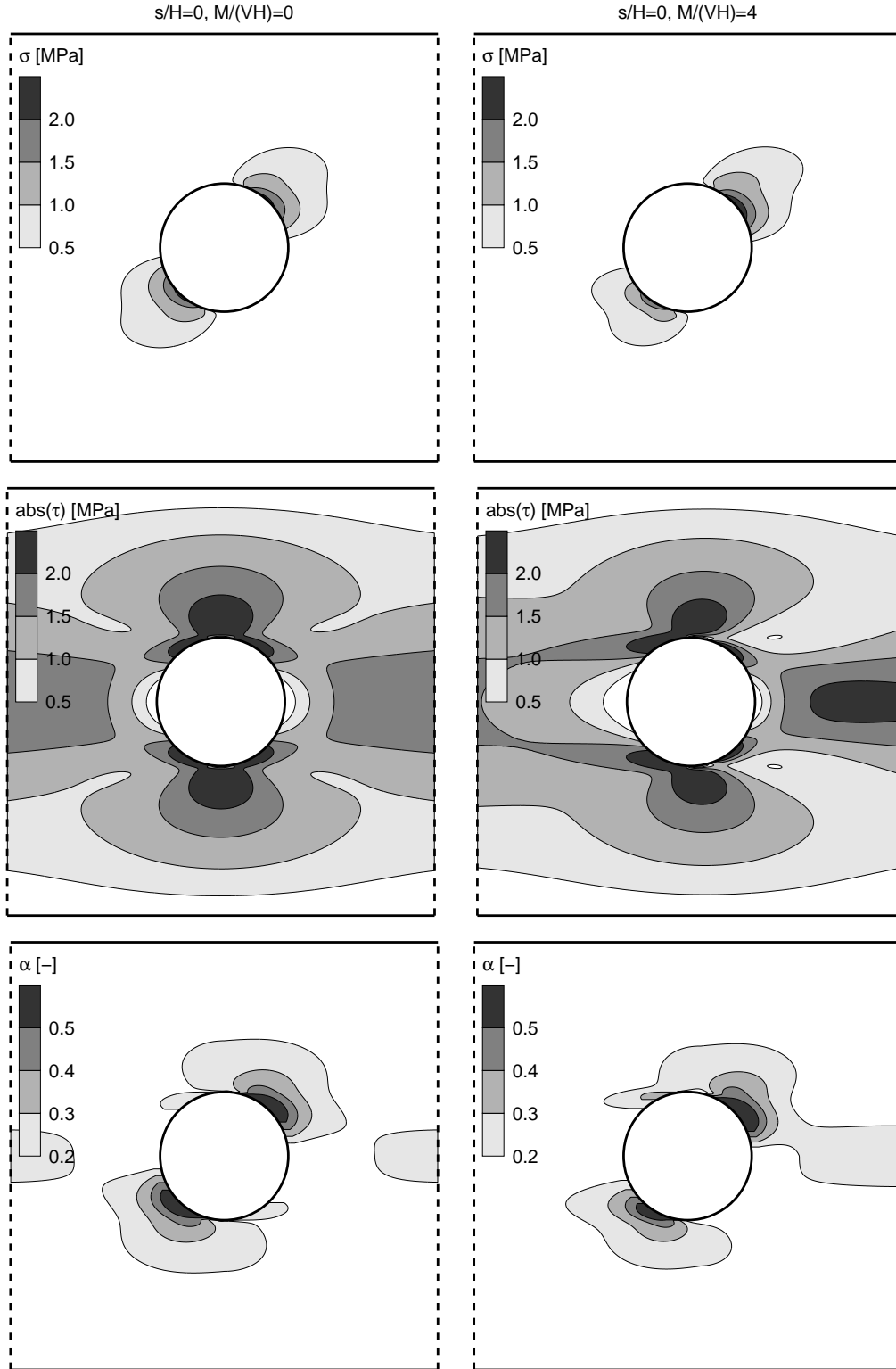
Figure 8.9: *Stress distributions σ, τ and α for beam geometry $H = 600$ mm, $T = 115$ mm, $\phi = 0.3H$. Applied loads correspond to PFM failure loads: $V/A_{net} = 1.43$ MPa for $M/(VH) = 0$ and $V/A_{net} = 1.35$ MPa for $M/(VH) = 4$.*
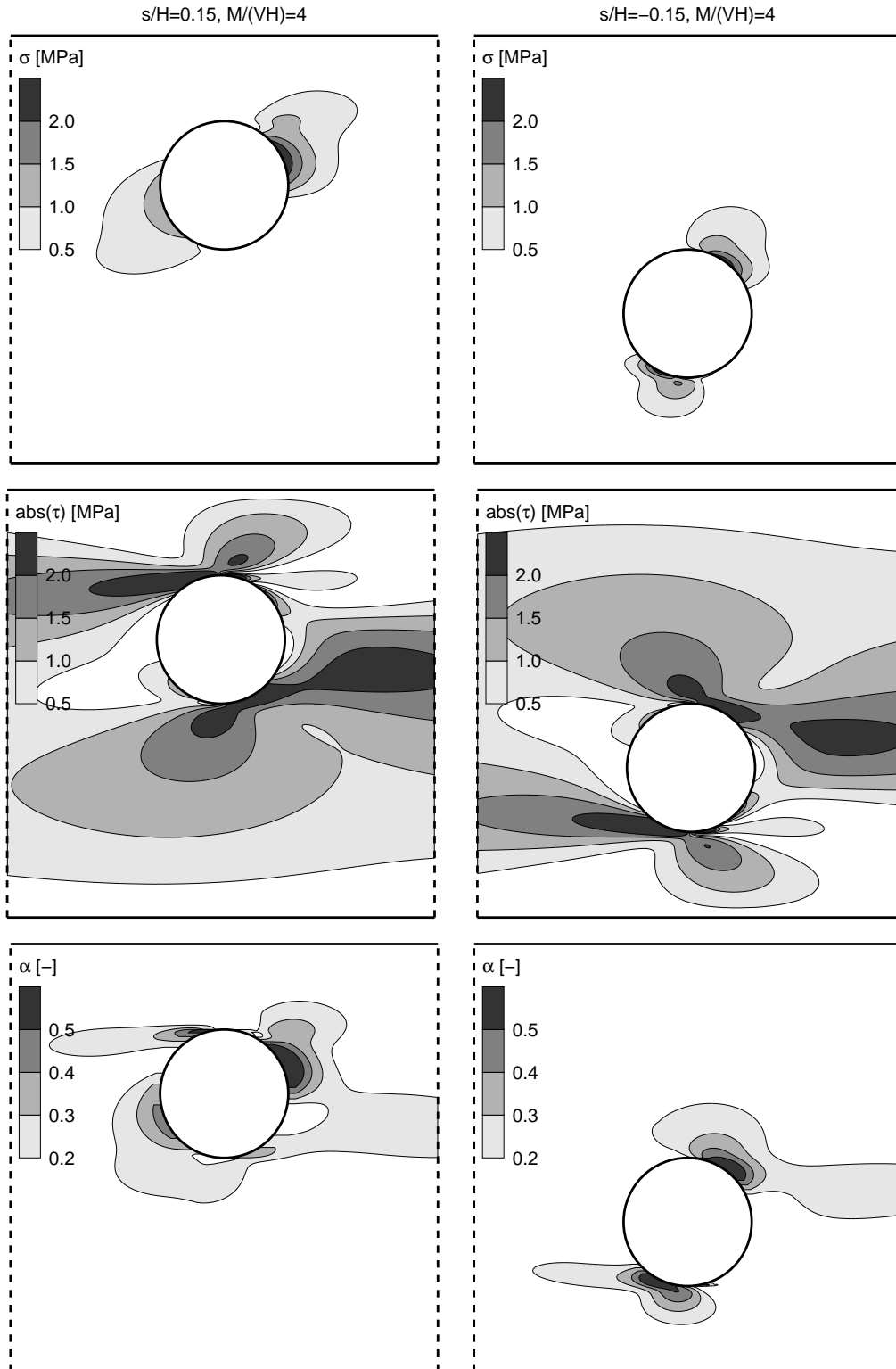
Figure 8.10: *Stress distributions σ, τ and α for beam geometry $H = 600$ mm, $T = 115$ mm, $\phi = 0.3H$. Applied loads correspond to PFM failure loads: $V/A_{net} = 1.15$ MPa for $s/H = 0.15$ and $V/A_{net} = 1.11$ MPa for $s/H = -0.15$.*

8.3 Verification

The verification of the probabilistic fracture mechanics method is based on comparison to experimental test results. The method is also compared to Weibull weakest link theory, conventional stress analysis and the mean stress method. The comparison to experimental test results is shown in Figure 8.11 for quadratic holes and in Figure 8.12 for circular holes from [2] and [16]. The test series notation in the figures refer to the notation used in Paper B. Some comments on the correlation between test results and the probabilistic fracture mechanics method are given below.

Bending moment to shear force ratio
The probabilistic fracture mechanics method seems to capture the the influence of the bending moment to shear force ratio well. The difference in strength for the considered bending moment to shear force ratios are however comparatively small.

Beam size
The probabilistic fracture mechanics method seems to capture the beam size effect well for the beams with $H = 450$, 630 and 900 mm. However, the method considerably overestimates the capacity for the small beams with $H = 180$ mm. One probable explanation is that the size of the potential fracture area a_m, used to determine mean stresses $\bar{\sigma}$ and $\bar{\tau}$, is too large in relation to the size of the small beams. Further comments on this is given in Chapter 9.

Hole placement with respect to beam height
The method predicts higher strength for test series AUh with a hole placed in the upper part of the beam ($s = H/6$) than for test series AMh with a centrically placed hole ($s = 0$), see Figure 8.11. The test results however shows the opposite relation. The difference in predicted strength is however small. For the small beams in the same figure, both test results and the probabilistic fracture mechanics method show lower strength for eccentrically placed holes. The strength reduction predicted by the method is however smaller than found in experimental tests.

Relative hole size with respect to beam height
The probabilistic fracture mechanics method seems to predict the influence of relative hole size well. As can be seen in Figure 8.12, the test results are comparatively scattered but the decrease in nominal shear strength seems in general fairly equal for the test results and the probabilistic fracture mechanics method.

Other methods
The conventional stress analysis methods (CSAσ and CSA$\sigma\tau$) and the mean stress method (MSM) show in general very poor agreement with the experimental test results. The Weibull weakest link theory (WEIσ and WEI$\sigma\tau$) shows overall fairly good correlation also concerning the beam size influence including the small beams.
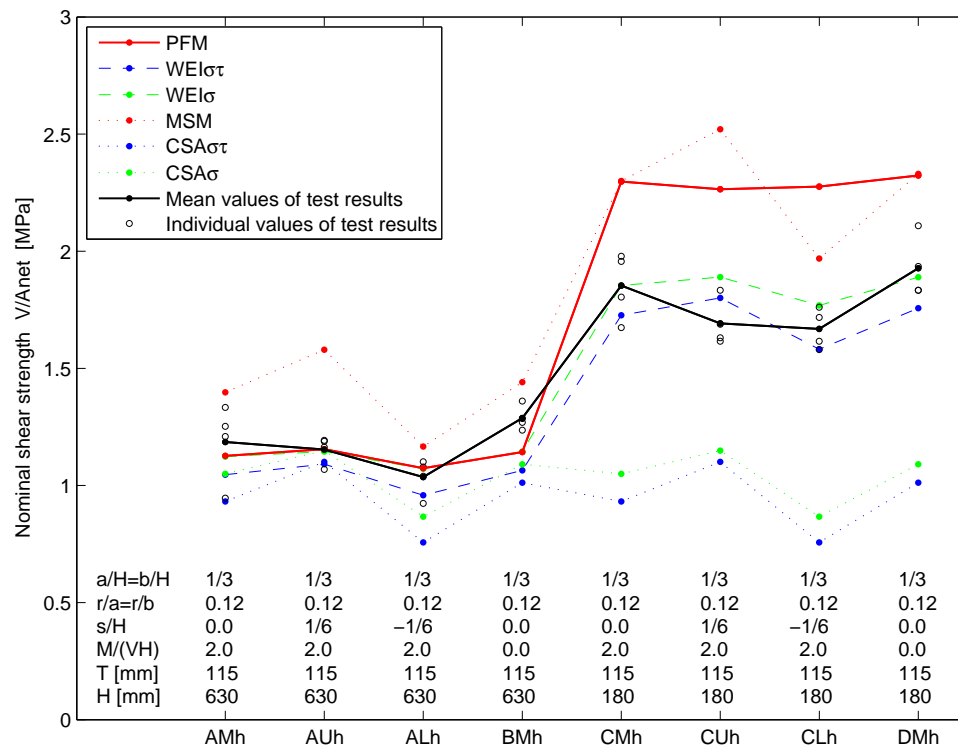
Figure 8.11: *Comparison to experimental test results for quadratic holes.*
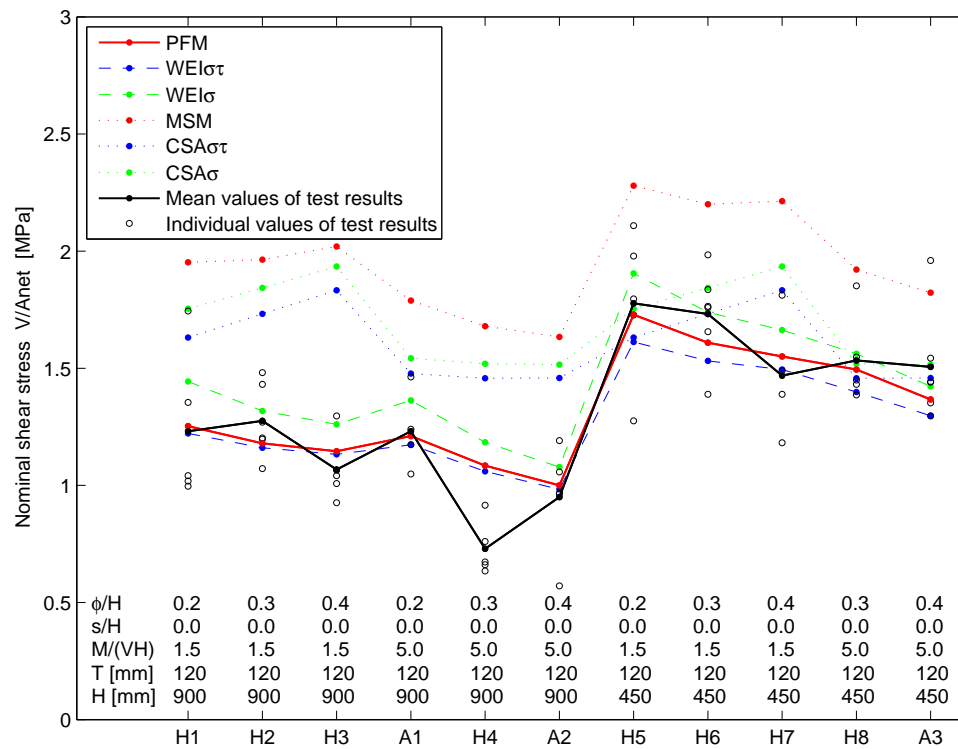
Figure 8.12: *Comparison to experimental test results for circular holes.*

Chapter 9

Concluding Remarks

Finding a simple, general and reliable method for design of glulam beams with holes seems difficult. Much effort has however been put into research within the field over the last decades. There is an obvious lack of knowledge which is reflected by the large differences concerning theoretical backgrounds and strength predictions between different design methods found in European timber engineering codes.

In order to increase the knowledge of the strength of glulam beams with holes and to increase the data base of experimental test results, full scale tests were carried out. One important finding from these tests is the strong beam size influence on the strength. This finding is in line with previous test results but the beam size effect is however not accounted for in all European timber engineering codes.

With the aim to investigate the possibilities for more accurate strength predictions of glulam beams with holes, a probabilistic fracture mechanics method is derived and implemented. The method is based on Weibull weakest link theory and the mean stress method. Combining these two methods means that the probabilistic fracture mechanics method takes the fracture energy and the stochastic nature of material properties into account. The method is consistent with Weibull weakest link theory in the sense that the same strength predictions are given by these two methods for an ideally brittle material. The probabilistic fracture mechanics method is also consistent with the mean stress method in the sense that the same strength predictions are given by these two methods for a material with deterministic material properties.

Good general features of the probabilistic fracture mechanics method are the ability to a analyze holes of arbitrary geometry and to consider the material properties that are believed to be the most important for strength of a glulam beam with a hole: material strength, fracture toughness and heterogeneity. Although of a general applicability, the method is furthermore simple in the sense that non-linear stress or fracture course analysis is not required. It is interesting that the probabilistic fracture mechanics method seems to be able to make a credible prediction of the influence of the curvature of the corners of a quadratic hole including sharp corners ($r = 0$). Weibull weakest link theory and conventional stress analysis methods predict zero beam strength for a hole with sharp corners.

The probabilistic fracture mechanics method seems to have an overall good ability to predict the strength based on the verification to experimental tests. One case when the method however obviously fails to make accurate predictions is small beams ($H = 180$ mm) where the strength is overestimated by about 30 %. A probable explanation is that the size of the potential fracture area a_m, used to determine the mean stresses, is too large in relation to the size of the small beams. The size of a fracture process region can, according to fracture mechanics, be expected to be governed by the properties of the material and to be independent of the size of the structure only as long as the structure is large as compared to the size of the fracture region. Further decrease of structural size implies decreased size of the fracture region. To overcome this problem, some kind of stress gradient related reduction of the length of the potential fracture area can be introduced for small beams.

Since the available experimental test results are limited, the extent to which the method can be verified is also limited. The present tests of beams with quadratic holes included tests of eccentrically placed holes, which seem to never have been tested before. Further full-scale testing is needed to increase the data base of test results for further verification and to increase the knowledge within the area. The influence of the different design parameters seems however to be rather complex.

There are also several other interesting design parameters which are not included in the this study. One example is influence of beam width T which was not analyzed in this study although the method gives a prediction according to Equation (7.4). Another example is the influence of a tensile or compressive axial force which would for example be of interest for design of glulam columns with holes. It seems that the combined action of axial force and bending neither has been tested nor analyzed. Another interesting load case not consider here is pure bending ($M/(VH) \to \infty$) which is of interest for straight beams but of even greater interest for tapered beams and curved beams. For these two load cases, the strength might however be limited by tensile or compressive failure parallel to grain and these failure modes are not considered in the present implementation. The probabilistic fracture mechanics method could possibly be generalized with respect to consideration of the normal stress along grain by modification of Equation (7.1) and corresponding modifications of the length of the potential fracture area a_{ms}.

A comparison of the overall ability to predict strength of different methods is presented in Figure 9.1, where the ratio between the theoretically predicted capacity and the capacity found in experimental tests is given. The considered methods are: the probabilistic fracture mechanics method (PFM), Weibull weakest link theory considering interaction of σ and τ (WEI$\sigma\tau$) and considering only σ (WEIσ), the mean stress method (MSM), conventional stress analysis considering interaction of σ and τ (CSA$\sigma\tau$) and considering only σ (CSAσ). Some code design methods are also included in the comparison: the empirically based method (method 1) and the "end-notched beam"-analogy method (method 2) found in Limträhandbok [6], the method in the German code DIN 1052 [5] and the Weibull-based design proposal presented by Höfflin and Aicher in [16] and [2]. The latter method is presented for circular holes, but is here used also for quadratic holes assuming $a = b = \phi$.

The experimental test results are the mean values of the test series that are also presented in Figure 8.11 and in Figure 8.12. The previously commented test series (H4) with somewhat deviating results in terms of a surprisingly low strength is however excluded from this comparison. A logarithmic scale is used in the comparison. Quadratic and circular marks represent test series with quadratic and circular holes respectively. Characteristic shear strength $f_{v,k} = 3.8$ MPa and characteristic perpendicular to grain tensile strength $f_{t,90,k} = 0.5$ MPa (based on values for GL 32h stated in [27]) are used for the code design methods. For the other six methods, the theoretical capacities are based on material properties stated in Table 8.1.

The probabilistic fracture mechanics shows good agreement compared to test results used in this comparison, with the exception of the four test series with small beams. The two methods based on Weibull weakest link theory (WEI$\sigma\tau$ and WEIσ) show overall good agreement. It is remarkable that the agreement is good also for the square holes with rounded corner $r/a = r/b \approx 0.12$, having in mind that Weibull theory predict an unrealistic zero strength for square holes with sharp corners. The "end-notched beam"-analogy method (Limträhandbok method 2) shows in general the most un-conservative strength predictions among the code design methods. It is however interesting that the scatter in ratio between theoretical and experimental strength is fairly low considering the beams with circular holes and quadratic holes separately. The overall agreement with experimental tests could easily be improve by some general reduction for beams with circular holes.
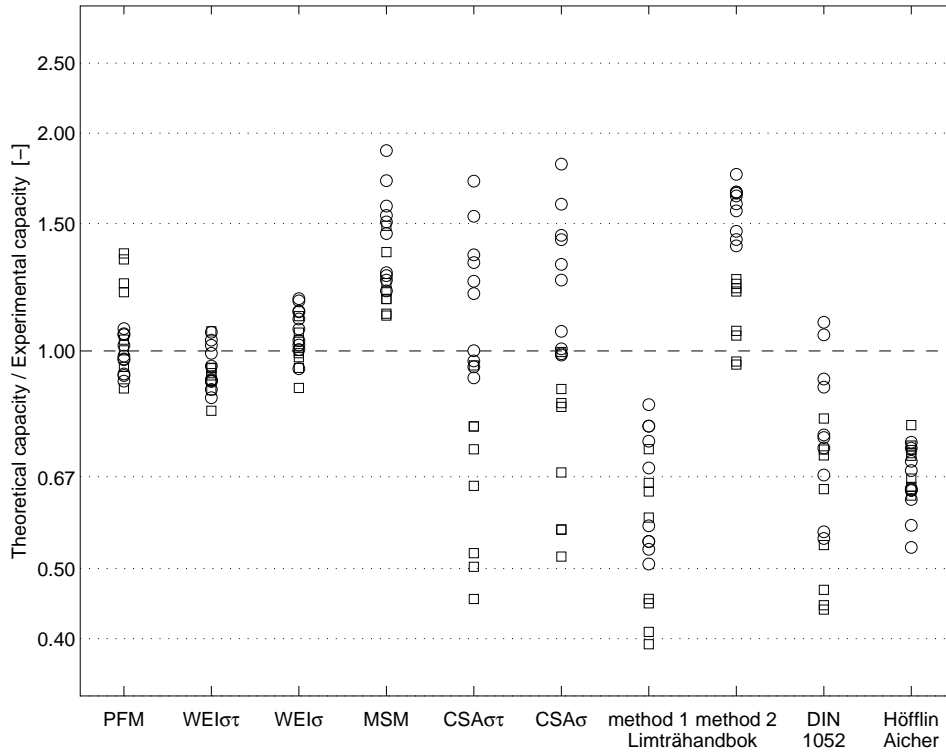
Figure 9.1: *Comparison of overall ability to predict strength of different methods for strength analysis including code design methods.*

Bibliography

[1] Aicher S., Schmidt J., Brunhold S.
Design of timber beams with holes by means of fracture mechanics
CIB-W18/28-19-4, Copenhagen, Denmark, 1995.

[2] Aicher S., Höfflin L.
Tragfähigkeit und bemessung von brettschichtholzträgern mit runden durchbrüchen –
Sicherheitsrelevante modifikationen der bemessungsverfahren nach Eurocode 5 und DIN 1052
MPA Otto-Graf-Institute, University of Stuttgart, 2006.

[3] Aicher S., Gustafsson P.J. (ed), Haller P., Petersson H.
Fracture mechanics models for strength analysis of timber beams with a hole or a notch –
A report of RILEM TC-133
Report TVSM-7134, Division of Structural Mechanics, Lund University, 2002.

[4] Bengtsson S., Dahl G.
Inverkan av hål nära upplag på hållfastheten hos limträbalkar
Byggnadsteknik II, Lund University, 1971.

[5] Blaß H.J., Ehlbeck J., Kreuzinger H., Steck G.
Erläuterungen zu DIN 1052:2004-08 –
Entwurf, berechnung und bemessung von holzbauwerken
2nd Edition including original text. DGfH innovations- und Service GmbH, München, 2005.

[6] Carling O.
Limträhandbok
Svenskt Limträ AB, Print & Media Center i Sundsvall AB, 2001.

[7] Danielsson H.
The strength of glulam beams with holes – A survey of tests and calculation methods
Report TVSM-3068, Division of Structural Mechanics, Lund University, 2007.

[8] *Eurocode 5:*
Design of timber structures - Part 1-1: General - Common rules and rules for buildings
EN 1995-1-1:2004 (E).

[9] *Eurocode 5:*
Design of timber structures - Part 1-1: General Rules-General rules and rules for buildings
prEN 1995-1-1: Final Draft 2002-10-09.

[10] Gustafsson P.J.
A study of strength of notched beams
CIB-W18A/21-10-1, Parksville, Vancouver Island, Canada, 1988.

[11] Gustafsson P.J., Enquist B.
Träbalks hållfasthet vid rätvinklig urtagning
Report TVSM-7042, Division of Structural Mechanics, Lund University, 1988.

[12] Gustafsson P.J., Serrano E.
Fracture mechanics in timber engineering – Some methods and applications
Proceedings of 1st RILEM Symposium on Timber Engineering, Stockholm, 1999.

[13] Gustafsson P.J., Petersson H., Stefansson F.
Fracture analysis of wooden beams with holes and notches
Proceedings of the Int. Wood Engineering Conference, New Orleans, USA, 1996.

[14] Gustafsson P.J.
Chapter 7: *Fracture perpendicular to grain – Structural applications*
In Thelandersson S., Larsen H.J. *Timber Engineering*
John Wiley & Sons Ltd, Chichester, England, 2003.

[15] Hallström S.
Glass fibre reinforcemed laminated timber beams with holes
Report 95-12, Department of Lightweight Structures, KTH, Stockholm, 1995.

[16] Höfflin L.
Runde durchbrüche in brettschichtholzträger –
Experimentelle und theoretische untersuchungen
MPA Otto-Graf-Institute, University of Stuttgart, 2005.

[17] Johannesson B.
Design problems for glulam beams with holes
Division of Steel and Timber structures, Chalmers University of Technology, Göteborg, 1983.

[18] Kolb H., Frech P.
Untersuchungen an durchbrochenen bindern aus brettschichtholz
Holz als Roh- und Werkstoff 35, p. 125-134, 1977.

[19] Kolb H., Epple A.
Verstärkung von durchbrochenen brettschichtholzbindern
Forchungs- und Materialprüfungsanstalt Baden-Württenberg, Stuttgart, 1985.

[20] Penttala V.
Reiällinen liimapuupalkki
Division of Structural Engineering, Helsinki Univeristy of Technology, Otaniemi, 1980.

[21] Petersson H.
Fracture design analysis of wooden beams with holes and notches.
Finite element analysis based on energy release rate approach.
CIB-W18/28-19-3, Copenhagen, Denmark, 1995.

[22] Pizio S.
Die anwendung der bruchmechanik zur bemessung von holzbauteilen, untersucht am
durchbrochen und am ausgeklinkten Träger
Publication 91:1, Baustatik und Stahlbau, ETH, Zürich, 1991.

[23] Rautenstrauch K., Franke S., Franke B.
Beanspruchungsanalyse von bauteilen aus voll- und brettschichtholz durch industri-
photogrammetrie am beispiel von ausklinkungen und durchbrüchen
Forchungsstelle 1 - Abschlussbericht Teil B, Bauhaus-Universität Weimar, 2007.

[24] Riipola K.
Timber beams with holes: Fracture mechanics approach
Journal of Structural Engineering, Volume 121, Issue 2, p. 225-239, 1995.

[25] Scheer C., Haase K.
Durchbrüche in brettschichtholzträger, Teil 1: Spannungstheoretische untersuchungen
Holz als Roh- und Werkstoff 58, p. 153-161, 2000.

[26] Scheer C., Haase K.
Durchbrüche in brettschichtholzträger, Teil 2: Bruchmechanische untersuchungen
Holz als Roh- und Werkstoff 58, p. 217-228, 2000.

[27] SS-EN 1194:1999
Träkonstruktioner – Limträ – Hållfasthetsklasser och bestämning av karakteristiska värden
SIS Förlag, Stockholm, 2000.

[28] Stefansson F.
Fracture analysis of orthotropic beams – Linear elastic and nonlinear methods
Report TVSM-3029, Division of Structural Mechanics, Lund University, 2001.

[29] Steiger R.
EMPA - Swiss Federal Laboratories for Materials Testing and Research
Personal communication.

[30] Weibull W.
A statistical theory of the strength of materials
Proceedings nr 151, Ingenjörsvetenskapsakademien, Stockholm, 1939.

Appendix A

Analytical solutions for beam examples

Derivation of global effective dimensionless stress parameter α_{global} for beam in bending with varying bending moment according to Weibull weakest link theory.
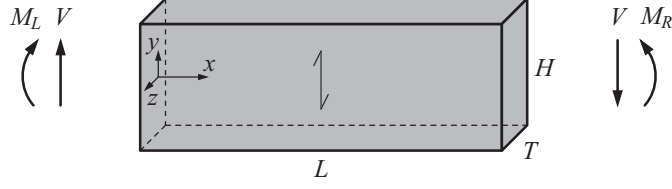
$$M(x) = M_R\left(\eta - \eta\frac{x}{L} + \frac{x}{L}\right) \qquad \text{where} \qquad \eta = \frac{M_L}{M_R} \qquad \text{and} \qquad 0 \leq \eta \leq 1$$

$$\sigma(x,y) = -\frac{M(x)}{I}y = -\frac{12M_R}{TH^3}\left(\eta - \eta\frac{x}{L} + \frac{x}{L}\right)y$$

$$\alpha(x,y) = \frac{\sigma(x,y)}{f_\sigma}$$

$$\alpha_{global} = \left(\frac{1}{\Omega_{ref}}\int_\Omega \alpha^m(x,y,z)\,d\Omega\right)^{1/m} =$$

$$= \left(\frac{1}{\Omega_{ref}}\int_\Omega \left(-\frac{12M_R}{TH^3 f_\sigma}\left(\eta - \eta\frac{x}{L} + \frac{x}{L}\right)y\right)^m d\Omega\right)^{1/m} =$$

$$= \frac{6M_R}{TH^2 f_\sigma}\left(\frac{1}{\Omega_{ref}}\frac{2^m}{H^m}\int_\Omega\left(-\left(\eta - \eta\frac{x}{L} + \frac{x}{L}\right)y\right)^m d\Omega\right)^{1/m} =$$

$$= \frac{6M_R}{TH^2 f_\sigma}\left(\frac{1}{\Omega_{ref}}\frac{2^m}{H^m}\int_{-\frac{T}{2}}^{\frac{T}{2}}1\,dz\int_{-\frac{H}{2}}^{0}(-y)^m dy\int_0^L\left(\eta - \eta\frac{x}{L} + \frac{x}{L}\right)^m dx\right)^{1/m} =$$

$$= \frac{6M_R}{TH^2 f_\sigma}\left(\frac{T}{\Omega_{ref}}\frac{2^m}{H^m}\left[-\frac{1}{m+1}(-y)^{m+1}\right]_{-\frac{H}{2}}^{0}\cdots\right.$$

$$\left.\cdots\left[\frac{1}{m+1}\left(\eta - \eta\frac{x}{L} + \frac{x}{L}\right)^{m+1}\frac{L}{1-\eta}\right]_0^L\right)^{1/m} =$$

$$= \frac{6M_R}{TH^2 f_\sigma}\left(\frac{T}{\Omega_{ref}}\frac{2^m}{H^m}\left(\frac{1}{m+1}\frac{H^{m+1}}{2^{m+1}}\right)\left(\frac{1}{m+1}\left(1-\eta^{m+1}\right)\frac{L}{1-\eta}\right)\right)^{1/m} =$$

$$= \frac{6M_R}{TH^2 f_\sigma}\left(\frac{LHT}{2\Omega_{ref}}\left(\frac{1}{m+1}\right)\left(\frac{1}{m+1}\frac{1-\eta^{m+1}}{1-\eta}\right)\right)^{1/m} =$$

$$= \frac{6M_R}{TH^2 f_\sigma}\left(\frac{LHT}{2\Omega_{ref}}\frac{1}{(m+1)^2}\frac{1-\eta^{m+1}}{1-\eta}\right)^{1/m}$$

Derivation of global effective dimensionless stress parameter α_{global} for beam in bending with constant bending moment according to Weibull weakest link theory.

$$
\begin{aligned}
M(x) &= M \\[2mm]
\sigma(y) &= -\frac{M}{I}y = -\frac{12M}{TH^3}y \\[2mm]
\alpha(y) &= \frac{\sigma(y)}{f_\sigma} \\[2mm]
\alpha_{global} &= \left(\frac{1}{\Omega_{ref}}\int_\Omega \alpha^m(x,y,z)\,d\Omega\right)^{1/m} = \\[2mm]
&= \left(\frac{1}{\Omega_{ref}}\int_\Omega \left(-\frac{12M}{TH^3 f_\sigma}y\right)^m d\Omega\right)^{1/m} = \\[2mm]
&= \frac{6M}{TH^2 f_\sigma}\left(\frac{1}{\Omega_{ref}}\frac{2^m}{H^m}\int_V (-y)^m\,d\Omega\right)^{1/m} = \\[2mm]
&= \frac{6M}{TH^2 f_\sigma}\left(\frac{1}{\Omega_{ref}}\frac{2^m}{H^m}\int_{-\frac{T}{2}}^{\frac{T}{2}}1\,dz\int_{-\frac{H}{2}}^{0}(-y)^m dy\int_0^L 1\,dx\right)^{1/m} = \\[2mm]
&= \frac{6M}{TH^2 f_\sigma}\left(\frac{LT}{\Omega_{ref}}\frac{2^m}{H^m}\left[-\frac{1}{m+1}(-y)^{m+1}\right]_{-\frac{H}{2}}^{0}\right)^{1/m} = \\[2mm]
&= \frac{6M}{TH^2 f_\sigma}\left(\frac{LT}{\Omega_{ref}}\frac{2^m}{H^m}\left(\frac{1}{m+1}\frac{H^{m+1}}{2^{m+1}}\right)\right)^{1/m} = \\[2mm]
&= \frac{6M}{TH^2 f_\sigma}\left(\frac{LHT}{2\Omega_{ref}}\frac{1}{m+1}\right)^{1/m}
\end{aligned}
$$

Derivation of global effective dimensionless stress parameter α_{global} for beam in bending with constant bending moment according to the probabilistic fracture mechanics method.
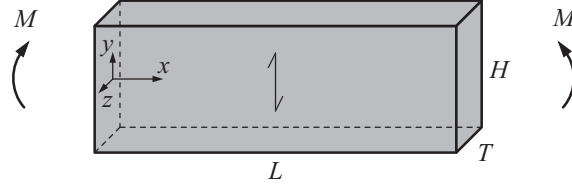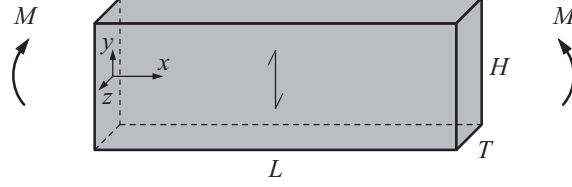
$$
\begin{aligned}
M(x) &= M \\
\sigma(y) &= -\frac{M}{I}y = -\frac{12M}{TH^3}y \\
\alpha(y) &= \frac{\bar{\sigma}(y)}{f_\sigma} \quad \text{where} \quad \bar{\sigma}(y) = \frac{1}{a_m}\int_{a_m}\sigma(y)\,dy \quad \text{and} \quad a_m = a_m(y)
\end{aligned}
$$

$$
a_m(y) = \begin{cases}
a_{ms} & \text{for} & -\frac{H}{2} \leq y < -\frac{H}{2}+\frac{a_{ms}}{2} & (1) \\[2mm]
2\left(\frac{H}{2}+y\right) & \text{for} & -\frac{H}{2}+\frac{a_{ms}}{2} \leq y < -\frac{H}{2}+a_{ms} & (2) \\[2mm]
2a_{ms} & \text{for} & -\frac{H}{2}+a_{ms} \leq y & (3)
\end{cases}
$$

$$
\text{where } a_{ms} = \frac{2E_I G_{Ic}}{\pi f_\sigma^2} \quad \text{since } k = 0
$$

$$
\bar{\sigma}(y) = \begin{cases}
\dfrac{1}{a_m}\displaystyle\int_{-\frac{H}{2}}^{-\frac{H}{2}+a_m} -\dfrac{12M}{TH^3}y\,dy = \dfrac{6M}{TH^2}\left(1-\dfrac{a_{ms}}{H}\right) & \text{for (1)} \\[4mm]
\dfrac{1}{a_m}\displaystyle\int_{y-\frac{am}{2}}^{y+\frac{am}{2}} -\dfrac{12M}{TH^3}y\,dy = -\dfrac{12M}{TH^3}y & \text{for (2)} \\[4mm]
\dfrac{1}{a_m}\displaystyle\int_{y-\frac{am}{2}}^{y+\frac{am}{2}} -\dfrac{12M}{TH^3}y\,dy = -\dfrac{12M}{TH^3}y & \text{for (3)}
\end{cases}
$$

$$\alpha_{global} = \left(\frac{1}{\Omega_{ref}} \int_{\Omega} \alpha^m(y) \, d\Omega \right)^{1/m} =$$

$$= \left(\frac{1}{\Omega_{ref}} \int_{\Omega} \left(\frac{\bar{\sigma}(y)}{f_{\sigma}} \right)^m d\Omega \right)^{1/m} =$$

$$= \left(\frac{1}{\Omega_{ref}} \int_{-\frac{T}{2}}^{\frac{T}{2}} 1 \, dz \int_{-\frac{H}{2}}^{0} \left(\frac{\bar{\sigma}(y)}{f_{\sigma}} \right)^m dy \int_{0}^{L} 1 \, dx \right)^{1/m} =$$

$$= \left(\frac{LT}{\Omega_{ref}} \left(\int_{-\frac{H}{2}}^{-\frac{H}{2}+\frac{a_{ms}}{2}} \left(\frac{6M}{TH^2 f_{\sigma}} \left(1 - \frac{a_{ms}}{H} \right) \right)^m dy + ... \right. \right.$$

$$\left. \left. ... + \int_{-\frac{H}{2}+\frac{a_{ms}}{2}}^{0} \left(-\frac{12M}{TH^3 f_{\sigma}} y \right)^m dy \right) \right)^{1/m} =$$

$$= \frac{6M}{TH^2 f_{\sigma}} \left(\frac{LT}{\Omega_{ref}} \left(\int_{-\frac{H}{2}}^{-\frac{H}{2}+\frac{a_{ms}}{2}} \left(1 - \frac{a_{ms}}{H} \right)^m dy + ... \right. \right.$$

$$\left. \left. ... + \int_{-\frac{H}{2}+\frac{a_{ms}}{2}}^{0} \left(-\frac{2}{H} y \right)^m dy \right) \right)^{1/m} =$$

$$= \frac{6M}{TH^2 f_{\sigma}} \left(\frac{LT}{\Omega_{ref}} \left(\left(1 - \frac{a_{ms}}{H} \right)^m \frac{a_{ms}}{2} + ... \right. \right.$$

$$\left. \left. ... + \left[\frac{1}{m+1} \left(-\frac{2}{H} y \right)^{m+1} \left(-\frac{H}{2} \right) \right]_{-\frac{H}{2}+\frac{a_{ms}}{2}}^{0} \right) \right)^{1/m} =$$

$$= \frac{6M}{TH^2 f_{\sigma}} \left(\frac{LT}{\Omega_{ref}} \left(\left(1 - \frac{a_{ms}}{H} \right)^m \frac{a_{ms}}{2} + \frac{1}{m+1} \left(1 - \frac{a_{ms}}{H} \right)^{m+1} \frac{H}{2} \right) \right)^{1/m} =$$

$$= \frac{6M}{TH^2 f_{\sigma}} \left(\frac{LHT}{2\Omega_{ref}} \left(1 - \frac{a_{ms}}{H} \right)^m \left(\frac{a_{ms}}{H} + \frac{1}{m+1} \left(1 - \frac{a_{ms}}{H} \right) \right) \right)^{1/m} =$$

$$= \frac{6M}{TH^2 f_{\sigma}} \left(1 - \frac{a_{ms}}{H} \right) \left(\frac{LHT}{2\Omega_{ref}} \left(\frac{a_{ms}}{H} + \frac{1}{m+1} - \frac{1}{m+1} \frac{a_{ms}}{H} \right) \right)^{1/m}$$

Paper A

Strength Tests of Glulam Beams with Quadratic Holes –
Test Report

Henrik Danielsson

Abstract

This report deals with strength tests of glulam beams with quadratic holes with rounded corners. A total of 36 individual tests were carried out, divided into nine test series with four nominally equal tests in each test series. There were four parameters varied within these test series: beam size, bending moment to shear force ratio, material strength class and also hole placement with respect to the height of the beam. The latter parameter seems to never have been investigated before since all previously performed tests found in the literature have been carried out on beams with holes placed centrically in the beam height direction. The test results indicate a strong size effect. The influence of eccentric placement of the hole on the crack load was found to be small.

Keywords: glulam, hole, strength, test, size effect, eccentric hole.

Acknowledgements

Lund, February 2008

Henrik Danielsson

Contents

1 Introduction

The tests presented in this report deals with the strength of glulam beams with holes. A total of 36 individual tests were carried out, divided into nine test series with four nominally equal tests in each test series. All holes were quadratic with rounded corners and with a side length equal to one third of the beam height. The study comprises investigations of primarily two interesting and potentially important design variables: *beam size effect* and *hole placement with respect to beam height.* Two other design parameters are also studied to some extent: *material strength class* and *bending moment to shear force ratio* at hole center.

Beam size
Two different beam cross section sizes were used within the test series, 115×180 mm^2 and 115×630 mm^2, in order to investigate the size dependence of the strength.

Hole placement with respect to beam height
Three different hole placements with respect to the height of the beam were tested, centrically placed holes and holes placed with its center in the upper or lower part of the beam respectively.

Material Strength Class
Two different material strength classes were used, homogeneous glulam of lamination strength class LS22 and combined glulam of lamination strength classes LS22 and LS15.

Bending moment to shear force ratio
Two different test setups were used concerning the bending moment to shear force ratio, one with the hole center placed in a position (in the length direction of the beam) with a combined state of shear force and bending moment and another setup where the hole is placed with its center at a point of zero bending moment.

Different hole placements with respect to the beam height seems to never have been investigated before since all previously performed tests found in the literature have been carried out on beams with holes placed centrically with respect to the beam height [1].

The report is organized in the following way. The nine test series and the different test setups, test procedures, recorded measures and other characteristics of the tests are presented in Section 2. The glulam beams are described concerning material strength class, lamellae size, density, moisture content and other material properties in Section 3. The results of the strength tests are presented in Section 4 and some concluding remarks on the results are given in Section 5.

2 Test series

The test series are in Table 1 described concerning name, number of tests, test setup, hole placement, strength class type, beam size and hole size. The geometric properties and the bending moment to shear force ratios at hole center for Test Setup 1 and Test Setup 2 are illustrated in Figure 1. The names of the test series consist of a three letter combination. All tests with the same first letter (A, B, C, D) have the same test setup and geometry with the exception of the hole placement which is described by the second letter (M=Middle, U=Upper, L=Lower) according to Figure 1. The last letter of the combination tells whether the beams are strength class homogeneous (h) or strength class combined (c).

Table 1: *Test series.*

Test series	Number of tests	Test setup	Hole placement	Strength class type	Beam size $T \times H$ [mm^2]	Hole size $a \times b$ [mm^2]	r [mm]
AMh	4	1	Middle	homogeneous	115×630	210×210	25
AMc	4	1	Middle	combined	115×630	210×210	25
AUh	4	1	Upper	homogeneous	115×630	210×210	25
ALh	4	1	Lower	homogeneous	115×630	210×210	25
BMh	4	2	Middle	homogeneous	115×630	210×210	25
CMh	4	1	Middle	homogeneous	115×180	60×60	7
CUh	4	1	Upper	homogeneous	115×180	60×60	7
CLh	4	1	Lower	homogeneous	115×180	60×60	7
DMh	4	2	Middle	homogeneous	115×180	60×60	7

Figure 1: *Test setups and hole placements.*

4

All tests were run in deformation control. The rate of total deformation was 0.02 mm/s for test series AMh (except AMh-1 were the rate was 0.05 mm/s), AMc, AUh, ALh and BMh while the rate of total deformation was 0.007 mm/s for test series CMh, CUh, CLh and DMh. These rates resulted in a test duration of approximately 20-30 minutes. The rate of total deformation referred to is the rate of the actuator in the testing machine. These rates of total deformations allowed careful observations of the two corners of the holes where cracks were expected during the loading procedure which enabled a careful investigation of the initiation and propagation of the cracks.

The following variables were recorded for all tests: the total deformation, applied load P, beam deflection δ and also vertical deformations d in the beam at the two failing corners of the hole. Four LVDT sensors were used to measure these deformations, one on each side of the beam at the two failing corners of the hole. A fifth LVDT sensor was used to measure the beam deflection δ. The placement of these sensors, glulam beam sizes and sizes of steel beams and support plates are shown in Figures 2 and 3.

For test series AMh, AMc, AUh, ALh, CMh, CUh and CLh the glulam beams were delivered with a total length which was longer than the span length of the test setup and there where two holes in each beam as shown in Figure 3. Hence, two test were performed on the same beam. For these test series, tests 1 and 2 and tests 3 and 4 were performed on the same beam. The larger beams ($H = 630$ mm) were by means of a roller type of support stabilized in the weak direction at three points along the beam length. Photos of the hole and the LVDT sensors are for some tests shown in Figure 4. Photos of the test setups used for the nine different test series are shown in Figure 5.
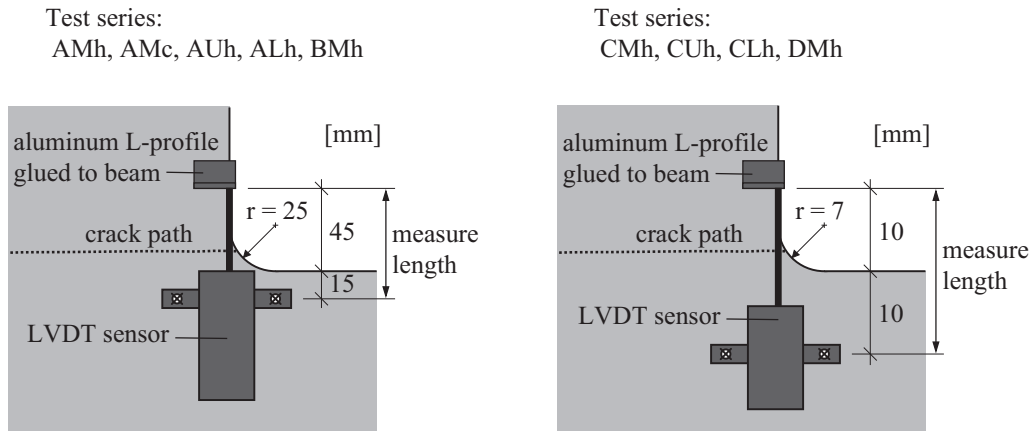
Figure 2: *Placement of LVDT sensors for measurement of deformation d.*
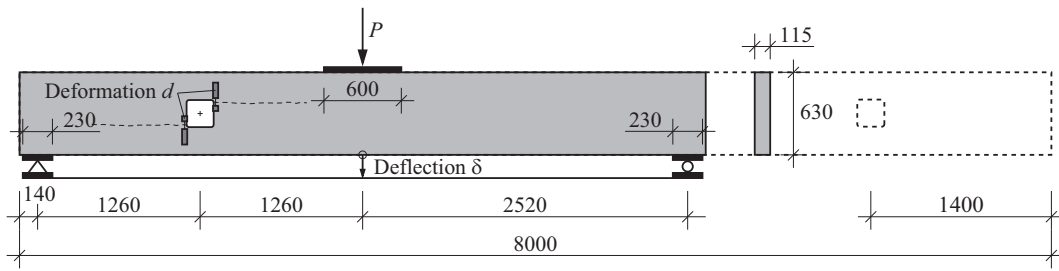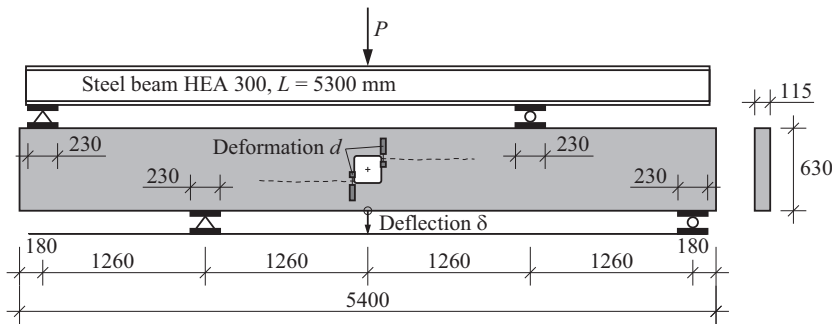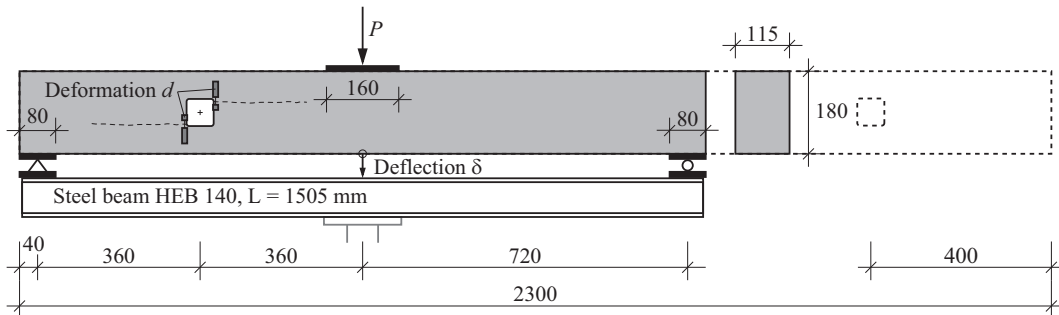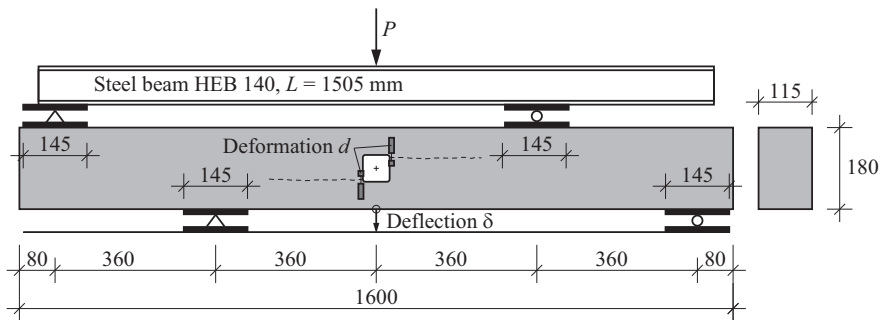
Figure 3: *Test setups with dimensions of glulam beams and steel parts.*
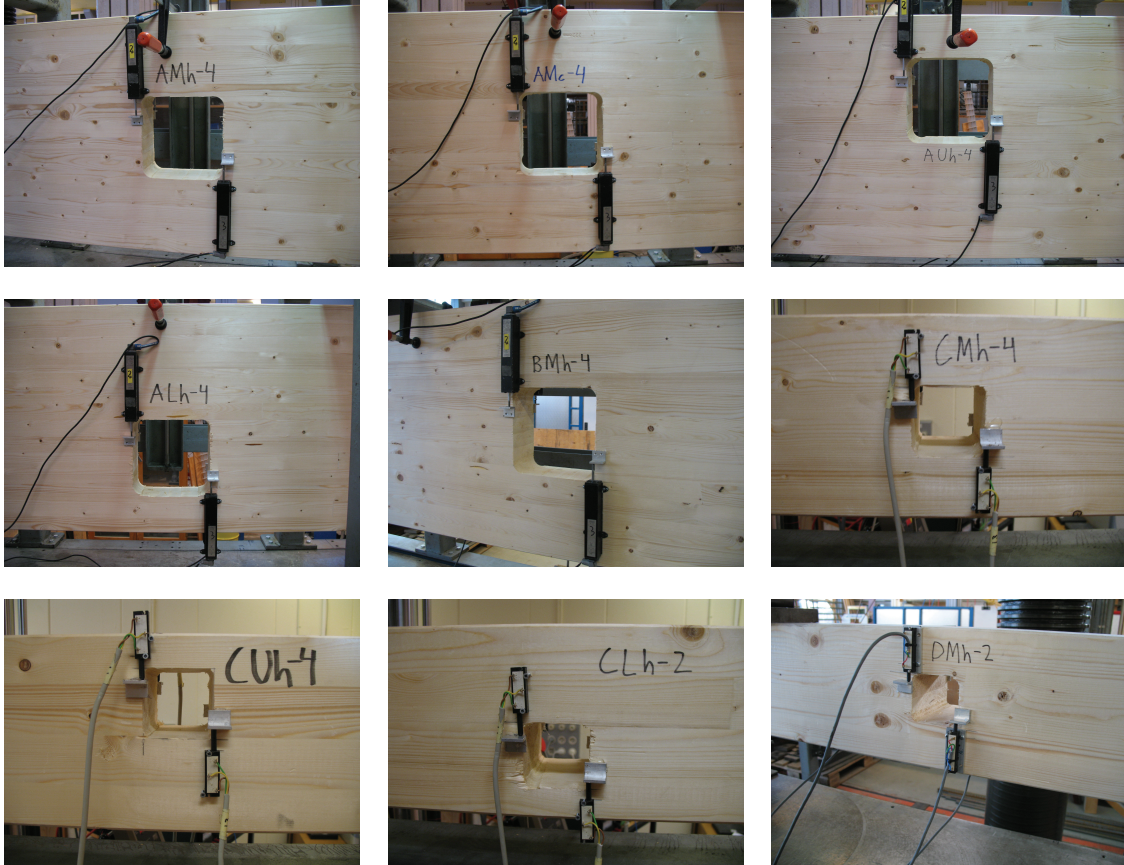
Figure 4: *Photos of the holes and LVDT sensors from test series: AMh, AMc and AUh (top); ALh, BMh and CMh (middle); CUh, CLh and DMh (bottom).*

Figure 5: *Photos of test setups used for test series AMh, AMc, AUh and ALh (top left); BMh (top right); CMh, CUh and CLh (bottom left) and DMh (bottom right).*

3 Materials

All glulam beams were produced and delivered by Töreboda Moelven AB. The beams were made of spruce (Lat. *Picea Abies*), glued with melamine-urea-formaldehyde (MUF) resin and delivered with pre-made holes. The lamella thickness was consistently 45 mm which means that there were 4 lamellae in the small beams (115×180 mm^2) and 14 lamellae in the large beams (115×630 mm^2). All small glulam beams were strength class homogeneous while both strength class homogeneous glulam and strength class combined glulam were represented among the large beams. The strength class combined glulam beams were produced with the three outmost lamellae on each side of lamination strength class LS22 and the remaining eight of lamination strength class LS15. The strength class homogeneous glulam beams were produced with lamination strength class LS22 throughout the entire beam cross section. The lamellae compositions of the cross sections are illustrated in Figure 6 and the material properties for these lamination strength classes are presented in Table 2. These material properties correspond to the requirements of lamella material properties for the different glulam strength classes in SS-EN 1194 [4]. There were no obvious differences in the average width of the growth rings, in the number of knots or any other visually observable property between the two lamination strength classes.

Table 2: *Material properties for lamination strength classes according to [3].*

		LS15	LS22
Characteristic tensile strength	[MPa]	14.5	22
Mean tensile Young's modulus	[MPa]	11 000	13 000
Density, 5th percentile	[kg/m^3]	350	390

The strength class homogeneous glulam beams correspond to glulam strength class GL32h according to SS-EN 1194 [4]. The strength class combined glulam beams correspond to the glulam strength class L40 according to Swedish BKR [2] and this class is usually considered to correspond to GL32c although this class should be composed of LS22 and LS18 according to SS-EN 1194.

The nominal beam cross section sizes 115×180 mm^2 and 115×630 mm^2 are used throughout this report although the real cross section sizes were measured to 114×178 mm^2 and 114×628 mm^2 respectively at moisture content corresponding to the moisture content at the time of testing. Figure 6 shows the arrangement and relative growth ring orientation of the lamellae in the cross sections and also the location of the holes in relation to the location of the glue lines. The placement of the holes and the direction of load was random with respect to the orientation of the growth rings. The holes were not perfectly shaped according to the dimensions in Table 1 although there were no major discrepancies. The corners of the holes in the small beams were however not ideally quarter circular in shape. The hole surfaces were not smoothed in any way.
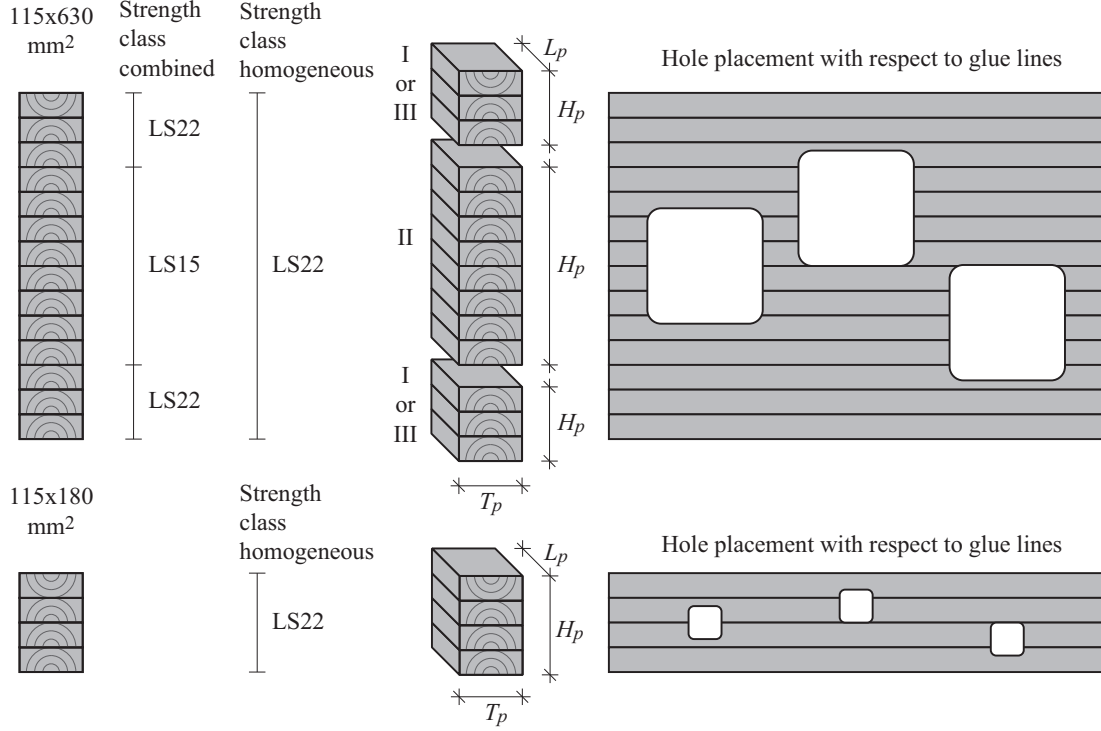
Figure 6: *Illustration of beam cross section composition and hole placement.*

The beams were delivered wrapped in plastic cover and with a moisture content believed to be approximately 12 %. From the time of delivery to the time of testing the beams were kept indoors in a climate of about 20 °C and 35 % RH. The beams were kept in the plastic covers until about ten minutes before testing in order to reduce the risk of any drying and development of any moisture gradient in the material. The moisture content u at time of testing and the density ρ were determined from samples of the tested beams. This was carried out by cutting a piece of length about 100 mm from the beam cross section. The pieces from the large beams where then cut into smaller pieces denoted I, II and III according to Figure 6. The volume V_{test} was determined by measuring the side lengths T_p, H_p and L_p and the mass at time of testing m_{test} was also determined. The pieces were then left to dry in a temperature of 105 °C until the mass was constant and the moisture content was considered to be zero. The moisture content u were for the individual parts determined according to Equation (1) and the mean value according to the same equation with the masses m_{test} and m_{dry} replaced by $\sum m_{test}$ and $\sum m_{dry}$ respectively. The density was determined in the same manner according to Equation (2). The measured data, the moisture content u and the density ρ are presented in Table 3.

$$u \ = \ \frac{m_{test} - m_{dry}}{m_{dry}} \qquad [\text{kg/kg] or [\%}] \tag{1}$$

$$\rho \ = \ \frac{m_{test}}{V_{test}} \qquad [\text{kg/m}^3] \tag{2}$$

Table 3: *Measured data, density ρ and moisture content u at time of testing.*

Test series	no.	piece	T_p [mm]	H_p [mm]	L_p [mm]	m_{test} [g]	m_{dry} [g]	u [%]	ρ [kg/m³]	
AMh	1,2	I	114	134	100	714.7	638.4	11.95	467.9	
		II	114	359	100	1850.4	1656.7	11.69	452.1	
		III	114	132	99	655.4	593.8	10.37	439.9	
AMh	3,4	I	114	132	100	625.2	565.6	10.54	415.5	
		II	114	359	102	1914.6	1719.3	11.36	458.6	
		III	114	133	101	641.2	579.7	10.61	418.7	
AMc	1,2	I	114	133	99	665.3	595.1	11.80	443.2	
		II	114	360	99	1802.2	1610.5	11.90		443.6*
		III	114	132	99	640.4	571.8	12.00	429.9	
AMc	3,4	I	114	134	98	711.2	633.6	12.25	475.1	
		II	114	360	99	1803.2	1607.1	12.20		443.8*
		III	114	131	100	681.9	610.3	11.73	456.6	
AUh	1,2	I	114	133	101	649.2	586.5	10.69	423.9	
		II	114	359	100	1889.3	1687.7	11.95	461.6	
		III	114	132	101	693.3	620.8	11.68	456.2	
AUh	3,4	I	114	133	102	722.6	649.7	11.22	467.2	
		II	114	360	102	1954.1	1751.5	11.57	466.8	
		III	114	132	101	721.5	648.8	11.21	474.7	
ALh	1,2	I	114	131	92	638.6	574.6	11.14	464.8	
		II	114	359	95	1857.7	1663.1	11.70	477.8	
		III	114	134	99	787.9	704.1	11.90	521.0	
ALh	3,4	I	114	130	94	671.6	601.3	11.69	482.1	
		II	114	359	96	1816.6	1629.5	11.48	462.4	
		III	114	134	99	797.8	709.5	12.45	527.5	
BMh	1	I	114	132	100	768.4	694.5	10.64	510.6	
		II	114	360	100	1876.6	1682.1	11.56	457.3	
		III	114	133	100	735.7	663.1	10.95	485.2	
BMh	2	I	114	133	98	702.2	631.8	11.14	472.6	
		II	114	359	99	1882.2	1675.9	12.31	464.5	
		III	114	132	99	704.6	633.2	11.28	473.0	
BMh	3	I	114	133	99	717.2	641.9	11.73	477.8	
		II	114	359	99	1781.6	1598.9	11.43	439.7	
		III	114	132	99	623.4	564.3	10.47	418.5	
BMh	4	I	114	133	101	765.0	686.1	11.50	499.6	
		II	114	360	99	1883.8	1688.8	11.55	463.7	
		III	114	131	99	749.4	668.4	12.12	506.9	
CMh	1,2		114	178	100	1021.2	908.7	12.38	503.3	
CMh	3,4		114	178	99	944.9	842.3	12.18	470.4	
CUh	1,2		114	178	99	987.6	879.7	12.27	491.6	
CUh	3,4		114	178	101	1065.9	946.9	12.57	520.1	
CLh	1,2		114	178	99	980.4	871.9	12.44	488.0	
CLh	3,4		114	178	100	1029.4	916.8	12.28	507.3	
DMh	1		114	178	99	948.0	845.3	12.15	471.9	
DMh	2		114	178	99	945.6	841.9	12.32	470.7	
DMh	3		114	178	99	960.3	854.6	12.37	478.0	
DMh	4		114	178	100	986.8	879.1	12.25	486.3	
mean								11.73	468.8	443.7*

* = lamination strength class LS15.

11

4 Results

Three different load levels are used to present and compare the test results:

Crack initiation shear force V_{c0}
Shear force at first crack development visually observable by the naked eye.

Crack shear force V_c
Shear force at the instant of crack development across the entire beam width.

Maximum shear force V_f
Shear force at instant of either a sudden crack propagation or a step-wise stable/unstable crack growth to the end of the beam.

The crack patterns for these load levels are illustrated in Figure 7 and some examples from the tests are given in Figures 8, 9 and 10 where dashed lines have been drawn under the cracks to emphasize their length and location.

The shear forces corresponding to the three definitions above are for all tests presented in Table 4 and Figures 11 and 12. The exact values of the presented shear forces were determined from visual observations during the testing with aid from the recorded beam deflection δ and the deformations d at the cracked corners of the hole. The crack initiation shear force V_{c0} is only given in the cases when there was a visually observable crack in the cross section before there was a crack spreading across the entire beam width at the given corner. The crack shear force V_c is given for both corner B and corner T for all tests. The length of the crack (in the beam length direction) at this level varies between the tests. For some tests, the crack was only one to a few centimeters in the length direction at this load level while other tests showed an instant crack propagation all the way to the end of the beam at this load level. The maximum shear force V_f is not given for test series BMh and DMh since the test setup for these test series is such that this load level is irrelevant. All forces refer to the shear force at hole center due to the externally applied load. The dead weights of the glulam beams are hence not taken into account. The dead weights of the steel beams used in test series BMh and DMh are however included in the presented loads.

The shear force V is plotted vs the beam deflection δ and the deformations d respectively in Figures 13 to 21 for all individual tests. The crack shear forces V_{cB} and V_{cT} for the individual tests are in these figures indicated in by dotted lines. The deformation d_B corresponds to the measurements from the LVDT sensors at corner B and d_T corresponds to measurements at corner T. Some plots lack deformations from one or more of the LVDT sensors at the corners of the holes due to technical problems. The beam deflections δ for test series CMh, CUh and CLh are presented as measured and is hence not compensated for the deflection in the steel beam (approximately 1 mm at $V = 30$ kN) used in the test setup.
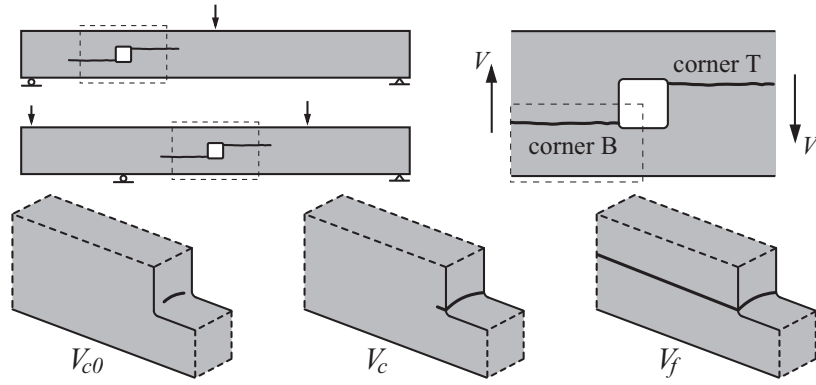
Figure 7: *Illustration of crack patterns for defined load levels.*
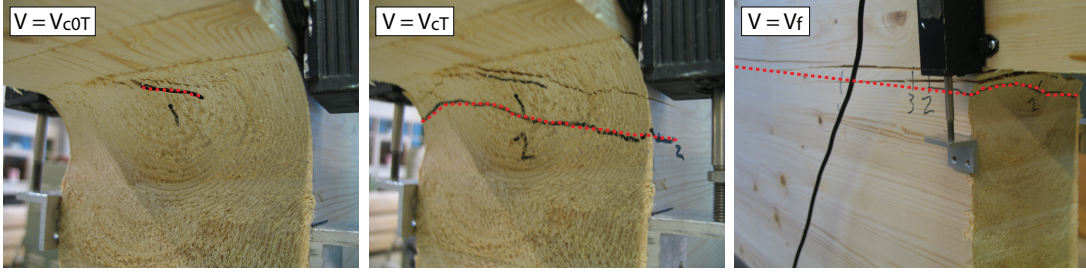
Figure 8: *Photos of crack patterns for corner T of ALh-4.*
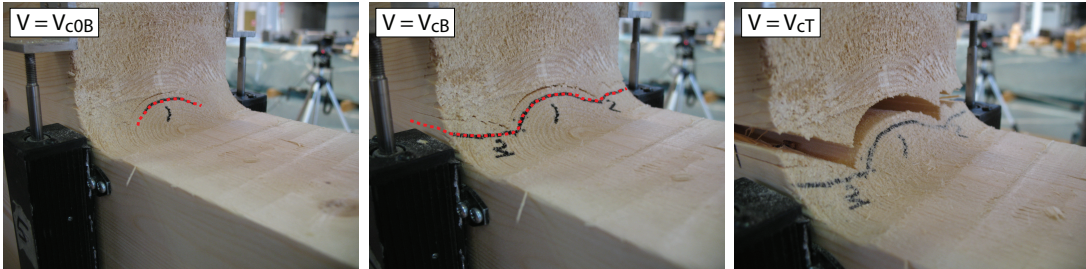
Figure 9: *Photos of crack patterns for corner B of BMh-4.*
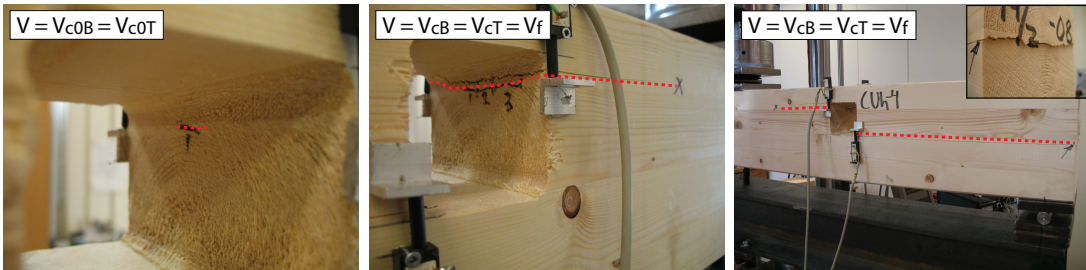
Figure 10: *Photos of crack patterns for CUh-4.*

13

Table 4: *Shear forces V for all test series.*

		V_{c0} [kN]				V_c [kN]				V_f [kN]	
		V_{c0B}	V_{c0T}	min		V_{cB}	V_{cT}	min			
AMh	1					47.6	45.7	45.7		52.1	
	2	47.5	47.5	47.5		71.4	64.4	64.4		71.4	
	3		42.0	42.0		58.4	58.4	58.4		58.4	
	4					60.5	60.5	60.5		60.5	
	mean (std)			44.8	(3.9)			57.3	(8.1)	60.6	(8.0)
AMc	1	61.0		61.0		64.3	64.3	64.3		64.3	
	2	48.0	44.4	44.4		49.7	51.3	49.7		63.6	
	3	45.0	40.0	40.0		51.2	51.2	51.2		52.8	
	4					49.1	47.7	47.7		54.4	
	mean (std)			48.5	(11.1)			53.2	(7.5)	58.8	(6.0)
AUh	1		28.6	28.6		59.2	57.6	57.6		59.2	
	2					51.6	59.0	51.6		60.5	
	3		55.1	55.1		56.2	56.2	56.2		56.2	
	4	47.5	54.6	47.5		57.4	57.4	57.4		57.4	
	mean (std)			43.7	(13.6)			55.7	(2.8)	58.3	(1.9)
ALh	1	50.2	41.5	41.5		53.9	50.2	50.2		58.9	
	2		43.7	43.7		54.5	52.1	52.1		69.6	
	3		40.0	40.0		64.8	53.2	53.2		64.8	
	4		39.5	39.5		57.0	44.6	44.6		69.8	
	mean (std)			41.2	(1.9)			50.0	(3.8)	65.8	(5.1)
BMh	1		51.9	51.9		61.3	61.3	61.3		-	
	2	59.4	49.0	49.0		65.7	65.7	65.7		-	
	3	61.4	56.0	56.0		62.1	62.1	62.1		-	
	4	48.5		48.5		59.7	68.7	59.7		-	
	mean (std)			51.4	(3.4)			62.2	(2.5)		
CMh	1	20.6	20.6	20.6		27.3	27.3	27.3		27.3	
	2	24.1	23.3	23.3		24.9	24.9	24.9		29.5	
	3	23.1	17.9	17.9		24.4	23.1	23.1		25.3	
	4	24.4	24.4	24.4		27.0	27.0	27.0		27.0	
	mean (std)			21.6	(2.9)			25.6	(2.0)	27.3	(1.7)
CUh	1	24.0	18.8	18.8		25.3	25.3	25.3		25.3	
	2		19.0	19.0		23.2	22.5	22.5		25.3	
	3	20.5	20.5	20.5		23.3	23.3	23.3		23.3	
	4	16.7	16.7	16.7		22.3	22.3	22.3		22.3	
	mean (std)			18.8	(1.6)			23.4	(1.4)	23.6	(2.2)
CLh	1		17.5	17.5		23.1	22.3	22.3		26.9	
	2	19.2	19.2	19.2		23.7	23.7	23.7		29.5	
	3	21.8	23.4	21.8		24.3	24.3	24.3		25.5	
	4					21.8	21.8	21.8		24.5	
	mean (std)			19.5	(2.2)			23.0	(1.2)	26.6	(2.2)
DMh	1	26.0	26.0	26.0		29.1	29.1	29.1		-	
	2					25.3	25.3	25.3		-	
	3	23.3		23.3		25.3	25.3	25.3		-	
	4	25.4	22.6	22.6		26.7	28.1	26.7		-	
	mean (std)			24.0	(1.8)			26.6	(1.8)		
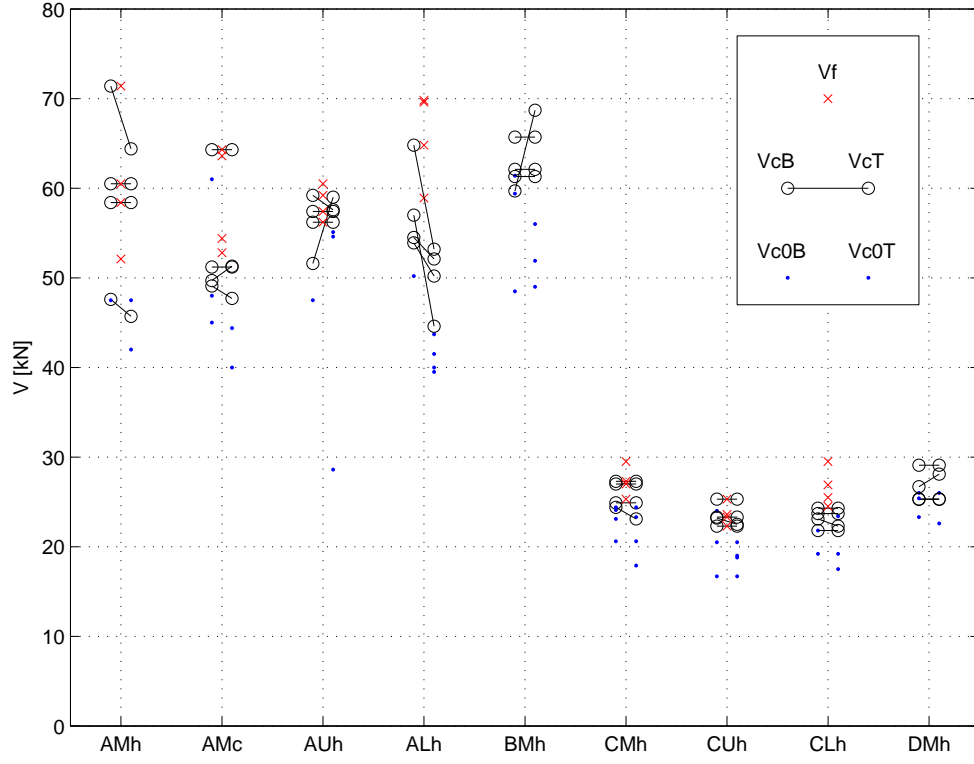
Figure 11: *Shear force V for all test series.*
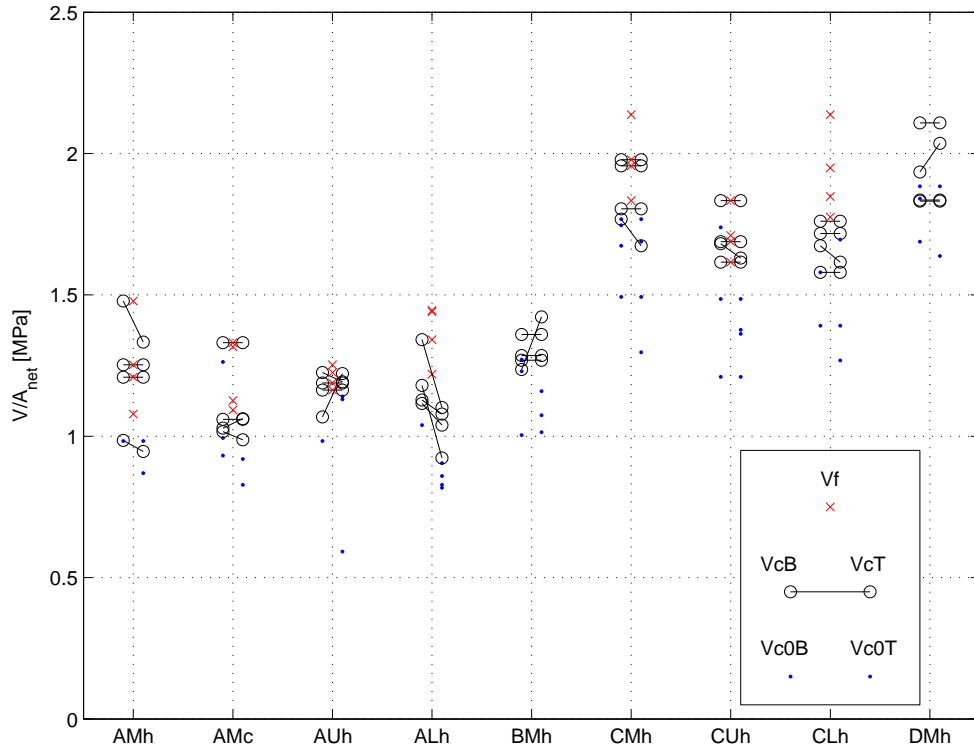
Figure 12: *Mean shear stress* $\tau = V/A_{net} = V/((H-b)T)$ *for all test series.*

15
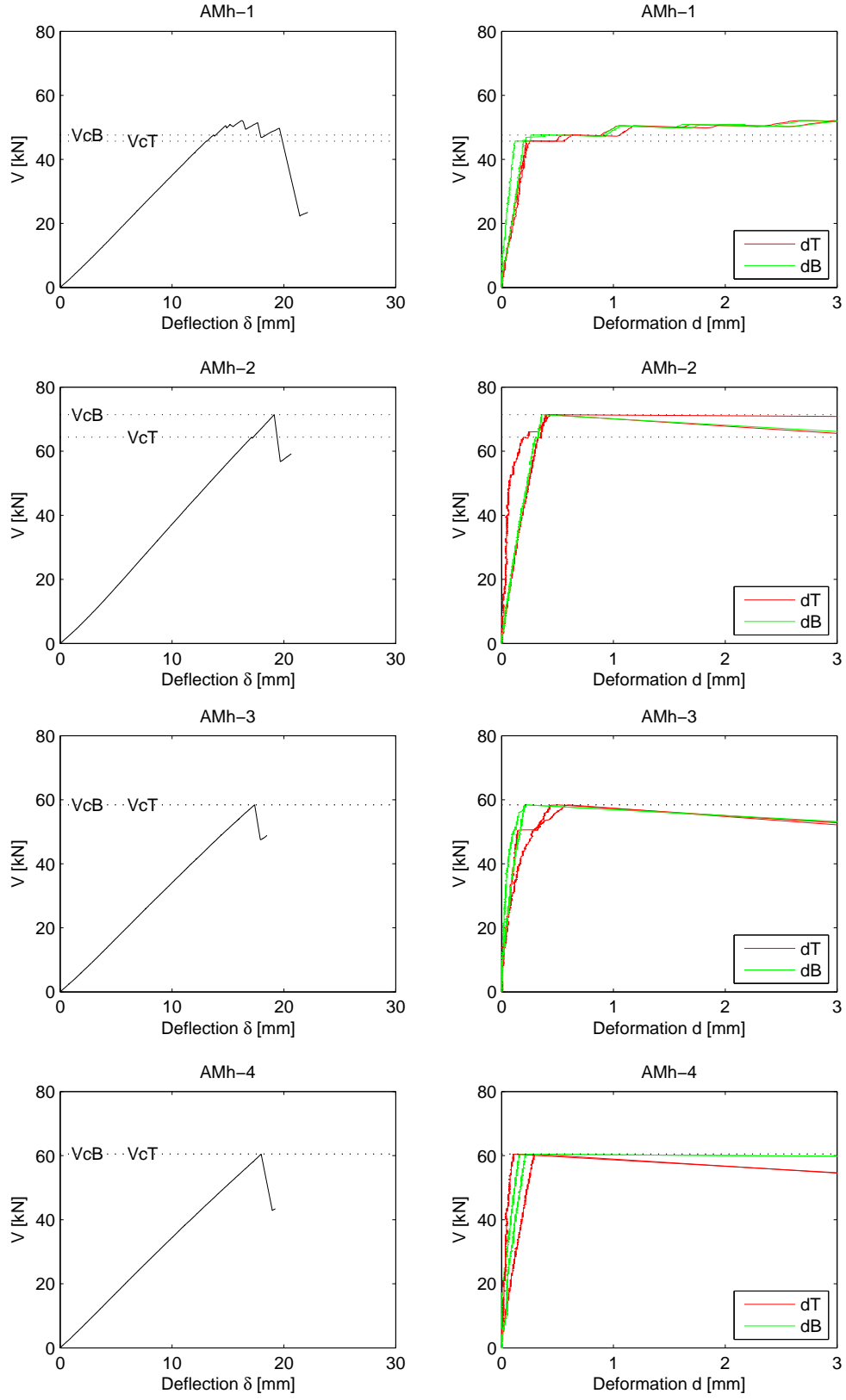
Figure 13: *Deflection δ and deformations d for test series AMh.*
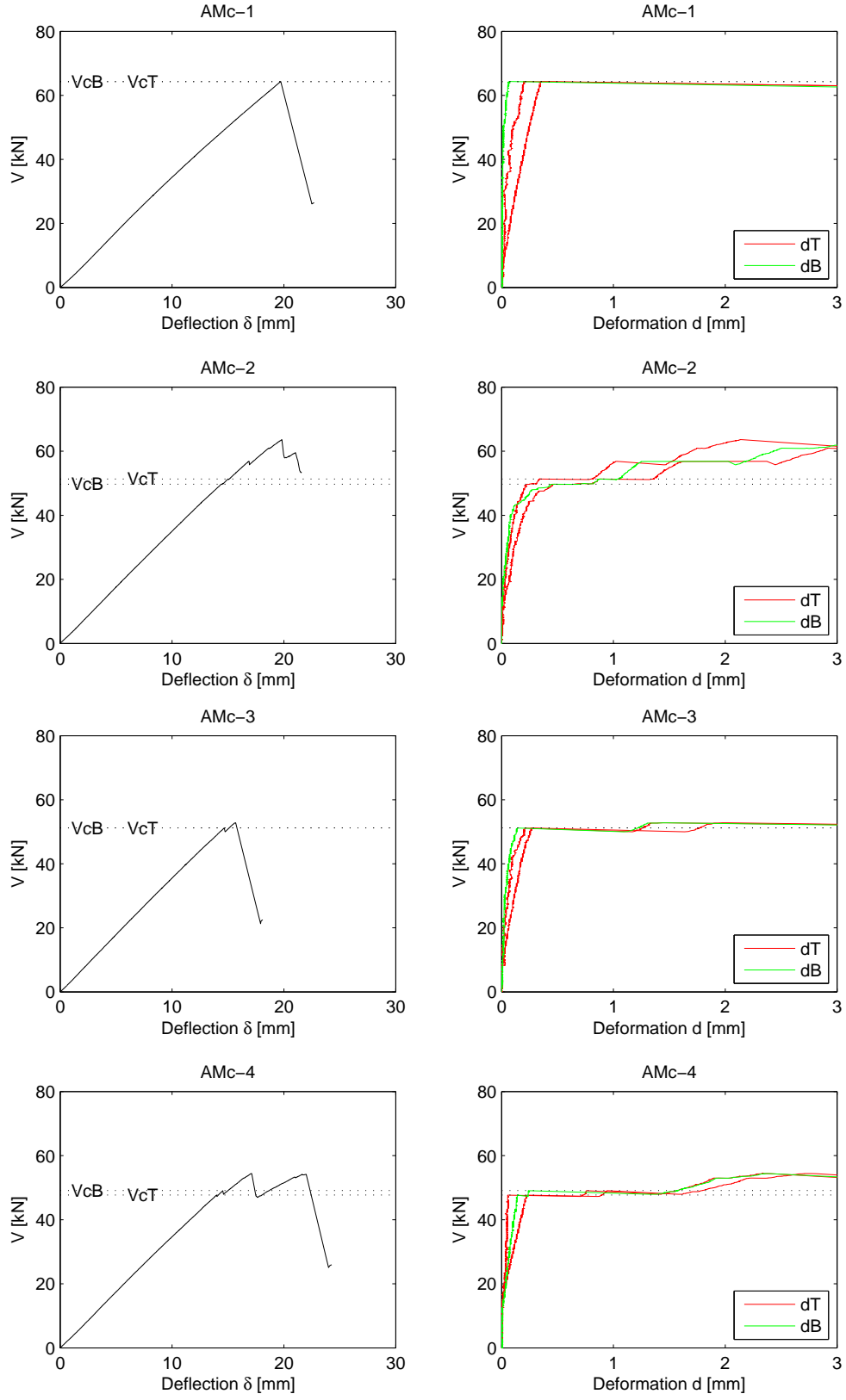
Figure 14: *Deflection δ and deformations d for test series AMc.*
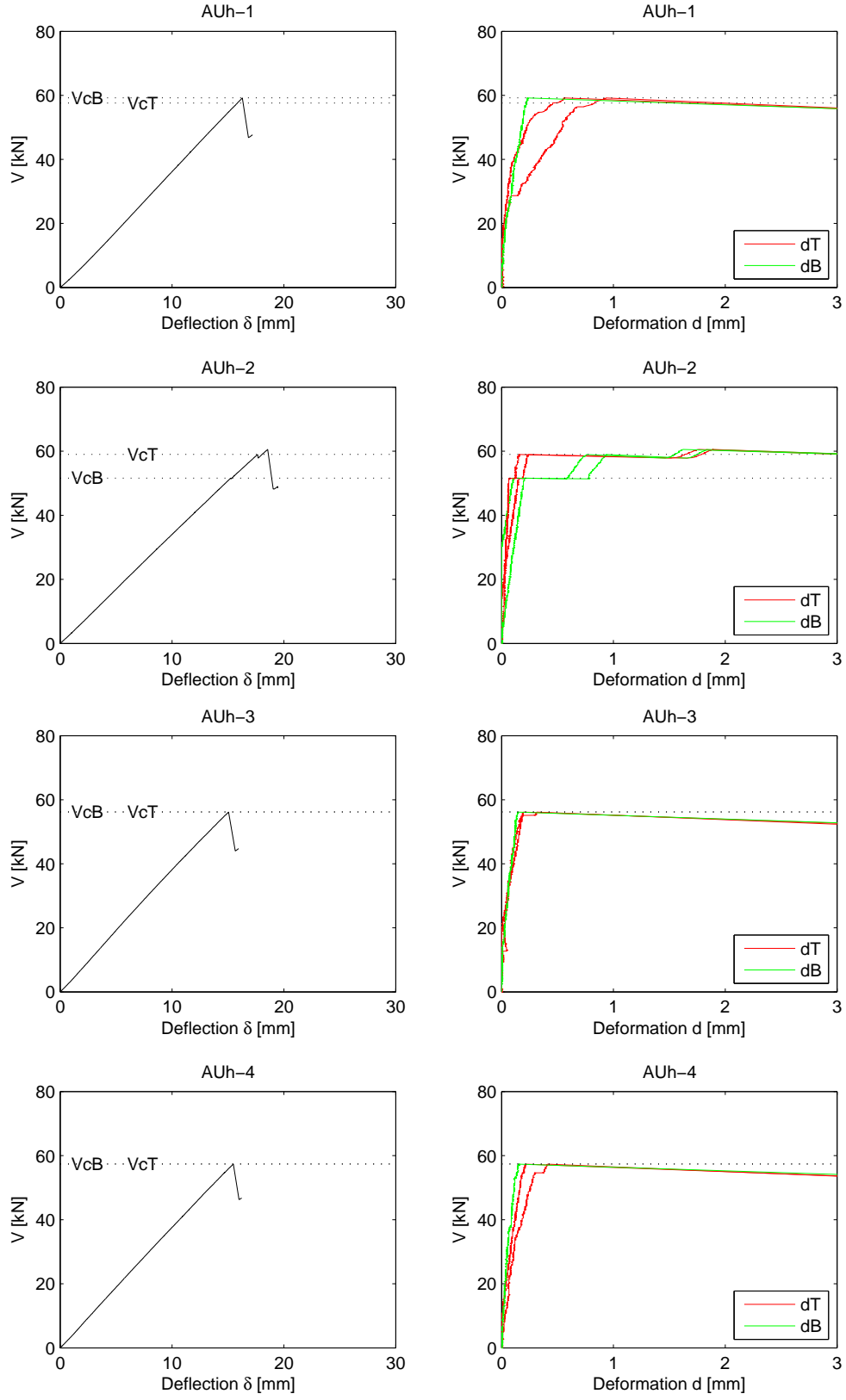
Figure 15: *Deflection δ and deformations d for test series AUh.*

18
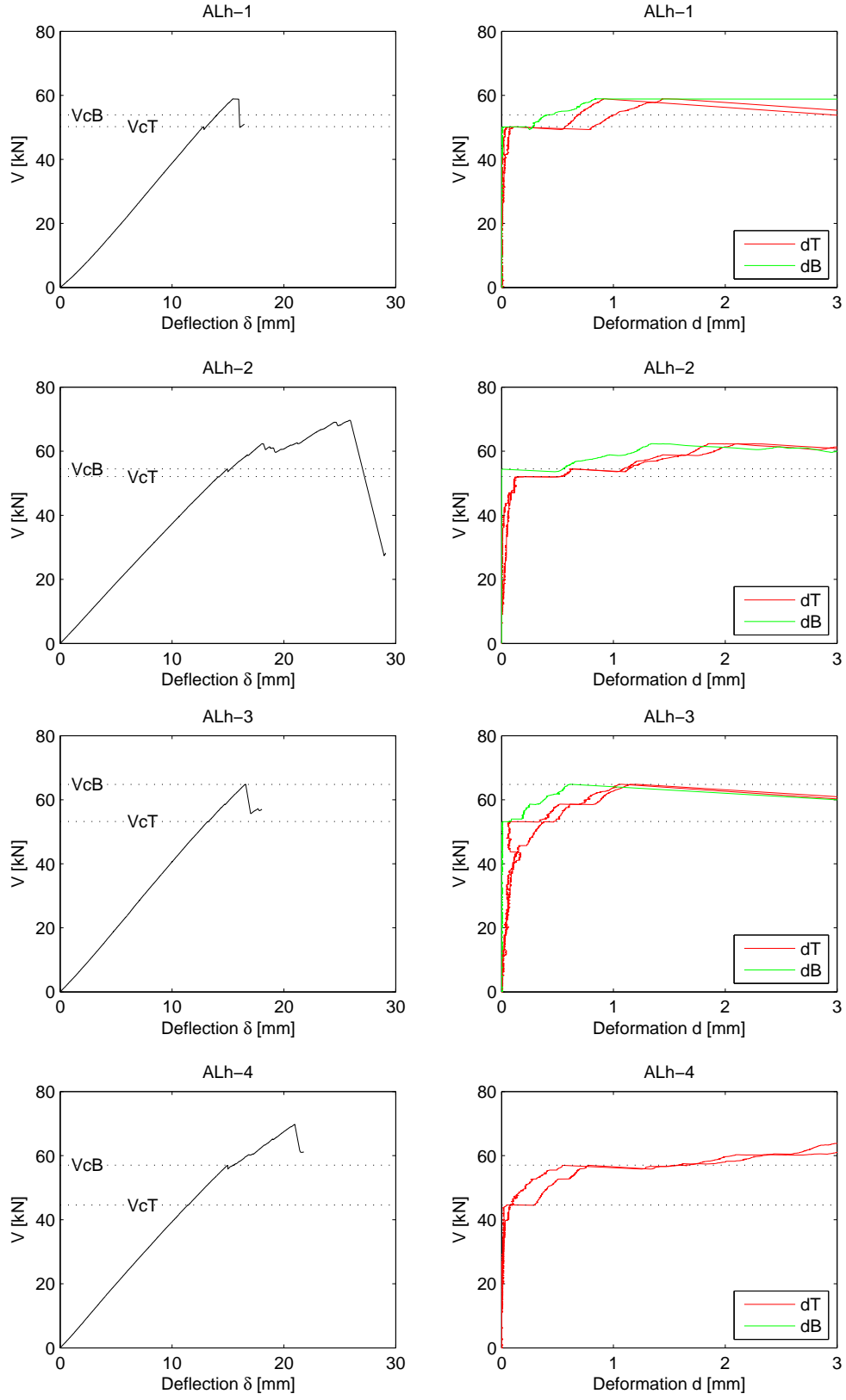
Figure 16: *Deflection δ and deformations d for test series ALh.*

19
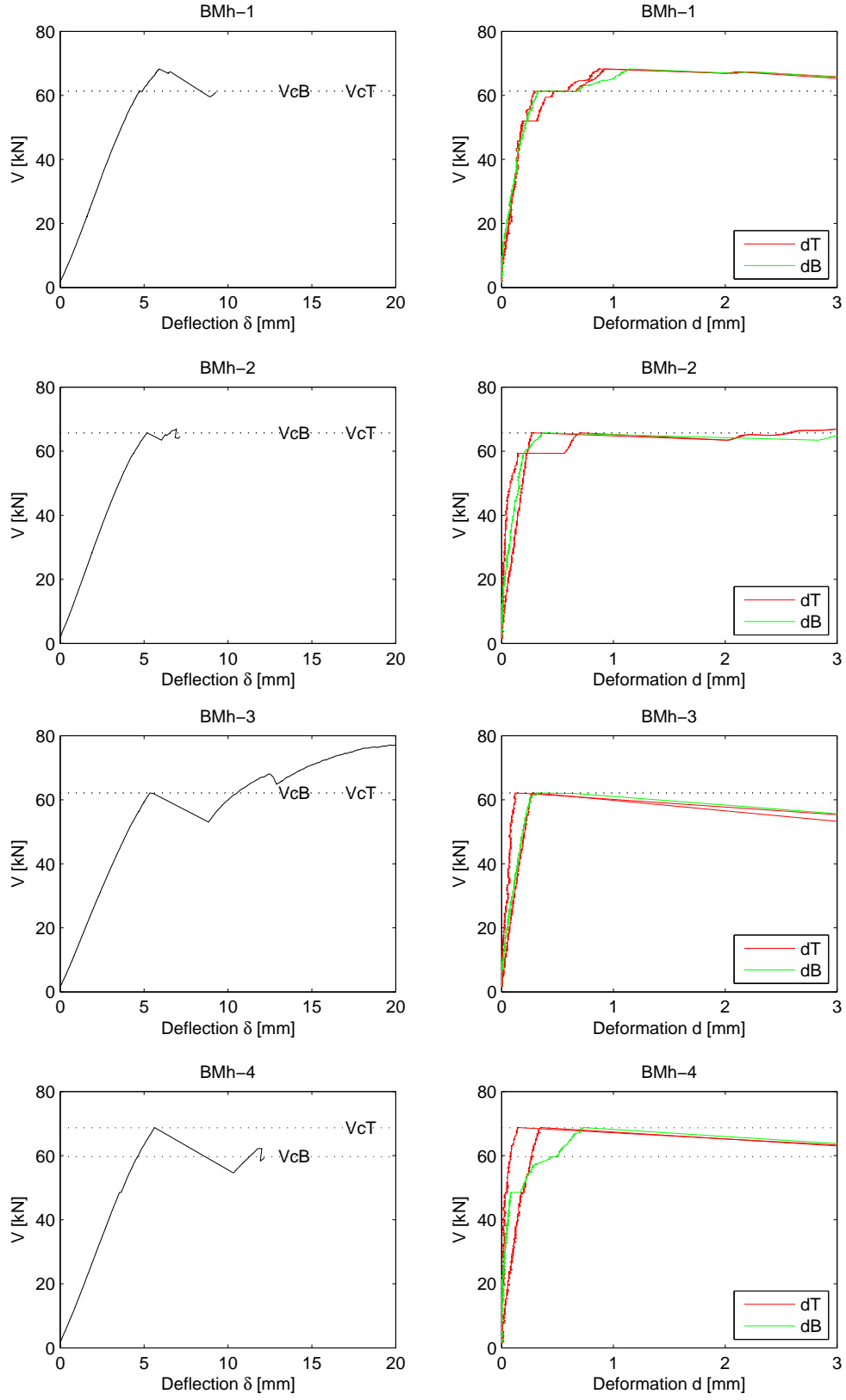
Figure 17: *Deflection δ and deformations d for test series BMh.*
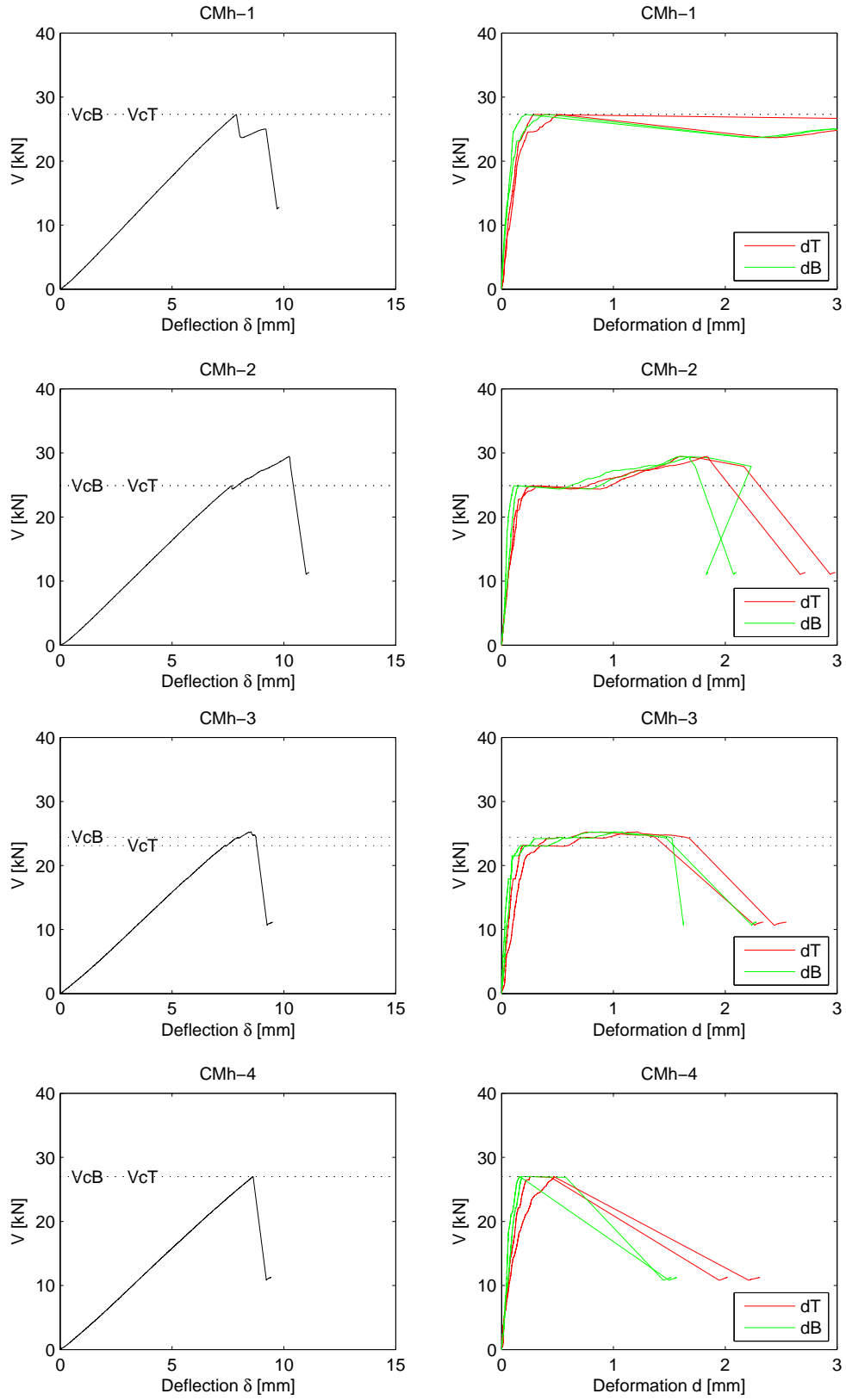
Figure 18: *Deflection δ and deformations d for test series CMh.*
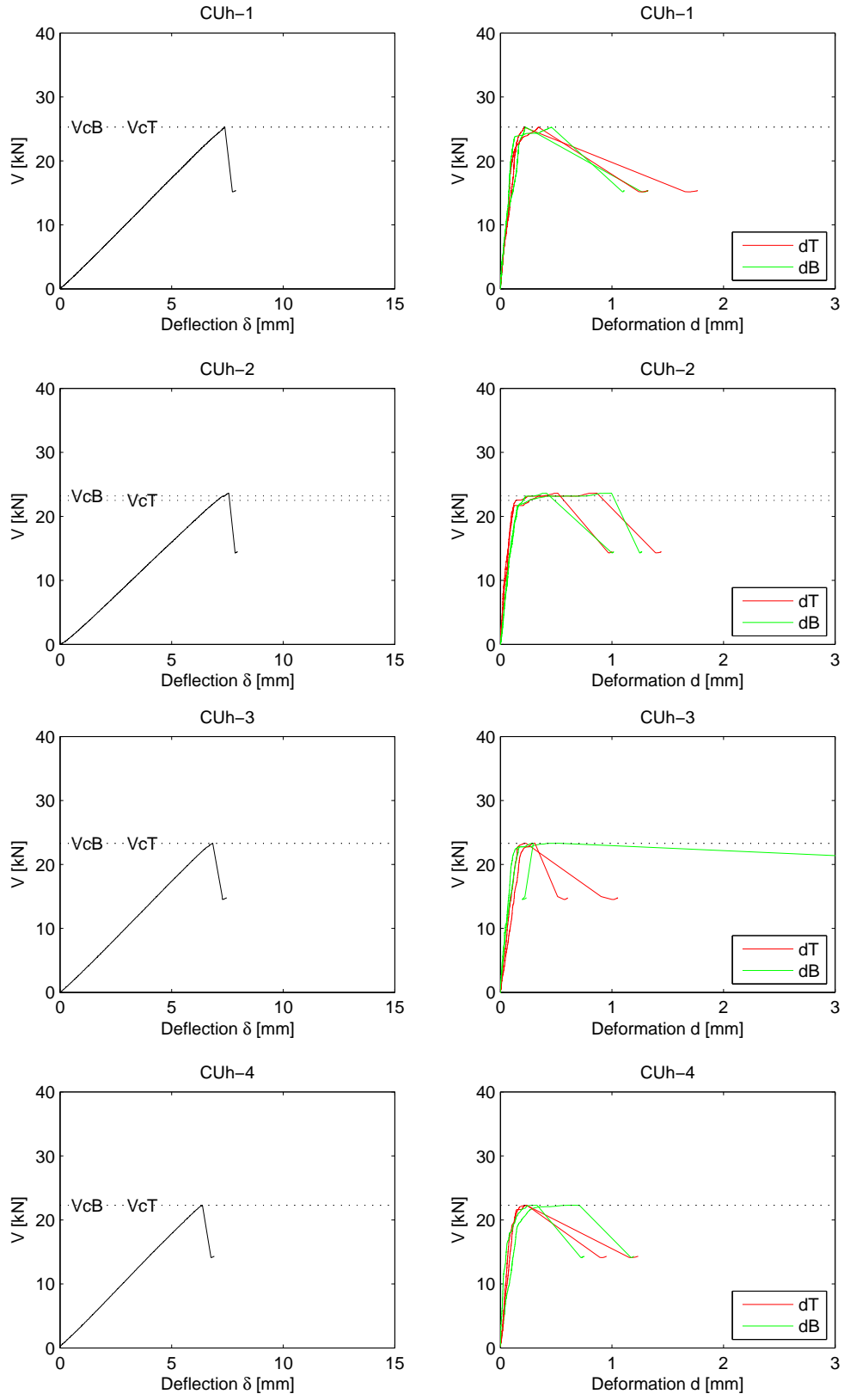
Figure 19: *Deflection δ and deformations d for test series CUh.*
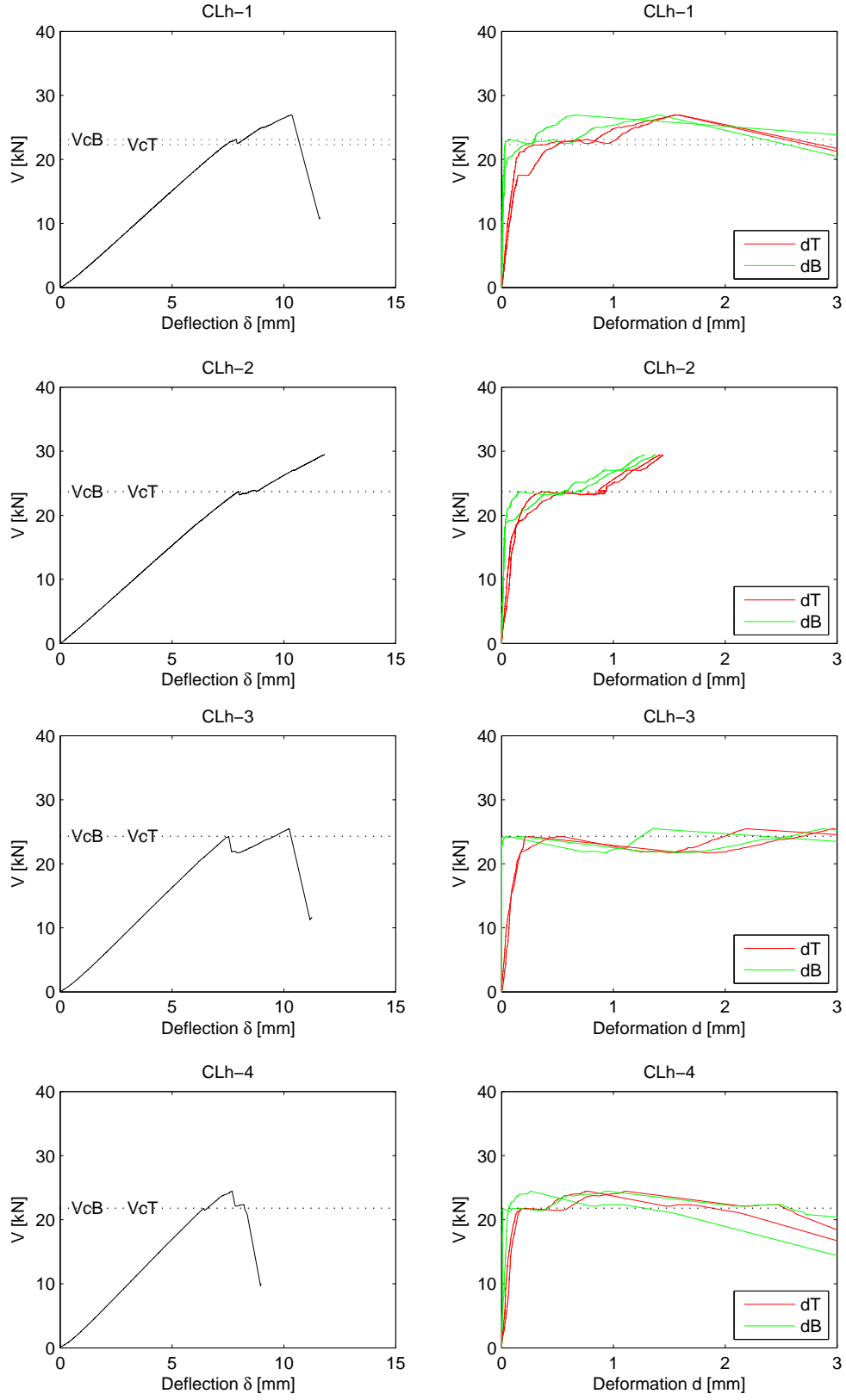
Figure 20: *Deflection δ and deformations d for test series CLh.*
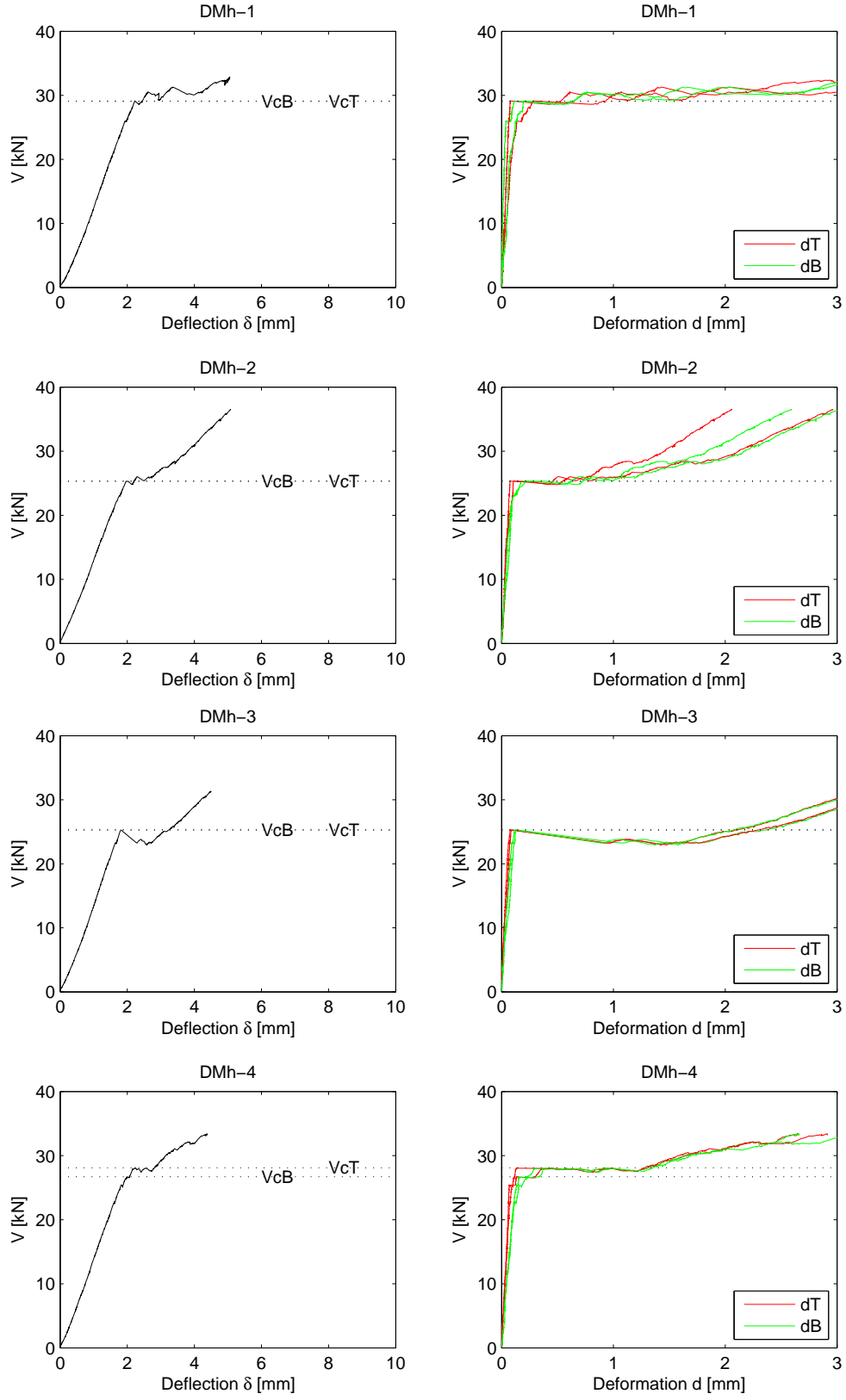
Figure 21: *Deflection δ and deformations d for test series DMh.*

5 Concluding remarks

Some comments on the test results concerning the influence of the four investigated design parameters are listed below.

Beam size
    The test results indicate a strong beam size effect on the relative strength as can be seen in Figure 12. Increasing the beam size by a factor 3.5 gave about 30-35 % reduction in nominal shear stress V/A_{net} at the instant of crack development across the entire beam width.

Hole placement with respect to beam height
    Slightly lower (approximately 5-15 % considering mean values) crack shear forces V_c were found for the beams with eccentrically placed holes compared to the beams with centrically placed holes. There is furthermore another interesting difference concerning the beams with eccentrically placed holes. Both among the large and the small beams the tests generally showed a more sudden crack propagation all the way to the end of beam for the beams with the hole placed in the upper part of the beam (test series AUh and CUh) compared to the beams with the hole placed in the lower part of the beam (test series ALh and CLh).

Material Strength Class
    There was no significant difference in the behavior between the material strength class homogeneous beams of test series AMh and the strength class combined beams of test series AMc. The results of these two test series are however comparatively scattered.

Bending moment to shear force ratio
    For beams with centrically placed holes, two different bending moment to shear force ratios were investigated. The beams with holes placed in a position of zero bending moment (test series BMh and DMh) shows on average slightly higher (approximately 5-10 % considering mean values) crack shear forces V_c compared to the beams with holes placed in a position of combined bending moment and shear force (test series AMh and CMh).

The scatter in the strength between nominally equal tests within a test series is not very large, the coefficient of variation of V_c being from 4 % to 14 % with an average of 8 %.

The test results furthermore show that it is more frequent with crack development across the entire beam width (V_c) at the upper corner T before the lower corner B than the other way around. The most frequent scenario is however that cracks develop simultaneously at both corners. The most common place for crack initiation (V_{c0}) is in the middle of the beam width although some tests showed a crack initiation all the way to one side of the beam width.

References

[1] Danielsson H.
The Strength of Glulam Beams with Holes – A Survey of Tests and Calculation Methods
Report TVSM-3068, Division of Structural Mechanics, LTH, Lund University, 2007.

[2] Boverket
(The National Board of Housing, Building and Planning)
Regelsamling för konstruktion – Boverkets konstruktionsregler BKR.
(Design Regulations)
Elanders Gotab, Vällingby, 2003.

[3] SP Sveriges Provnings- och Forskningsinstitut
(SP Swedish National Testing and Research Institute)
Lamination strength classes for glued laminated timber according to EN 1194.
PM, 2002-06-14.

[4] SS-EN 1194:1999
Träkonstruktioner – Limträ – Hållfasthetsklasser och bestämning av karakteristiska värden.
(Glued laminated timber – Strength classes and determination of characteristic values.)
SIS Förlag, Stockholm, 2000.

Paper B

Strength of Glulam Beams with Holes –
Tests of Quadratic Holes and Literature Test Results Compilation

Henrik Danielsson and Per Johan Gustafsson

**INTERNATIONAL COUNCIL FOR RESEARCH AND INNOVATION
IN BUILDING AND CONSTRUCTION**

WORKING COMMISSION W18 - TIMBER STRUCTURES

STRENGTH OF GLULAM BEAMS WITH HOLES –
TESTS OF QUADRATIC HOLES AND
LITERATURE TEST RESULT COMPILATION

H Danielsson

P J Gustafsson

Division of Structural Mechanics, Lund University

SWEDEN

MEETING FORTY ONE

ST. ANDREWS

CANADA

AUGUST 2008

Strength of Glulam Beams with Holes – Tests of Quadratic Holes and Literature Test Result Compilation

Henrik Danielsson and Per Johan Gustafsson

Division of Structural Mechanics, Lund University, Sweden

1 Background

Looking at design recommendations for glulam beams with holes in European timber engineering codes over the last decades, it can be seen that the strength design has been treated in many different ways. The theoretical backgrounds on which the recommendations are based shows fundamental differences and there are major discrepancies between the strength estimations according to the different codes as well as between tests and estimations according to codes [5]. The contemporary version of Eurocode 5 [7] does not state any equations concerning design of glulam beams with holes and the recommendations in the German code DIN 1052 [3] concerning rectangular holes were withdrawn during the fall of 2007. The absence of design recommendations indicates a need for further investigations of the subject. There are, however, several tests found in the literature concerning the strength of glulam beams with holes. Two of the most recent and more comprehensive studies were presented by Höfflin in 2005 [10] and by Aicher and Höfflin in 2006 [1]. These studies dealt exclusively with beams with circular holes. Although the test results found in literature all in all represent much work, important parameters such as mode of loading, beam size and hole placement have often been varied only within a very limit range. Among other limitations, it seems that all available test results relate to glulam beams with holes that are centrically placed with respect to the beam height [5].

2 Strength tests of glulam beams with quadratic holes

2.1 Test series and test setups

Experimental tests of the strength of glulam beams with quadratic holes have been carried out at the Division of Structural Mechanics at Lund University and they are in detail reported in [6]. The study comprised investigations of four design variables: *bending moment to shear force ratio at hole center*, *material strength class*, *beam size effect* and the previously overlooked design variable of *hole placement with respect to beam height*. Two different test setups were used to investigate the influence of bending moment to shear force ratio. Three different hole placements were used for one of the test setups to investigate the influence of hole placement with respect to beam height. The size effect was investigated for each combination of test setup and hole placement by using two test series with a scale factor of 3.5 for the length and height dimensions while the width was kept constant. All holes had rounded corners and a side length equal to 1/3 of the beam height. Altogether, the study consists of nine separate test series with four nominally equal tests in each series according to Table 1 and Figure 1.

Table 1: *Description of test series.*

Test series	Number of tests	Test setup	Hole placement	Strength class type	Beam size $T \times H$ [mm]	Hole size $a \times b$ [mm]	r [mm]
AMh	4	1	Middle	homogeneous	115×630	210×210	25
AMc	4	1	Middle	combined	115×630	210×210	25
AUh	4	1	Upper	homogeneous	115×630	210×210	25
ALh	4	1	Lower	homogeneous	115×630	210×210	25
BMh	4	2	Middle	homogeneous	115×630	210×210	25
CMh	4	1	Middle	homogeneous	115×180	60×60	7
CUh	4	1	Upper	homogeneous	115×180	60×60	7
CLh	4	1	Lower	homogeneous	115×180	60×60	7
DMh	4	2	Middle	homogeneous	115×180	60×60	7

Figure 1: *Test setups and hole placements.*

2.2 Materials

The beams were all made of spruce (Lat. *Picea Abies*) and glued with melamine-urea-formaldehyde (MUF) resin. The lamella thickness was consistently 45 mm. All beams except the beams of test series AMc were of strength class homogeneous glulam. The strength class combined beams of test series AMc were composed of lamination strength class LS22 in the three outmost lamellae on each side and of lamination strength class LS15 in the remaining eight lamellae. The strength class homogeneous glulam beams were composed of lamination strength class LS22 throughout the entire beam height. The requirements on the two lamination strength classes are stated in [15] as: characteristic tensile strength, 14.5 and 22 MPa; mean tensile Young's modulus, 11 000 and 13 000 MPa and density (5th percentile), 350 and 390 kg/m^3 for LS15 and LS22, respectively. The homogeneous beams correspond to the requirements in SS-EN 1194 [16] for glulam strength class GL 32h. The strength class combined beams correspond to the Swedish strength class L40. The mean value of the moisture content at the time of testing was measured to 11.7 % and the mean densities for the two different lamination strength classes was measured to 444 kg/m^3 and 469 kg/m^3 for LS15 and LS22, respectively.

2.3 Test Results

Three different load levels are used to present and compare the test results according to the definitions in Figure 2. The test results are presented in Figure 3 and in Table 2. The crack initiation shear force V_{c0} is only given in the cases when there was a visually observable crack in the cross section before there was a crack spreading across the entire beam width at the given corner. The crack shear force V_c is given for both corner B and corner T for all tests. The maximum shear force V_f is not given for test series BMh and DMh since the test setup for these test series is such that this load level is irrelevant.

Crack initiation shear force V_{c0}
Shear force at first crack development visually observable by the naked eye.

Crack shear force V_c
Shear force at the instant of crack development across the entire beam width.

Maximum shear force V_f
Shear force at instant of either a sudden crack propagation or a step-wise stable/unstable crack growth to the end of the beam.

Figure 2: *Definitions and illustrations of load levels.*

Figure 3: *Shear forces V for the three load levels and all tests in all nine test series.*

3

Table 2: *Beam cross section, hole size, hole placement, bending moment to shear force ratio and test results for the three defined load levels for all tests in all nine test series.*

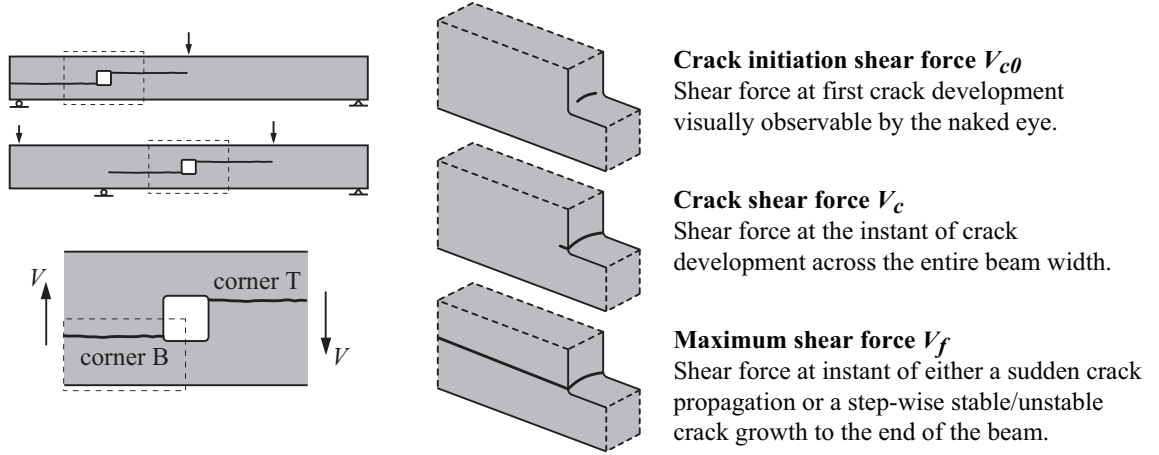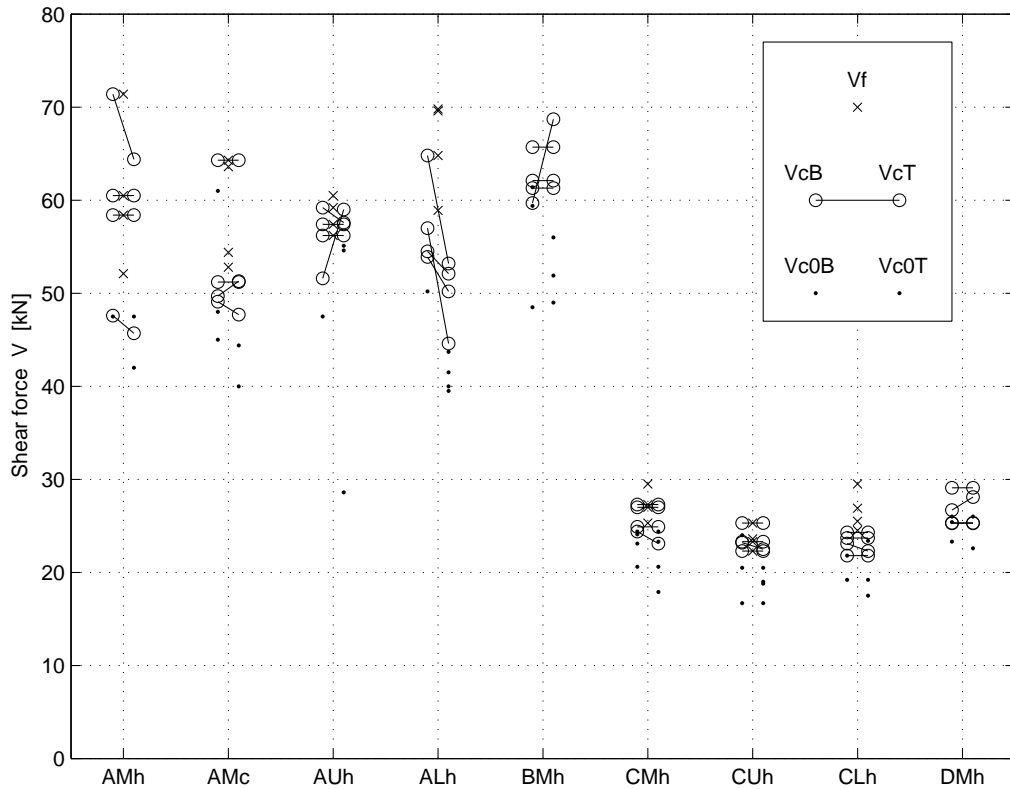| Test series	$T \times H$	$a \times b$	r	hole placement	$\frac{M}{VH}$		V_{c0}			V_c			V_f
							V_{c0B}	V_{c0T}	min	V_{cB}	V_{cT}	min	
	[mm]	[mm]	[mm]		[-]		[kN]	[kN]	[kN]	[kN]	[kN]	[kN]	[kN]
AMh	115×630	210×210	25	middle	2.0	1				47.6	45.7	45.7	52.1
						2	47.5	47.5	47.5	71.4	64.4	64.4	71.4
						3		42.0	42.0	58.4	58.4	58.4	58.4
						4				60.5	60.5	60.5	60.5
						mean			44.8			57.3	60.6
						(std)			(3.9)			(8.1)	(8.0)
AMc	115×630	210×210	25	middle	2.0	1	61.0		61.0	64.3	64.3	64.3	64.3
						2	48.0	44.4	44.4	49.7	51.3	49.7	63.6
						3	45.0	40.0	40.0	51.2	51.2	51.2	52.8
						4				49.1	47.7	47.7	54.4
						mean			48.5			53.2	58.8
						(std)			(11.1)			(7.5)	(6.0)
AUh	115×630	210×210	25	upper	2.0	1		28.6	28.6	59.2	57.6	57.6	59.2
						2				51.6	59.0	51.6	60.5
						3		55.1	55.1	56.2	56.2	56.2	56.2
						4	47.5	54.6	47.5	57.4	57.4	57.4	57.4
						mean			43.7			55.7	58.3
						(std)			(13.6)			(2.8)	(1.9)
ALh	115×630	210×210	25	lower	2.0	1	50.2	41.5	41.5	53.9	50.2	50.2	58.9
						2		43.7	43.7	54.5	52.1	52.1	69.6
						3		40.0	40.0	64.8	53.2	53.2	64.8
						4		39.5	39.5	57.0	44.6	44.6	69.8
						mean			41.2			50.0	65.8
						(std)			(1.9)			(3.8)	(5.1)
BMh	115×630	210×210	25	middle	0.0	1		51.9	51.9	61.3	61.3	61.3	-
						2	59.4	49.0	49.0	65.7	65.7	65.7	-
						3	61.4	56.0	56.0	62.1	62.1	62.1	-
						4	48.5		48.5	59.7	68.7	59.7	-
						mean			51.4			62.2	
						(std)			(3.4)			(2.5)	
CMh	115×180	60×60	7	middle	2.0	1	20.6	20.6	20.6	27.3	27.3	27.3	27.3
						2	24.1	23.3	23.3	24.9	24.9	24.9	29.5
						3	23.1	17.9	17.9	24.4	23.1	23.1	25.3
						4	24.4	24.4	24.4	27.0	27.0	27.0	27.0
						mean			21.6			25.6	27.3
						(std)			(2.9)			(2.0)	(1.7)
CUh	115×180	60×60	7	upper	2.0	1	24.0	18.8	18.8	25.3	25.3	25.3	25.3
						2		19.0	19.0	23.2	22.5	22.5	25.3
						3	20.5	20.5	20.5	23.3	23.3	23.3	23.3
						4	16.7	16.7	16.7	22.3	22.3	22.3	22.3
						mean			18.8			23.4	23.6
						(std)			(1.6)			(1.4)	(2.2)
CLh	115×180	60×60	7	lower	2.0	1		17.5	17.5	23.1	22.3	22.3	26.9
						2	19.2	19.2	19.2	23.7	23.7	23.7	29.5
						3	21.8	23.4	21.8	24.3	24.3	24.3	25.5
						4				21.8	21.8	21.8	24.5
						mean			19.5			23.0	26.6
						(std)			(2.2)			(1.2)	(2.2)
DMh	115×180	60×60	7	middle	0.0	1	26.0	26.0	26.0	29.1	29.1	29.1	-
						2				25.3	25.3	25.3	-
						3	23.3		23.3	25.3	25.3	25.3	-
						4	25.4	22.6	22.6	26.7	28.1	26.7	-
						mean			24.0			26.6	
						(std)			(1.8)			(1.8)	

4

2.4 Comments concerning test results

The scatter in the strength between nominally equal tests within a test series is not very large, the coefficient of variation of $V_{c,min}$ being from 4 % to 14 % with an average of 8 %. The test results furthermore show that it was more frequent with crack development across the entire beam width at the upper corner T before the lower corner B than the other way around. The most frequent scenario was, however, that cracks developed simultaneously at both corners. The most common place for crack initiation was in the middle of the beam width although some tests showed a crack initiation all the way to one side of the beam width. Some further comments on the test results concerning the influence of the four investigated design parameters are listed below. When nothing else is stated, the crack shear force V_c refers to the minimum of V_{cB} and V_{cT}.

Bending moment to shear force ratio: For beams with centrically placed holes, two different bending moment to shear force ratios were investigated. The beams with holes placed in a position of zero bending moment (test series BMh and DMh) shows on average slightly higher (approximately 5-10 % considering mean values) crack shear forces V_c compared to the beams with holes placed in a position of combined bending moment and shear force (test series AMh and CMh).

Material Strength Class: There was no significant difference in the behavior between the material strength class homogeneous beams of test series AMh and the strength class combined beams of test series AMc. The results of these two test series are, however, comparatively scattered.

Beam size: The test results indicate a strong beam size effect on the strength. Increasing the beam size by a factor 3.5 gave about 30-35 % reduction in nominal shear stress V_c/A_{net}.

Hole placement with respect to beam height: Slightly lower (approximately 5-15 % considering mean values) crack shear forces V_c were found for the beams with eccentrically placed holes compared to the beams with centrically placed holes. There is furthermore another interesting difference concerning the beams with eccentrically placed holes. Both among the large and the small beams the tests generally showed a more sudden crack propagation all the way to the end of beam for the beams with the hole placed in the upper part of the beam (test series AUh and CUh) compared to the beams with the hole placed in the lower part of the beam (test series ALh and CLh).

3 Previous tests of glulam beams with holes

3.1 Compilation of test results in literature

A compilation of previously performed tests of glulam beams with holes from various sources is presented in Table 3. The tests are described concerning beam cross section, hole design, bending moment to shear force ratio, number of tests and results corresponding to the three load levels defined in Figure 2. All holes were centrically placed with respect to beam height. Load levels V_{c0} and V_c refers to the minimum of the values for the two corners, if values for both corners are given in the original source. A more comprehensive compilation including further details such as material strength class, moisture content, how well the definition of load levels correspond with the ones found in the original sources, etc. is found in [5].

Table 3: *Compilation of test results of glulam beams with holes. n = number of tests.*

Reference		$T \times H$	$\square : a \times b$ $\bigcirc : \phi$	r	$\frac{M}{VH}$	n	V_{c0} mean	(std)	V_c mean	(std)	V_f mean	(std)
		[mm]	[mm]		[-]	[-]	[kN]	[kN]	[kN]	[kN]	[kN]	[kN]
Bengtsson & Dahl	[2]	90×500	300×150	0	1.20	2					39.0	(0.3)
		90×500	200×100	0	1.20	2					49.6	(1.1)
Kolb & Frech	[12]	80×550	250×250	?	0.91	2					32.7	(2.1)
		80×550	250×150	?	0.91	2					44.0	(2.8)
		80×550	250×250	?	1.82	2					33.8	(1.1)
		80×550	250×150	?	1.82	2					35.4	(4.0)
Penttala	[13]	90×500	200×200	?	1.60	1					33.8	
		90×500	400×200	?	1.60	1	25.0				31.3	
		90×500	600×200	?	1.60	1	20.8				30.0	
		115×800	400×200	?	1.25	1					69.1	
		115×800	200×200	?	1.25	1	52.5				84.4	
Johannesson	[11]	90×500	250×250	25	1.30	2			26.8	(0.5)	28.5	(2.8)
		90×500	250×250	25	2.80	2			22.2	(2.3)	25.6	(0.6)
		140×400	600×200	25	2.25	1			30.0		37.0	
		88×495	125×125	25	2.53	4			40.4	(11.1)		
		88×495	375×125	25	2.53	4			37.7	(6.4)		
		88×495	370×370	25	2.53	4			9.1	(2.1)		
		88×495	735×245	25	2.53	4			12.8	(1.1)		
		88×495	1100×370	25	2.53	4			4.2	(0.3)		
Pizio	[14]	120×400	180×180	0	1.05	2	24.1	(12.4)	30.6	(3.1)	63.7	(4.6)
		120×400	180×90	0	1.05	2	37.2	(15.4)	54.9	(3.4)	75.5	(1.6)
		120×400	180×10	0	1.05	2	92.5	(26.3)	103.3	(14.8)	103.3	(14.8)
		120×400	180×90	0	1.05	1	56.6		71.0		84.5	
		120×400	180×10	0	1.05	1	110.1		110.1		110.1	
		120×400	360×180	0	1.75	2	21.7	(2.3)	23.3	(0.0)	24.8	(2.1)
		120×400	10×180	0	1.75	1	34.0		34.0		34.0	
		120×400	360×180	0	1.75	1	19.2		21.1		28.8	
		120×400	10×180	0	1.75	2	30.0	(1.1)	33.8	(0.0)	33.8	(0.0)
		120×400	180×90	0	1.75	3	45.8	(11.2)	54.2	(7.0)	54.2	(0.7)
		120×400	180×180	0	1.05	2	20.6	(4.9)	26.8	(3.8)	70.0	(11.2)
Hallström	[9]	90×315	400×150	25	2.78	5			11.9	(1.5)		
		90×315	400×150	0	2.78	5			12.2	(1.1)		
		90×315	400×150	25	2.78	5			12.2	(0.5)		
		90×315	400×150	25	?	1			12.2			
		165×585	600×295	25	?	4			27.1	(1.9)		
Bengtsson & Dahl	[2]	90×500	$\phi250$		1.20	2					38.4	(1.2)
		90×500	$\phi150$		1.20	1					52.5	
Penttala	[13]	90×500	$\phi255$		1.20	1					33.8	
		90×500	$\phi250$		2.10	1					31.6	
		90×500	$\phi150$		1.20	1					51.3	
		115×800	$\phi400$		1.03	1	57.1				65.9	
		115×800	$\phi300$		2.00	1					89.5	
Johannesson	[11]	90×500	$\phi250$		1.30	2			29.6	(5.4)	36.5	(4.3)
		90×500	$\phi250$		2.80	2			33.2	(2.6)	37.5	(3.5)
		90×500	$\phi250$		0.60	2			33.8	(7.1)	41.7	(4.1)
		90×500	$\phi125$		0.60	2			-		40.1	(0.1)
		88×495	$\phi125$		2.53	4			51.9	(4.6)		
		88×495	$\phi396$		2.53	4			16.1	(1.5)		
Hallström	[9]	90×315	$\phi150$		2.78	5			24.5	(3.5)		
Höfflin [10]	H1	120×900	$\phi180$		1.50	5	69.2	(23.2)	106.4	(27.8)	128.1	(19.2)
	H2	120×900	$\phi270$		1.50	6	65.3	(22.1)	96.4	(11.7)	108.7	(6.7)
	H3	120×900	$\phi360$		1.50	5	48.0	(8.4)	69.2	(9.0)	88.6	(15.6)
	H4	120×900	$\phi270$		5.00	5	43.1	(8.3)	55.1	(8.6)	84.2	(18.0)
	H5	120×450	$\phi90$		1.50	5	62.8	(15.6)	76.8	(13.8)	82.1	(7.6)
	H6	120×450	$\phi135$		1.50	6	38.8	(6.0)	65.5	(7.6)	67.9	(7.0)
	H7	120×450	$\phi180$		1.50	4	34.6	(7.4)	47.6	(8.5)	51.8	(5.9)
	H8	120×450	$\phi135$		5.00	5	34.7	(18.2)	58.0	(7.1)	63.4	(6.5)
Aicher & Höfflin [1]	A1	120×900	$\phi180$		5.00	4	66.4	(21.5)	106.4	(15.0)	111.6	(13.1)
	A2	120×900	$\phi360$		5.00	5	46.7	(15.3)	61.6	(15.0)	79.9	(3.2)
	A3	120×450	$\phi180$		5.00	6	42.4	(9.6)	48.8	(7.7)	53.7	(8.0)
		$120 \times 450^*$	$\phi180$		5.00	3	15.4	(3.1)	37.9	(6.8)	44.8	(2.5)
		$120 \times 900^*$	$\phi360$		5.00	3	33.5	(13.6)	49.6	(17.4)	66.6	(6.9)

* = curved beam, radius of curvature = $H/0.03$

6

3.2 Influence of bending moment to shear force ratio

Figure 4 illustrates the influence of the bending moment to shear force ratio on the strength. The results indicate a only a small influence of the bending moment on the crack shear force V_c. There is however one exception: The test series with $T \times H = 120 \times 900$ mm^2 and $\phi = 270$ mm shows a 43 % reduction in the crack shear force V_c for $M/(VH) = 5.0$ compared to $M/(VH) = 1.5$. It is worth pointing out that the mean value of the crack shear force is lower for the test series with $T \times H = 120 \times 900$ mm^2, $M/(VH) = 5.0$ and $\phi = 270$ mm than it is for the test series with equal cross section and bending moment to shear force ratio but with a larger hole, $\phi = 360$ mm, as can be seen in Figure 4 and in Table 3.
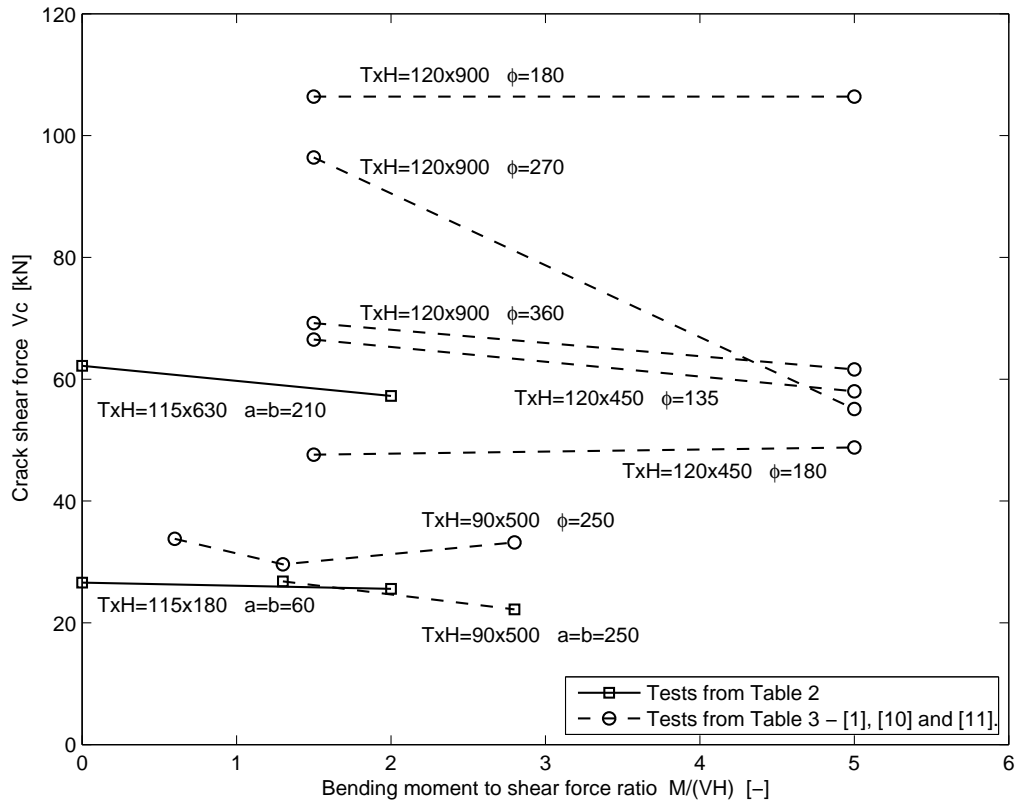

Figure 4: *Influence on strength of bending moment to shear force ratio for nominally equal tests concerning beam cross section, material strength class, hole size and hole placement.*

3.3 Influence of beam size

The present tests of glulam beams with quadratic holes indicated a strong beam size effect. Figure 5 shows the test series mean of the nominal shear stress V_c/A_{net} vs. beam height H for these tests and tests presented in [1] and [10]. Test results connected with lines represent test series which are equal concerning bending moment to shear force ratio, material strength class, beam width and hole size to beam height ratio but with different beam height H. The beam size effect can be expressed according to $V_c/A_{net} \sim H^{-m}$ where the parameter m describing the beam size effect can be determined from two test series of different size scale. The values of m are for the nine pair of test series given in Figure 5. It can be seen that the tests from [1] and [10] and relating to circular holes indicate a stronger beam size effect than the tests relating to quadratic holes presented in Section 2. The value of the parameter

$m = 1.07$ for test series with $M/(VH) = 5.0$ and $\phi = 0.3H$ is substantially higher than the value for the other eight pair of test series. This deviating result is due to the test series with $T \times H = 120 \times 900$ mm^2, $M/(VH) = 5.0$ and $\phi = 270$ mm. The result of that series gave also the deviating result with respect to influence of bending moment according to Figure 4 and showed lower strength than the corresponding beam with a larger hole, $\phi = 360$ mm.
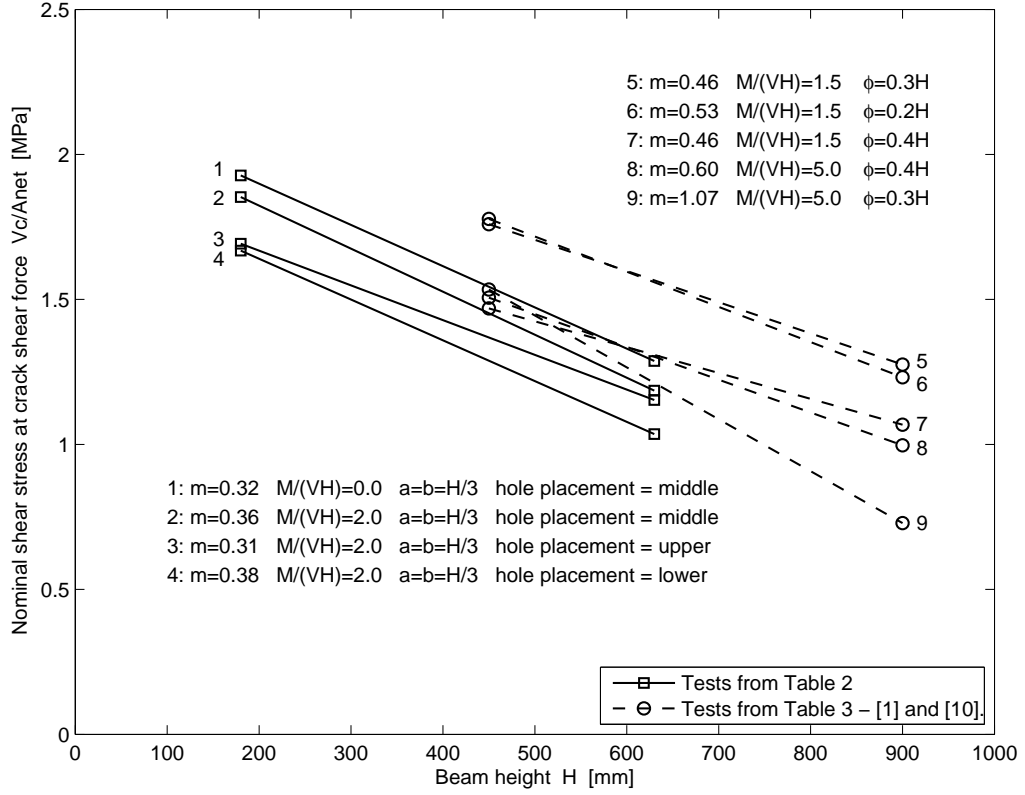

Figure 5: *Influence on strength of beam size (beam height, beam length and hole size uniformly scaled) for otherwise nominally equal tests.*

4 Comparison of design codes and test results

In order to make a simple evaluation of some of the proposed design recommendations, a comparison between test results and the shear force capacities according to codes is presented. The characteristic shear force capacities according to the following three methods are used in the comparison; (1) the empirically based method found in Swedish code of practise *Limträhandbok* [4], (2) The "end-notched beam analogy"-method found in a previous version of Eurocode 5 (prEN 1995-1-1 [8]) and also found in *Limträhandbok* and (3) the design method found in the German code DIN 1052 [3] (recently withdrawn for rectangular holes). The present results of beams with quadratic holes and test results of straight beams with circular holes presented in [1] and [10] are used in the comparison. The beams of test series AMc are considered to correspond to strength class GL 32c while the material strength class of all other beams is GL 32h. The following strength values (taken from SS-EN 1194 [16]) are used when determining characteristic capacities according to codes; $f_{v,k} = 3.8$ MPa and $f_{t,90,k} = 0.5$ MPa for GL 32h and $f_{v,k} = 3.2$ MPa and $f_{t,90,k} = 0.45$ MPa for GL 32c. Characteristic values for the beam test results $V_{i,k}$ and the coefficient of variation *cov* are determined according to Equations (1) and (2)

8

$$V_{i,k} = \bar{V}_i \cdot (1 - 1.645 \cdot cov) \tag{1}$$

$$cov = \sqrt{\frac{1}{n_{tot} - 1} \sum_{i=1}^{n_i} \sum_{j=1}^{n_j} \left(\frac{\bar{V}_i - V_{ij}}{\bar{V}_i} \right)^2} \tag{2}$$

where n_{tot} is the total number of individual tests, n_i is the number of test series, n_j is the number of individual tests within the test series, $\bar{V}_i$ is the mean value of the crack shear force V_c for test series i and V_{ij} is the individual value of the crack shear force V_c for test j in test series i. For the beams with quadratic holes, the minimum crack shear force $V_c = \min(V_{cB}, V_{cT})$ of the test results according to Table 2 and the overall coefficient of variation $cov = 7.55$ % based on these 36 test is used to determine the characteristic values $V_{i,k}$. For the beams with circular holes, the crack shear force V_c according to Table 3 and the overall coefficient of variation $cov = 15.3$ % based on these 56 tests is used to determine the characteristic values $V_{i,k}$. The comparison between tests and codes is presented in Table 4 and in Figure 6 for the quadratic holes and in Figure 7 for the circular holes. The test series notations for circular holes (H1-H8 and A1-A3) refer to notations in Table 3.

Comparing the characteristic values $V_{i,k}$ based on the test results and the characteristic strength values V_{code} according to codes, some observations are worth pointing out. *Limträ-handbok* and DIN 1052 underestimates the capacity of all test series with quadratic holes. This underestimation is more severe for the test series with small beams since the beam size effect is not taken into account in any way in these two codes. The test results of beams with quadratic holes do however not indicate the strong size effect suggested by Eurocode 5. This code is on the unsafe side for all test series with quadratic and circular holes, but shows a fairly good ability to predict relative influence of the various parameters.

Table 4: *Test results and characteristic shear force capacities according to codes in kN.*

| Test series | Test results | | Characteristic shear force capacities V_{code} according to codes | | |
	mean $\bar{V}_i$	characteristic $V_{i,k}$	*Limträhandbok* empirical method	Eurocode 5 prEN 1995-1-1	DIN 1052
AMh	57.3	50.1	36.6	60.1	41.8
AMc	53.2	46.6	30.8	50.6	37.6
AUh	55.7	48.8	36.6	53.3*	35.9*
ALh	50.0	43.8	36.6	53.3*	35.9*
BMh	62.2	54.5	36.6	60.1	50.2
CMh	25.6	22.4	10.5	32.1	11.9
CUh	23.4	20.5	10.5	28.5*	10.2*
CLh	23.0	20.2	10.5	28.5*	10.2*
DMh	26.6	23.3	10.5	32.1	14.3
H1	106.4	79.6	83.7	176.4	116.5
H2	96.4	72.2	66.4	134.7	88.2
H3	69.2	51.8	51.9	108.0	72.8
A1	106.4	79.6	83.7	176.4	78.1
H4	55.1	41.3	66.4	134.7	63.8
A2	61.6	46.1	51.9	108.0	54.9
H5	76.8	57.5	41.8	109.4	58.3
H6	65.5	49.0	33.2	95.8	44.1
H7	47.6	35.6	25.9	77.9	36.4
H8	58.0	43.4	33.2	95.8	31.9
A3	48.8	36.5	25.9	77.9	27.4

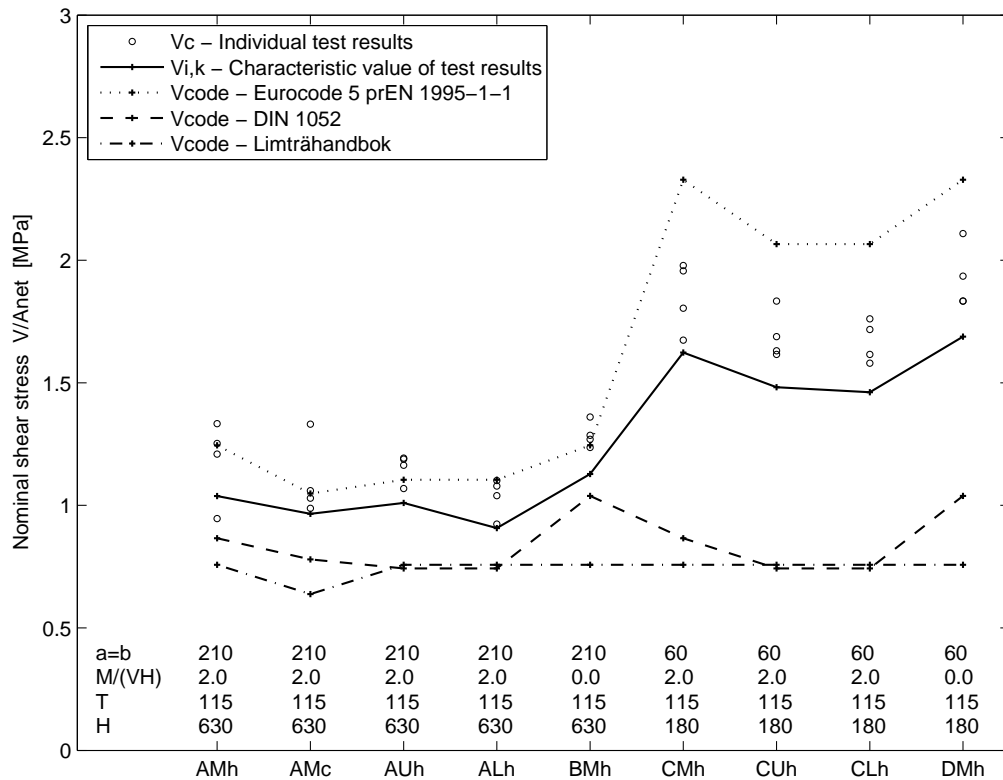* = Hole placement with respect to beam height not according to regulations in code.

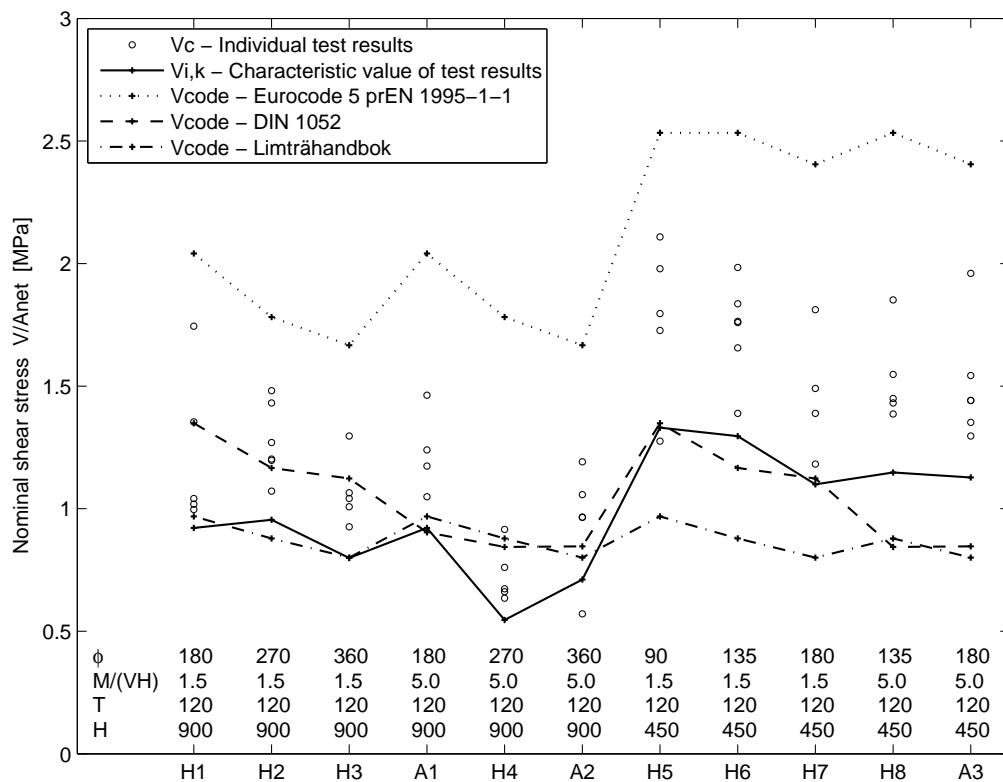Figure 6: *Comparison of codes and test results for quadratic holes.*

Figure 7: *Comparison of codes and test results for circular holes.*

References

[1] Aicher S., Höfflin L.
Tragfähigkeit und Bemessung von Brettschichtholzträgern mit runden Durchbrüchen –
Sicherheitsrelevante Modifikationen der Bemessungsverfahren nach Eurocode 5 und DIN 1052
MPA Otto-Graf-Institute, University of Stuttgart, 2006.

[2] Bengtsson S., Dahl G.
Inverkan av hål nära upplag på hållfastheten hos limträbalkar
Master's Thesis, Byggnadsteknik II, Lund University, 1971.

[3] Blaß H.J., Ehlbeck J., Kreuzinger H., Steck G.
Erläuterungen zu DIN 1052:2004-08 – Entwurf, Berechnung und Bemessung von Holzbauwerken
2nd Edition including original text. DGfH innovations- und Service GmbH, München, 2005.

[4] Carling O.
Limträhandbok
Svenskt Limträ AB, Print & Media Center i Sundsvall AB, 2001.

[5] Danielsson H.
The Strength of Glulam Beams with Holes – A Survey of Tests and Calculation Methods
Report TVSM-3068, Division of Structural Mechanics, Lund University, 2007.
(available for download at: www.byggmek.lth.se/english/publications/)

[6] Danielsson H.
Strength Tests of Glulam Beams with Quadratic Holes – Test Report
Report TVSM-7153, Division of Structural Mechanics, Lund University, 2008.
(available for download at: www.byggmek.lth.se/english/publications/)

[7] *Eurocode 5: Design of timber structures - Part 1-1: General - Common rules and rules for buildings*
EN 1995-1-1:2004 (E).

[8] *Eurocode 5: Design of timber structures - Part 1-1: General Rules-General rules and rules for buildings*
prEN 1995-1-1: Final Draft 2002-10-09.

[9] Hallström S.
Glass fibre reinforcemed laminated timber beams with holes
Report 95-12, Department of Lightweight Structures, Royal Institute of Technology, Stockholm, 1995.

[10] Höfflin L.
Runde Durchbrüche in Brettschichtholzträger – Experimentelle und theoretische Untersuchungen
Dissertation, MPA Otto-Graf-Institute, University of Stuttgart, 2005.

[11] Johannesson B.
Design problems for glulam beams with holes
Dissertation, Div. of Steel and Timber structures, Chalmers University of Technology, Göteborg, 1983.

[12] Kolb H., Frech P.
Untersuchungen an durchbrochenen Bindern aus Brettschichtholz
Holz als Roh- und Werkstoff 35, p. 125-134, 1977.

[13] Penttala V.
Reiällinen liimapuupalkki
Publication 33, Division of Structural Engineering, Helsinki Univeristy of Technology, Otaniemi, 1980.

[14] Pizio S.
Die Anwendung der Bruchmechanik zur Bemessung von Holzbauteilen,
untersucht am durchbrochen und am ausgeklinkten Träger
Publication 91:1, Dissertation, Baustatik und Stahlbau, ETH, Zürich, 1991.

[15] SP – Sveriges Provnings- och Forskningsinstitut
Lamination strength classes for glued laminated timber according to EN 1194
PM, 2002-06-14.

[16] SS-EN 1194:1999
Träkonstruktioner – Limträ – Hållfasthetsklasser och bestämning av karakteristiska värden
SIS Förlag, Stockholm, 2000.

Paper C

*A Probabilistic Fracture Mechanics Method
for Strength Analysis of Glulam Beams with Holes*

Henrik Danielsson and Per Johan Gustafsson

A Probabilistic Fracture Mechanics Method
for Strength Analysis of Glulam Beams with Holes

Henrik Danielsson · **Per Johan Gustafsson**

Abstract A probabilistic fracture mechanics method for strength analysis of glulam beams with holes is presented. The method is based on a combination of Weibull weakest link theory and the mean stress method which is a generalization of linear elastic fracture mechanics. Combining these two methods means that the fracture energy and the stochastic material properties are taken into account. The probabilistic fracture mechanics method is evaluated by comparison to experimental test results. The method shows good ability to predict strength, with the exception of very small beams where the capacity is overestimated. The comparison to experimental tests deals also with other methods for strength analysis including code design methods.

H. Danielsson · P.J. Gustafsson
Division of Structural Mechanics, Lund University, Sweden
P.O. Box 118, SE-221 00, Lund, Sweden
E-mail: henrik.danielsson@byggmek.lth.se
E-mail: per_j.gustafsson@byggmek.lth.se

1 Introduction

Introducing a hole through a glulam beam drastically changes the stress state and reduces the strength significantly due to the high perpendicular to grain tensile stresses and the shear stresses appearing in the vicinity of the hole. It is however sometimes necessary to make a hole, for example for installations. Wood is weak when loaded in tension perpendicular to grain and fracture caused by this type of loading commonly has a brittle course, which emphasizes the need for careful design.

Finding a simple, general and reliable design method is however a difficult task. Looking at European timber engineering design codes over the last decades, it can be seen that strength design of glulam beams with holes have been treated in many different ways. The theoretical background on which the recommendations are based show fundamental differences and there are also major discrepancies between strength predictions according to different codes as well as between codes and experimental tests (Danielsson 2007; Danielsson and Gustafsson 2008). The lack of knowledge is further reflected by the fact that the contemporary version of the European timber code EC5 (Eurocode 5 2004) does not state any equation concerning design of beams with holes and the recommendations in the German timber code DIN 1052 (Blaß, Ehlbeck, Kreuzinger and Steck 2005) were withdrawn for rectangular holes during 2007 since they were believed to lead to unsafe design.

The hypothesis in this study is that accurate strength predictions for glulam beams with holes can be obtained by what can be referred to as a *probabilistic fracture mechanics method*. A proposal for such a method is briefly outlined in (Gustafsson and Serrano 1999) and will be further developed here. The considered method is based on a combination of Weibull weakest link theory and the mean stress method which is a generalization of linear elastic fracture

mechanics. Combining these two methods means that the nonzero fracture energy and the stochastic nature of the material properties are taken into account.

The aim with the study is to investigate the possibilities of the proposed method. Specifically, the influence of four important design parameters on the strength is considered for both quadratic and circular holes: bending moment to shear force ratio, beam size, hole placement with respect to beam height and relative hole size with respect to beam height. Strength predictions according to the probabilistic fracture mechanics method is also compared to experimental test results and other methods for strength analysis including code design methods.

2 Methods for rational strength analysis

There are a few basically different methods for rational strength analysis based on linear elastic stress analysis. The dominating method in timber engineering is what can be referred to as *conventional stress analysis* (CSA) with some failure criterion based on the stresses in a point. Deterministic and ideally brittle material behavior is assumed, meaning that the strength properties are homogeneous throughout the body and that the fracture energy is assumed to be zero. This type of strength analysis method is of little use for glulam beams with a hole due to the high stress gradients in the vicinity of the hole. The *Weibull weakest link theory* (Weibull 1939) is, just as CSA, based on the assumptions of a linear elastic and ideally brittle material. The material strength properties are however allowed to be heterogenous and the method is hence stochastic. Weibull theory have been applied to glulam beams with circular holes (Höfflin 2005). A general drawback of Weibull theory and CSA is however that they cannot be applied to strength analysis of structural elements with a stress singularity caused by a crack or a sharp notch (Gustafsson 1988). In *linear elastic fracture mechanics* (LEFM), is infinite material strength assumed and the global strength is instead governed by fracture energy properties. LEFM suffers however from one major limitation: it is based on the assumption of an existing crack giving rise to a square root stress singularity. The theory can however be modified (generalized) in order to overcome this limitation. The *mean stress method*, presented in (Gustafsson 2002), is one such generalization. The basic idea of this method is to consider the mean tensile and shear stresses acting across a potential fracture area. These stresses, which has a finite value also for the case of presence of a stress singularity, are then used in a conventional stress based failure criterion. The mean stress method have been applied to glulam beams with holes (Gustafsson 2002) and have recently also been applied to steel-timber dowel joints (Sjödin and Serrano 2008).

3 A probabilistic fracture mechanics method

The derivation of the probabilistic fracture mechanics method (PFM) considered here starts with a reformulation of the Weibull theory. Based on analysis of different volumes and stress distributions with equal probability of failure, the following expression can be obtained

$$\frac{\sigma_{max}}{f} = \left(\frac{1}{\Omega_{ref}} \int_\Omega \left(\frac{\sigma(x,y,z)}{f_{ref}} \right)^m d\Omega \right)^{1/m} \tag{1}$$

where σ_{max} is the maximum stress in the body of volume Ω and with stress distribution $\sigma(x,y,z)$, f is the mean of σ_{max} at the instant of failure, f_{ref} is the mean strength valid for a homogeneous stress distribution in the reference volume Ω_{ref} and m is the Weibull shape parameter related to the scatter in material strength.

The ratio σ_{max}/f can be interpreted as a *global effective dimensionless stress parameter* α_{global} and $\sigma(x,y,z)/f_{ref}$ as an *effective dimensionless stress field* $\alpha(x,y,z)$ defined in the volume Ω. The expression can then be rewritten as

$$\alpha_{global} = \left(\frac{1}{\Omega_{ref}} \int_\Omega \alpha^m(x,y,z) \, d\Omega \right)^{1/m} \tag{2}$$

where the value of α_{global} for $\alpha(x,y,z)$ in Ω corresponds to equal probability of failure as the constant value of $\alpha(x,y,z) = \alpha_{global}$ for a homogeneous stress in Ω_{ref}. Since f_{ref} is here defined as the mean strength of Ω_{ref}, $\alpha_{global} = 1.0$ will for Ω give the mean failure value of σ_{max}. It is in calculation of the external load that give $\alpha_{global} = 1.0$ convenient that $\sigma(x,y,z)$ and thus also $\alpha(x,y,z)$ and α_{global} are proportional to the load.

Acknowledging the heterogeneity in the material strength in this way, the strength prediction will depend both on the volume and the distribution of the stresses but the material is still assumed to behave ideally brittle. To account also for the fracture toughness of the material, other choices of the effective dimensionless stress field than stated above can be made. In accordance with the mean stress method, it can be useful to consider the mean stresses acting across a potential fracture area. Assuming plane stress conditions and a fracture plane which coincides with the grain direction, the effective dimensionless stress field can be chosen according to

$$\alpha(x,y) = \left(\left(\frac{\bar{\sigma}(x,y)}{f_\sigma} \right)^2 + \left(\frac{\bar{\tau}(x,y)}{f_\tau} \right)^2 \right)^{1/2} \tag{3}$$

where $\bar{\sigma}(x,y)$ and $\bar{\tau}(x,y)$ are the mean values of the perpendicular to grain tensile stress σ and the shear stress τ in the potential fracture area and f_σ and f_τ are the corresponding mean strengths valid for the reference volume Ω_{ref}. If the mean stress perpendicular to grain is compressive, this contribution is ignored and the effective dimensionless stress is determined by the mean shear stress only.

The size of the potential fracture area is related to the size of the fracture process region at the instant of start of unstable crack growth and is defined by the plane stress width and a length a_{ms} in the grain direction (Gustafsson 2002). The length a_{ms} is derived in such a way that the mean stress method will give the same strength prediction for a body in a homogeneous state of stress as CSA and give the same strength prediction as LEFM for a body with a square root stress singularity. For a potential fracture area starting from a surface of the body, this length is found to be

$$a_{ms} = \frac{2}{\pi} \frac{E_I G_{IC}}{f_\sigma^2} \frac{E_x}{E_y} \left(\frac{G_{IIc}}{G_{Ic}} \right)^2 \frac{1}{4k^4} \cdots$$

$$\left(\sqrt{1 + 4k^2 \sqrt{\frac{E_y}{E_x} \frac{G_{Ic}}{G_{IIc}}} } - 1 \right)^2 \left(1 + k^2 \frac{f_\sigma^2}{f_\tau^2} \right) \quad (4)$$

$$\text{where } E_I = \sqrt{ \frac{2E_x E_y}{\sqrt{\frac{E_x}{E_y}} + \frac{E_x}{2G_{xy}} - \nu_{yx} \frac{E_x}{E_y}} }$$

where E_x, E_y, G_{xy} and ν_{yx} are the elastic stiffness parameters (Poisson's ratio defined as $\nu_{yx} = -\varepsilon_x/\varepsilon_y$ for uniaxial loading in the y-direction), G_{Ic} and G_{IIc} are the mode I and mode II critical energy release rates (which are equal to the fracture energies for an ideally linear elastic material) and $k = \bar{\tau}/\bar{\sigma}$ is the mixed mode ratio. The grain direction is here represented by the x-direction.

The expression in Equation (4) is valid for a potential fracture area starting from the surface of the considered body, which corresponds to initiation of fracture at a surface defect. The integration of $\alpha(x,y)$ should however be carried out over the entire considered volume meaning that also interior points need to be considered. For an interior point, a defect in the material can be interpreted as an interior crack which has two tips and the potential fracture area is hence taken as twice that valid for a surface crack. For points which are not on a surface, but neither far from them, some approximation needs to be made. Aiming for a smooth transition when moving between these two extremes, the length of the potential fracture area a_m is in the present implementation determined as illustrated in Figure 1 and expressed mathematically in Equation (5).
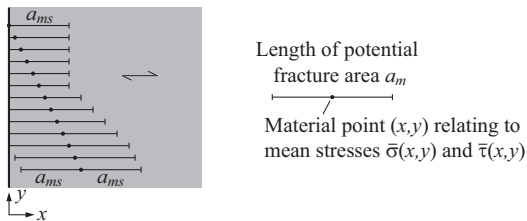

Fig. 1 Interpretation of the length of the potential fracture area for different locations of a material points with respect to a surface at $x = 0$.

$$a_m(x) = \begin{cases} a_{ms} & \text{for} & 0 \le x < a_{ms}/2 \\ 2x & \text{for} & a_{ms}/2 \le x < a_{ms} \\ 2a_{ms} & \text{for} & a_{ms} \le x \end{cases} \quad (5)$$

The physical interpretation of the method is that all points in the body are considered as potentially weak points where fracture initiation may occur. The material is, due to fracture toughness and ductility, assumed to have the ability to distribute the stresses over the fracture area and it is hence the mean stresses acting within this area that are considered. In accordance with Weibull theory, the resistance to fracture is not homogeneous but viewed as a stochastic property.

The strength prediction of PFM depends, among other parameters, on the value of the Weibull shape parameter m and the fracture energy parameters G_{Ic} and G_{IIc}. For an ideally brittle material ($G_{Ic} = G_{IIc} = 0$), the method will break down to Weibull theory. This is also true for a body with a homogeneous stress distribution, since the mean stresses are equal to the actual stresses. PFM will also approach Weibull theory for increasing size of the considered body since the relative size of the potential fracture area decreases. For a material which is assumed to show fracture ductility but where the material properties are assumed to be deterministic ($m \to \infty$), PFM will break down to the mean stress method meaning that the potential fracture area with the most severe combined action of $\bar{\sigma}$ and $\bar{\tau}$ will be decisive. For the special case of a deep crack in a large body, the mean stress method will in turn break down to conventional LEFM. For an ideally brittle material with deterministic properties, the strength prediction of PFM will be the same as according to CSA and the material point with the most severe combined action of σ and τ will be decisive.

4 Method for strength analysis of glulam beams with holes by probabilistic fracture mechanics

4.1 Determination of stress fields

The stress fields $\sigma(x,y)$ and $\tau(x,y)$ are determined by 2D plane stress finite element analysis by the commercial software ABAQUS. The entire beam is not modeled but only a certain part of the beam close to the hole according to Figure 2. The reason for adopting this approach is that it decreases the computational demands and enables an easy way of changing load conditions. The geometry is defined by the beam height H, beam width T, hole side lengths a and b, hole corner radius r and position of hole center relative to the neutral axis of the beam s. A circular hole can formally be regarded as a quadratic hole with diameter $\phi = a = b = 2r$. The length of the beam part considered for the finite element stress analysis is $1.5H + 1.5H$. The shear forces V and the bending moments M_L and M_R are applied as parabolic shear

stress distributions and linear normal stress distributions respectively. The load condition is represented by the bending moment to shear force ratio $M/(VH)$ at hole center.

An orthotropic and linear elastic material model is used with stiffness properties according to Table 1. 8-node plane stress quadrilateral elements with biquadratic displacement interpolation and reduced integration are used. Dynamic and geometrical non-linear effects are not included in the analysis. Due to the geometry, there are high stress gradients around the hole which in general means that a fine mesh is needed to describe the stress accurately. This problem is however less pronounced since the effective dimensionless stress field is based on the mean stresses for an area. The minimum element size in the regions with high stress gradient should however be considerably smaller than the size of the potential fracture area for which the mean stresses are determined. A typical finite element mesh used for the stress analysis is shown in Figure 3.
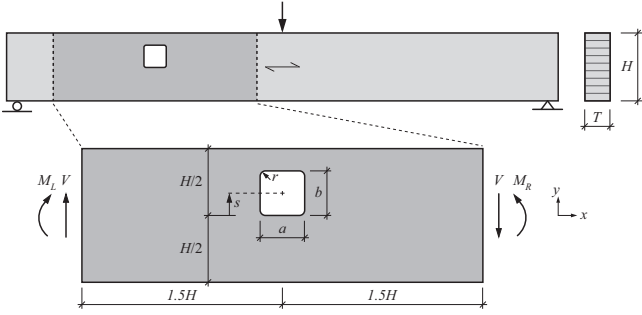
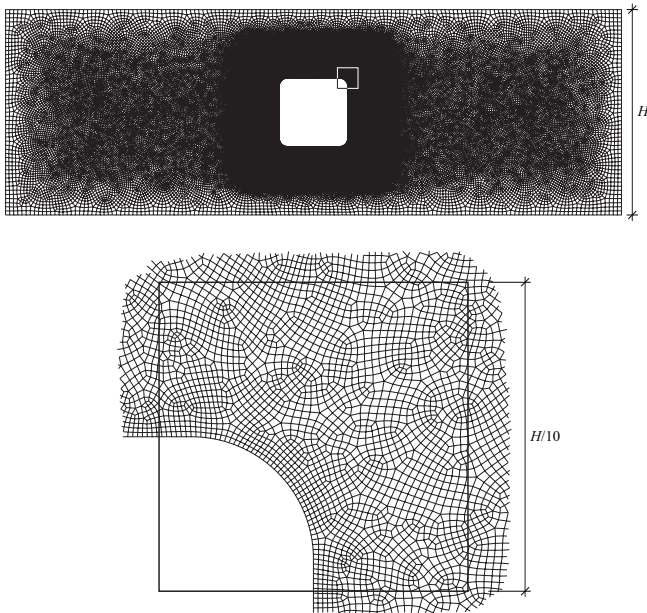
Fig. 2 Beam geometry, hole geometry and applied loads.

Fig. 3 Typical finite element mesh used for the stress analysis.

4.2 Determination of mean stresses

The output from the finite element stress analysis is taken as the stresses σ and τ in the nodal points of the elements. These stresses are then interpolated at *reference points* in an evenly distributed grid in the body. The distance between the reference points is equal in x- and y-directions and is denoted a_{rp}. For the presented numerical calculations is $a_{rp} = H/1000$. The mean stresses $\bar{\sigma}(x,y)$ and $\bar{\tau}(x,y)$ are determined at all reference points by numerical integration of the stresses within the potential fracture area a_m associated with the specific reference point. The size of the potential fracture depends on the mixed mode ratio $k = \bar{\tau}/\bar{\sigma}$ and determining the mean stresses is hence an iterative process. In this implementation, this iteration is however ignored and the mixed mode ratio is assumed to be determined with sufficient accuracy by the ratio between the stresses in the considered reference point $k = \tau/\sigma$.

The mean stresses must be determined in a part of the beam somewhat smaller than the one used for the finite element stress analysis. The reason for this is that the mean stresses in an interior material point of the body represent stress of both sides of the material point in the x-direction. The mean stresses are for the presented numerical calculations determined within a length $0.75H + 0.75H$.

4.3 Stress integration and strength prediction

The strength prediction according to the probabilistic fracture mechanics method is implicitly given by the value of the global effective dimensionless stress parameter α_{global} which is determined by integration of the effective dimensionless stress field $\alpha(x,y)$ according to Equation (2). This integration is carried out numerically according to

$$\alpha_{global} = \left(\frac{T a_{rp}^2}{\Omega_{ref}} \sum_{i=1}^{n} \alpha^m(x_i, y_i) \right)^{1/m} \tag{6}$$

where n is the number of reference points in the body and $\alpha(x_i, y_i)$ is the effective dimensionless stress at reference point i according to Equation (3). The criterion $\alpha_{global} = 1.0$ gives the mean global failure load since α_{global} is proportional to the applied loads and the strength prediction in terms of shear force at failure $V_{failure}$ is hence given by

$$V_{failure} = \frac{1}{\alpha_{global}} V_{FE} \tag{7}$$

where V_{FE} is the shear force applied in the finite element stress analysis and α_{global} is the value obtained from Equation (6) for this applied shear force.

An illustration of typical distributions of σ, τ, α and α^m in the vicinity of a hole are shown in Figure 4. It is from the distribution of α^m evident that the two regions that contributes significantly to α_{global} are very small. The illustration is based on the material properties stated in Table 1. Beam geometry and load condition are $H = 600$ mm, $T = 115$ mm, $a = b = 0.30H$, $r/a = r/b \approx 0.14$, $s = 0$, $M/(VH) = 4.0$ and the applied load corresponds to the PFM failure load, $V/A_{net} = 1.16$ MPa.
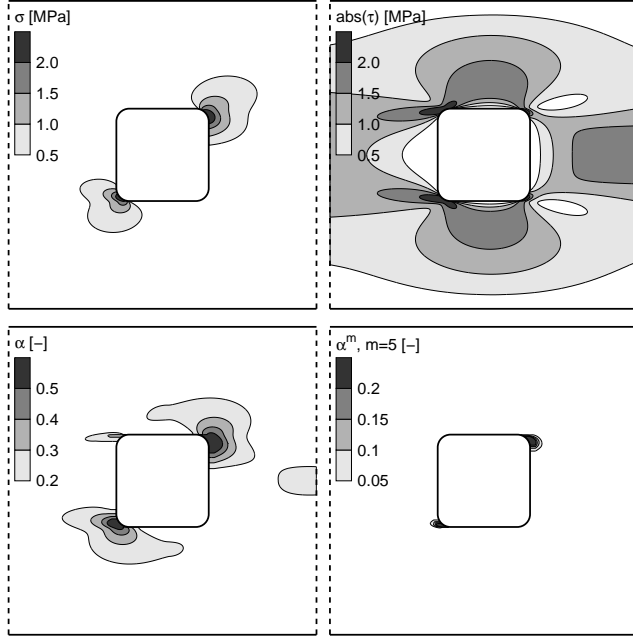
Fig. 4 Distributions of σ, τ, α and α^m in the vicinity of a hole.

4.4 Material properties

The material properties used for the numerical calculations are given in Table 1. The stiffness properties E_{xx}, E_{yy}, G_{xy} and ν_{xy} are assumed to correspond to mean values valid for glulam strength class GL 32h. The material strengths f_σ and f_τ and the fracture energies G_{Ic} and G_{IIc} are based on values used in (Gustafsson 2002). The values of the reference volume Ω_{ref} and the Weibull shape parameter m relate to experimental tests of the strength for homogeneous tensile stress perpendicular to grain. The reference volume Ω_{ref} is determined from the empirical relation

$$f_\sigma/f_0 = 1.5(\Omega_{ref}/\Omega_0)^{-0.2} \qquad (8)$$

where $f_0 = 1.0$ MPa and $\Omega_0 = 10^6$ mm^3 which is found in (Gustafsson 2003). The chosen value of the Weibull shape parameter, $m = 5$, corresponds to the volume influence in the above given equation and also to about 23 % coefficient of variation in strength.

Table 1 Material properties used in the PFM calculations.

Modulus of elasticity $\parallel$	E_{xx}	13 700	MPa
Modulus of elasticity $\perp$	E_{yy}	460	MPa
Shear Modulus	G_{xy}	850	MPa
Poisson's ratio	ν_{xy}	0.35	-
Tensile strength $\perp$	f_σ	3.0	MPa
Shear strength	f_τ	9.0	MPa
Fracture energy mode I	G_{Ic}	0.300	Nmm/mm^2
Fracture energy mode II	G_{IIc}	1.050	Nmm/mm^2
Reference volume	Ω_{ref}	31250	mm^3
Weibull shape parameter	m	5	-

5 Verification: Beam in bending

In order to verify the numerical implementation, the method is applied to a beam in bending according to Figure 5. For this loading and geometry, an analytical solution is derived in (Danielsson 2009) according to

$$M_{failure} = \frac{TH^2 f_\sigma}{6} \frac{1}{1 - a_{ms}/H} \cdots$$
$$\left(\frac{LHT}{2\Omega_{ref}} \left(\frac{a_{ms}}{H} + \frac{1}{m+1} - \frac{1}{m+1} \frac{a_{ms}}{H} \right) \right)^{-1/m} \quad (9)$$
$$\text{where} \quad a_{ms} = \frac{2E_I G_{Ic}}{\pi f_\sigma^2} \qquad \text{since } k = 0$$

The results for the special cases of the mean stress method and Weibull theory are found by $m \to \infty$ and $a_{ms} = 0$ respectively. The strength prediction according to the analytical solutions (dashed and solid lines) and the numerical solutions (marks) are for different values of m and G_{Ic} shown in Figures 6 and 7 for the probabilistic fracture mechanics method (PFM), Weibull theory (WEI), the mean stress method (MSM) and also according to conventional stress analysis (CSA) with failure criterion $\sigma = f_\sigma$. The numerical implementation of PFM gave almost exactly the same results as the analytical solution. The verification is based on a beam of dimension $L = 2H = 2T = 200$ mm and with direction of grain in y-direction. The material properties other than the ones illustrated in these two figures are as stated in Table 1. Applying a pure bending moment gives a mixed mode ratio $k = 0$ and with the given material properties the length of the potential fracture area is $a_{ms} \approx 21$ mm.
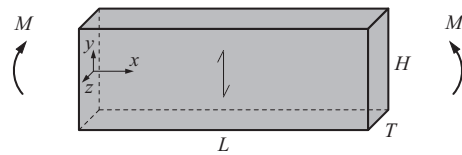

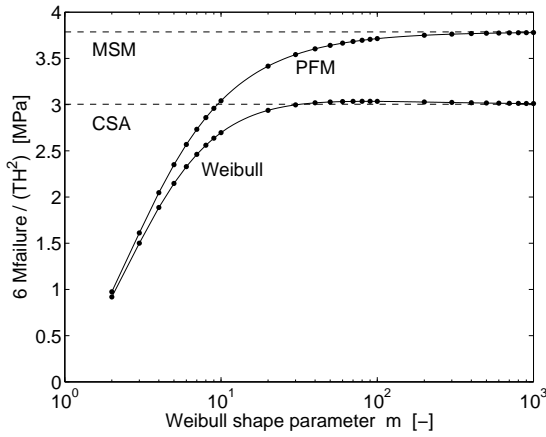**Fig. 5** Beam in bending for verification of numerical implementation.

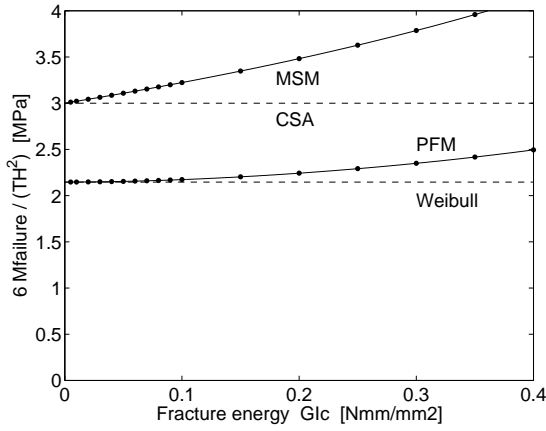**Fig. 6** Predicted strengths $6M_{failure}/(TH^2)$ versus m.

Fig. 7 Predicted strengths $6M_{failure}/(TH^2)$ versus G_{Ic}.

6 Parameter study and verification

The relative influence on the strength of the four design parameters investigated are illustrated in Figure 8 for a beam with a quadratic hole with rounded corners and in Figure 9 for a beam with a circular hole. The illustrations are based on a reference beam according to the figures. For each of the four graphs in the respective figures, one of the design parameters is varied while the others are constant. The nominal shear strength V/A_{net} is 1.35 MPa for the reference beam with a circular hole ($r/\phi = 0.5$), 1.16 MPa for the reference beam with a quadratic hole and rounded corners ($r/a = r/b \approx 0.14$) and 1.14 MPa for a corresponding quadratic hole with sharp corners ($r = 0$).

Verification of PFM is carried out by comparison to experimental test results. Strength tests of beams with quadratic holes with rounded corners were performed at Lund University (Danielsson 2008). The design parameters primarily studied in this test programme were: bending moment to shear force ratio, beam size and hole placement with respect to beam height. For beams with circular holes is verification made by means of test results presented in (Höfflin 2005; Aicher and Höfflin 2006). These studies are two of the most

recent and most comprehensive test programmes on glulam beams with circular holes and the design parameters primary studied were: bending moment to shear force ratio, beam size and relative hole size with respect to beam height. The comparison concerning these tests is shown in Figure 10 for the quadratic holes and in Figure 11 for circular holes. All beams of the presented tests are of material strength class GL 32h.

Some comments on the strength predictions and on their correlation to the experimental test results concerning the four design parameters are given below:

Bending moment to shear force ratio
PFM predicts a comparatively small influence of the bending moment to shear force ratio for holes centrically placed with respect to beam height. This agrees rather well with the overall behavior found in the tests. The difference in strength for the considered bending moment to shear force ratios are however comparatively small. According to PFM, the influence of bending moment to shear force ratio seems to a large extent to depend on the hole placement with respect to beam height. This is commented below.

Beam size
The beam size seems to be the most influential parameter out of the four investigated design parameters. PFM predicts a strong beam size influence on the strength which was also found in the experimental tests. The method seems to capture the beam size effect well for the beams with $H = 450$, 630 and 900 mm. However, the method considerably overestimates the capacity for the small beams with $H = 180$ mm. Comments regarding this is found in Section 8.

Hole placement with respect to beam height
Concerning hole placement with respect to beam height, the influence on the strength predicted by PFM is rather complex. For the reference beams in Figure 10 and Figure 11 where $M/(VH) = 4$, the strength is greater for the centrically placed holes than for the eccentrically placed ones. Further calculations showed that this difference in strength increases with increasing bending moment to shear force ratio (Danielsson 2009). For holes placed in a position where $M/(VH) = 0$, the method however predicts greater strength for eccentrically placed holes than for centrically placed ones. PFM predicts higher strength for test series AUh with a hole placed in the upper part of the beam ($s = H/6$, $M/(VH) = 2$) than for test series AMh with a centrically placed hole ($s = 0$, $M/(VH) = 2$), see Figure 10. The test results however show the opposite relation. The difference in predicted strength is however small. For the small beams in the same figure, both PFM and the test results show lower strength for eccentrically placed holes. The strength reduction predicted by PFM is however somewhat smaller than found in experimental tests.

Relative hole size with respect to beam height

PFM predicts decreasing nominal shear strength with increasing relative hole size. In general, the method suggests greater strength for a beam with a circular hole compared to a beam with a quadratic hole for $a = b = \phi$. The strength reduction for increasing hole size is further greater for the quadratic holes than for the circular holes. Increasing the holes size from $\phi = a = b = 0.20H$ to $0.40H$, the nominal shear strength is reduced by about 25 % for the quadratic holes and about 15 % for the circular holes. Compared to experimental test results, PFM seems to predict the influence of relative hole size well. As can be seen in Figure 11, the decrease in nominal shear strength seems in general fairly equal for the test results and PFM.
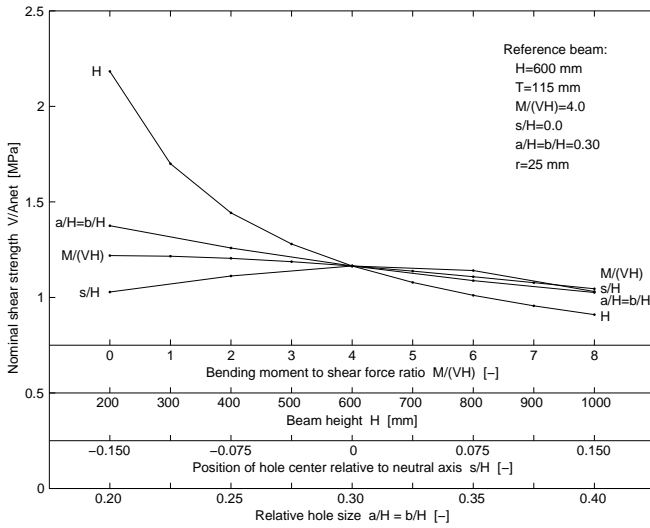
Fig. 10 Comparison to experimental test results for quadratic holes.

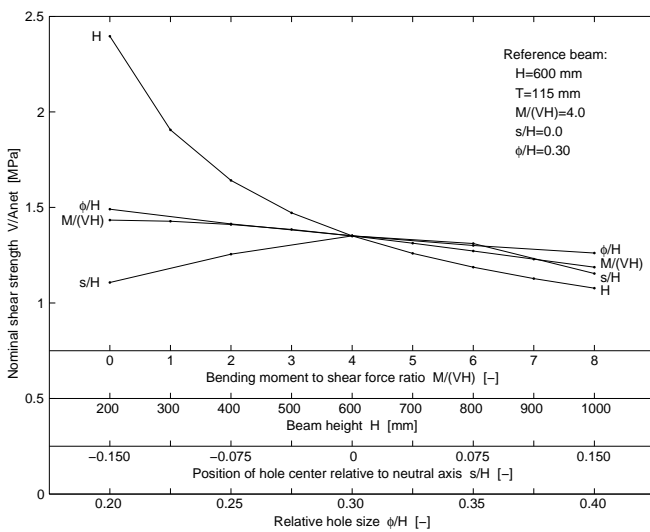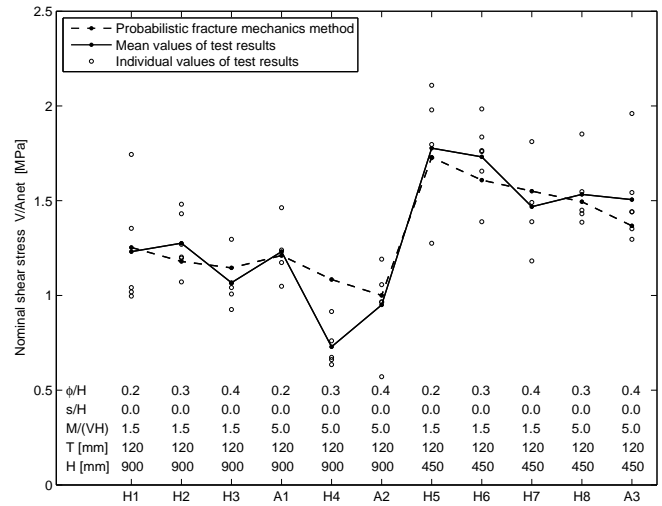**Fig. 8** Influence of design parameters for a beam with a quadratic hole.
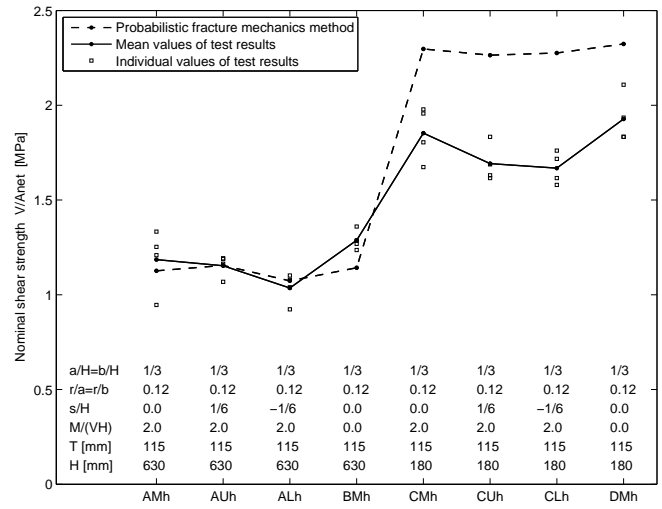
Fig. 11 Comparison to experimental test results for circular holes.

7 Comparison of methods for strength analysis

A comparison of the overall ability to predict strength of different methods is presented in Figure 12, where the ratio between the theoretically predicted capacity and the capacity found in experimental tests are given. The test results are the mean values of the test series also presented in Figures 10 and 11. Test series H4 in Figure 11 is however excluded from this comparison since it shows a deviating result in terms of a considerably lower strength compared to the other test series. Quadratic and circular marks represent test series with quadratic and circular holes respectively and a logarithmic scale is used for the comparison.

The considered methods are: the probabilistic fracture mechanics method (PFM), Weibull theory considering interaction of σ and τ (WEI$\sigma\tau$) and considering only σ (WEIσ), the mean stress method (MSM), conventional stress analy-

Fig. 9 Influence of design parameters for a beam with a circular hole.

sis considering interaction of σ and τ (CSAστ) and considering only σ (CSAσ). Some code design methods are also included in the comparison: the empirically based method (method 1) and the "end-notched beam"-analogy method (method 2) in Limträhandbok (Carling 2001), the German code DIN 1052 (Blaß 2005) and the Weibull-based design proposal by Höfflin and Aicher (Höfflin 2005; Aicher and Höfflin 2006). The latter method is presented for circular holes only, but is here used also for quadratic holes assuming $a = b = \phi$. The "end-notched beam" method is identical to the design method found in a previous draft version of EC 5. Characteristic strengths $f_{v,k} = 3.8$ MPa and $f_{t,90,k} = 0.5$ MPa are used for the code design methods (SS-EN 1194:1999 2000). The theoretical capacities for the other six methods are based on material properties stated in Table 1.

PFM shows good agreement compared to the test results, with the exception of the four test series with small beams and quadratic holes as previously mentioned. The two methods based on Weibull theory (WEIστ and WEIσ) show overall good agreement compared to the test results used in this comparison. It is remarkable that the agreement is good also for square holes, having rounded corners with $r/a = r/b \approx 0.12$, since Weibull theory predicts an unrealistic zero strength for square holes with sharp corners $r = 0$.

The "end-notched beam"-analogy method (Limträhandbok method 2) shows the most un-conservative strength predictions among the code design methods. It is however interesting that the scatter in ratio between theoretical and experimental strength is fairly low considering the beams with circular and quadratic holes separately. The overall agreement with experimental test could easily be improve by using some general reduction for beams with circular holes.
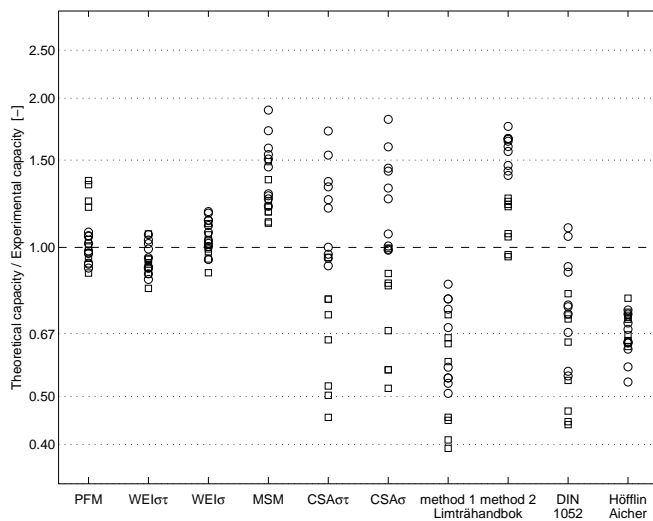

Fig. 12 Comparison of strength found in experimental tests and predicted strength according different methods for strength analysis.

8 Concluding remarks

The probabilistic fracture mechanics method seems to have good ability to predict the strength of glulam beams with holes, with the exception of small beams. An overestimation of about 30 % was found for the small beams ($H = 180$ mm). One probable explanation is that the size of the potential fracture area a_m, used to determine mean stresses, is too large in relation to the size of the small beams. The size of a fracture process region can, according to fracture mechanics, be expected to be governed by the properties of the material and to be independent of the size of the structure only as long as the structure is large as compared to the size of the fracture region. Further decrease in structural size implies decreased size of the fracture region. To overcome this problem, some kind of stress gradient related reduction of the length of the potential fracture area can be introduced for small beams. Such a reduction should give good correlation to experimental test results also for small beams.

Since the available experimental test results are limited, the extent to which the method can be verified is also limited. The present tests of beams with quadratic holes included tests of eccentrically placed holes, which seem to never have been tested before. There are however for example no test of circular holes with eccentric placement with respect to beam height.

There are also several other interesting design parameters which are not included in the parameter study presented here. One example is the influence of a tensile or compressive axial force on the strength which would for example be of interest for design of glulam columns with holes. It seems that the combined action of axial force and bending neither have been tested or analyzed. Another load case that would be of interest to analyze is pure bending, $M/(VH) \to \infty$. This kind of loading is of interest for design of straight beams but of even greater interest in relation to design of tapered beams and curved beams.

Good general features of the probabilistic fracture mechanics method are the ability to a analyze holes of arbitrary geometry and to consider the material properties that are believed to be the most important for strength of a glulam beam with a hole: material strength, fracture toughness and heterogeneity. Although of a general applicability, the method is furthermore simple in the sense that non-linear stress or fracture course analysis is not required. Generalization of PFM with respect to consideration of the normal stress along grain by modification of Equations (3) and (4) may be relevant in several applications, for example in analyzes of cases of pure bending.

A more thorough description of the probabilistic fracture mechanics method, a more comprehensive parameter study and a brief review of the code design methods considered here is presented in (Danielsson 2009).

References

Aicher S, Höfflin L (2006) Tragfähigkeit und bemessung von brettschichtholzträgern mit runden durchbrüchen – Sicherheitsrelevante modifikationen der bemessungsverfahren nach Eurocode 5 und DIN 1052. MPA Otto-Graf-Institute, University of Stuttgart

Blaß HJ, Ehlbeck J, Kreuzinger H, Steck G (2005) Erläuterungen zu DIN 1052:2004-08 – Entwurf, berechnung und bemessung von holzbauwerken. 2nd Edition including original text, DGfH innovations- und Service GmbH, München

Carling O (2001) Limträhandbok. Svenskt Limträ AB, Print & Media Center i Sundsvall AB

Danielsson H (2007) The strength of glulam beams with holes – A survey of tests and calculation methods. Report TVSM-3068, Division of Structural Mechanics, Lund University

Danielsson H (2008) Strength tests of glulam beams with quadratic holes – Test report. Report TVSM-7153, Division of Structural Mechanics, Lund University

Danielsson H, Gustafsson PJ (2008) Strength of glulam beams with holes – Tests of quadratic holes and literature test result compilation. CIB-W18/41-12-4, St Andrews, Canada

Danielsson H (2009) The strength of glulam beams with holes – A probabilistic fracture mechanics method and experimental tests. Report TVSM-3069, Division of Structural Mechanics, Lund University

Eurocode 5 (2004) Eurocode 5 - Design of timber structures. EN 1995-1-1:2004(E)

Gustafsson PJ, Enquist B (1988) Träbalks hållfasthet vid rätvinklig urtagning. Report TVSM-7042, Division of Structural Mechanics, Lund University

Gustafsson PJ, Serrano E (1999) Fracture Mechanics in Timber Engineering – Some Methods and Applications. Proceedings of 1st RILEM Symposium on Timber Engineering, Stockholm

Gustafsson (2002) Mean stress approach and initial crack approach. In Aicher S, Gustafsson PJ (ed), Haller P, Petersson H; Fracture mechanics models for strength analysis of timber beams with a hole or a notch – A report of RILEM TC-133. Report TVSM-7134, Division of Structural Mechanics, Lund University

Gustafsson PJ (2003) Chapter 7: Fracture perpendicular to grain – Structural applications. In Thelandersson S, Larsen HJ (ed:s); Timber Engineering. John Wiley & Sons Ltd, Chichester

Höfflin L (2005) Runde durchbrüche in brettschichtholzträger – Experimentelle und theoretische untersuchungen. MPA Otto-Graf-Institute, University of Stuttgart

Sjödin J, Serrano E (2008) A numerical study of methods to predict the capacity of multiple steel-timber dowel joints. Holz Roh Werkst 66: 447-454

SS-EN 1194:1999 (2000) Träkonstruktioner – Limträ – Hållfasthetsklasser och bestämning av karakteristiska värden. SIS Förlag, Stockholm

Weibull W (1939) A statistical theory of the strength of materials. Proceedings nr 151, The Royal Swedish Institute for Engineering Research, Stockholm